

# **Integrated Multistep Photochemical and Thermal Continuous Flow Reactions; Production of Bicyclic Lactones with Kilogram Productivity.**

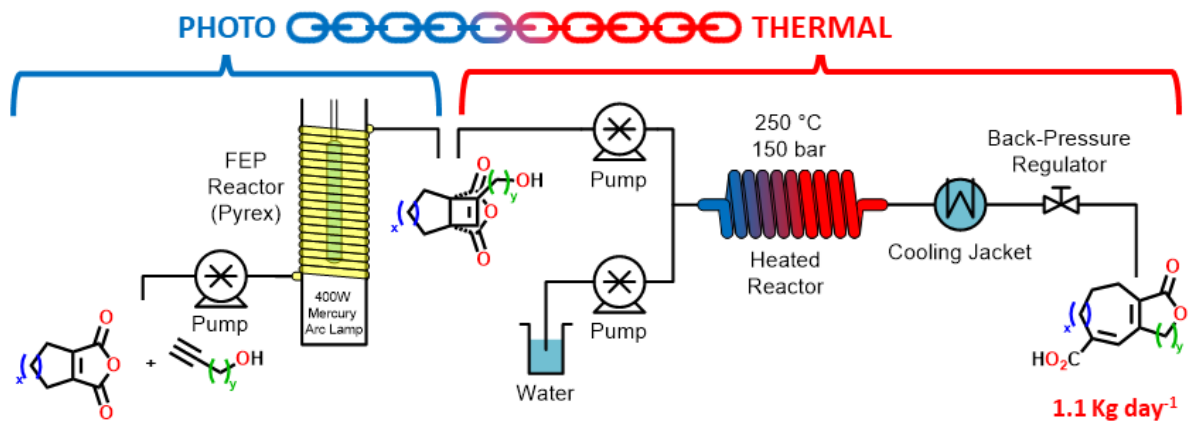
Rowena A. Howie,<sup>a</sup> Luke D. Elliott,<sup>b</sup> Surajit Kayal,<sup>a</sup> Xue-Zhong Sun,<sup>a</sup> Magnus W. D. Hanson-Heine,<sup>a</sup> Jonathan Hunter,<sup>a</sup> Charlotte A. Clark,<sup>a</sup> Ashley Love,<sup>a</sup> Christopher Wiseall,<sup>a</sup> Darren S. Lee,<sup>a</sup> Martyn Poliakoff,<sup>a</sup> Kevin I. Booker Milburn<sup>b</sup> and Michael W. George<sup>\*a</sup>

<sup>a</sup>School of Chemistry, University of Nottingham, University Park, Nottingham, NG7 2RD, UK

<sup>b</sup>School of Chemistry, University of Bristol, Cantock's Close, Bristol, BS8 1TS, UK.

\*Email: [mike.george@nottingham.ac.uk](mailto:mike.george@nottingham.ac.uk)

# TOC Graphic



## **Abstract**

Combining continuous photochemistry and flow reactions in high temperature/high pressure water has enabled us to integrate a multi-step sequence into a single process with a reduction in reaction time to <10 min compared to >24 hr in batch. At the same time, applying this approach to different substrates has allowed us to increase previously low yields to levels high enough to make those reactions potentially useful for multi-stage synthesis. In this paper, we describe the [2+2] cycloaddition / fragmentation of 3,4,5,6-tetrahydrophthalic anhydride and propargyl alcohol and analogous compounds leading to bicyclic lactones to demonstrate how photochemistry and thermal chemistry can be combined using continuous flow techniques to create complex structures on a relatively large scale. We show how photochemical and high temperature water flow reactors can be used to carry out a three- step reaction sequence as a single integrated and continuous process. The reaction time has been reduced by exploiting the enhanced acidity of high temperature water/acetonitrile mixtures. The overall process is demonstrated on an equivalent productivity of a > 1 kg/day productivity using lab scale equipment. Our approach should be simple to scale-up in an appropriate facility, for larger scale production of chemicals. Process analytical technology and modelling were used to support the reaction development, while UV and IR time resolved spectroscopy have been used to provide a deeper understanding of the reaction mechanism.

## **Keywords**

Organic Photochemistry, Flow Chemistry, Integrated Chemical Processes and High Temperature Water.

## Introduction

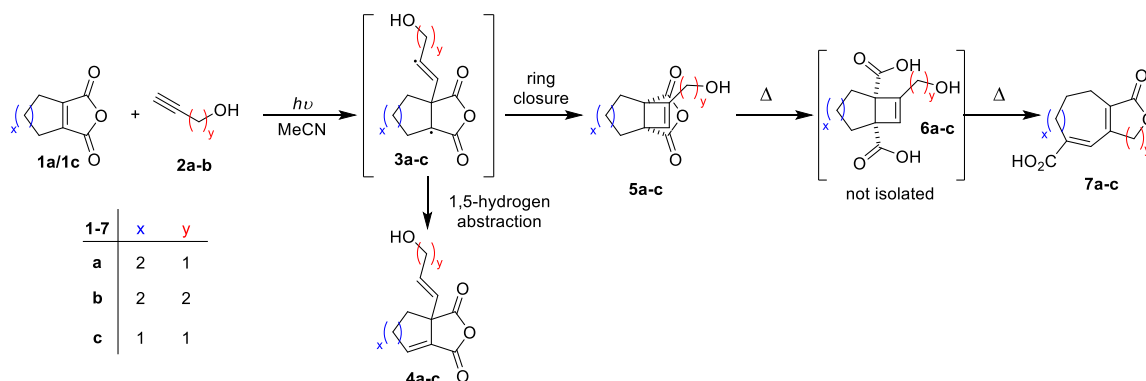
There is increasing use of continuous chemical synthesis in both academia and industry. In this context, one unmet goal is the ability to efficiently integrate continuous flow photochemistry with thermal chemistry to construct complex molecules in a more sustainable manner particularly for pharmaceutical, specialty chemical, and flavor and fragrance applications.<sup>1</sup> This need for integration has been driven by efficient and innovative syntheses and has been accompanied by developments in continuous flow reactors which simplify the problems of scaling up photochemical reactions.<sup>2</sup> Whilst the recent explosion in the use of visible light mediated photoredox reactions has offered new pathways for cross coupling and late stage functionalization, the structures generated can often be accessed by traditional means. Excited state photochemistry on the other hand, offers rapid access to sp<sup>3</sup> rich scaffolds often unobtainable by thermal and catalytic routes. Although the basic reactions have been known for many years, the products obtained are starting to be appreciated as novel scaffolds in their own right.<sup>3</sup> The focus on photochemistry has, in part, been facilitated by the increasing application of continuous flow chemistry, additionally, the unique reactivity of the often strained photochemical products can be exploited to further diversify the molecular space and complexity.<sup>4</sup>

There is considerable interest in applying the release of strain within organic molecules to create versatile building blocks and complex scaffolds. This has proved to be a powerful and widely used approach in thermal chemistry, where releasing the high ring strain in, for example, cyclopropanes and cyclobutanes lead to many possibilities for ring-opening in synthesis.<sup>5,6</sup> This interest in ring-opening has coincided with a renaissance in organic photochemistry, partly prompted by the ability of photochemistry to promote transformations that are not accessible by more traditional synthetic routes,<sup>7</sup> and particularly relevant to this paper, to easily introduce strain into organic molecules.

The scale-up problems of photochemistry are principally concerned with ensuring that every molecule in a large volume of reaction mixture is exposed to sufficient light to promote the desired transformation. Flow chemistry can be particularly useful for photochemistry because it enables reaction mixtures to be irradiated in a relatively narrow pathlength with much better light penetration than in a larger tank reactor. Such flow reactors can be used to produce kilogram quantities of compounds either by scaling out (i.e. several reactors in parallel) or by scaling up with highly efficient reactors in combination with high power light sources.<sup>8</sup> Of course, continuous flow chemistry also offers advantages in thermal reactions, such as those that release ring strain mentioned above. These advantages include (i) improved temperature control because of enhanced heat transfer, (ii) the opportunity to link the separate stages of a multi-step synthesis into a single, cleaner process by 'daisy-chaining' a number of different reactors in series and (iii) access to new operating windows (e.g. operating with traditional solvents well above their boiling points) which can widen the scope of known transformations. Superheating of solvents has particularly striking effects in the case of water because, at higher temperatures, H-bonding is weakened with a drop in dielectric constant and increased solubility of organic compounds (e.g. at 300 °C, H<sub>2</sub>O has solvent properties similar to those of acetone); at the same time, the ionic product of water increases giving enhanced concentrations of both [H]<sup>+</sup> and [OH]<sup>-</sup>, opening up the possibility of acid catalysis in the *absence of added acid*.<sup>9</sup>

Thus, there is a considerable attraction in the concept of creating a single continuous flow process to link photochemical and thermal reactors which first create strained structures and then release that strain to generate complex molecular architectures. The challenge, however, is how to match the productivity rates (g/h) of the photochemical and thermal processes so that the

reactors can be successfully integrated into a single chain, smoothly converting starting materials into desired product(s) with high selectivity and good productivity.



**Scheme 1.** Synthesis of 8,5-bicyclic lactone **7a**. Photochemical addition of **1** and **2** results in a mixture of non-bridged and bridged photoproducts (**4** and **5**) via a common intermediate, biradical **3**. Hydrolysis and subsequent ring opening and lactonization of the bridged photoproduct leads to the desired product **7**. The size of the two rings in **7** can be altered by adjusting size of both starting materials; the larger ring from the carbocycle of **1** ( $x$ ) and the smaller ring by the altering the length of the chain in **2** ( $y$ ).

In this paper we use the [2+2] cycloaddition / fragmentation of 3,4,5,6-tetrahydrophthalic anhydride (THPA, **1a**) and propargyl alcohol (**2a**) and analogous compounds as a case study to show how photochemistry and thermal chemistry can be combined using continuous flow techniques to create complex structures, found in natural products<sup>10</sup> and of potential use for drug discovery,<sup>11</sup> on a relatively large scale. We show how we have taken a series of photochemical and thermal reactions leading to a bicyclic lactone, **7a** in scheme 1, and have integrated them into a single process in continuous flow. The reaction was first reported over 25 years ago,<sup>12</sup> and then used in model studies towards the natural product pachylactone<sup>13</sup> and to study the thermal electrocyclic ring opening scope.<sup>14</sup> Together these papers established that the yields of the final ring-expanded product varied considerably with different sized rings; that is from 84% for **7a**, the 8/5 compound, to as little as 6% for the 7/5 analog and, as might be expected, the rate of converting the diester of **6a** to **7a** increased with temperature (e.g. maximum yield of **7a** was achieved in 28 hours in refluxing xylene (bp 139 °C) but only 7 hours in diglyme (bp 162 °C).

Although excellent yields of **7a** were obtained in these early studies, the ability to scale-up and hence to fully exploit the methodology was severely limited by the efficiency of the initial photochemical step and the sluggishness of the final thermal step. In this paper we demonstrate that to successfully address this challenge requires a combination of engineering, fundamental chemistry and reactor modelling, which results in a short reaction time in a flowing high-temperature water reactor to increase the productivity transforming a 24-hour acid reflux to a ca. 10-minute residence time. Our multi-faceted approach to this reaction has the following aims: (i) to study the photophysics of the reaction to gain greater insight into the excited state behavior of the substrate; (ii) to optimize the photochemical cycloaddition and thermal fragmentation for optimal productivity and sustainability and (iii) to combine- photochemical and thermal steps into a single streamlined continuous flow process. Our initial optimization focused on the parent **1a/2a** reaction but we also demonstrate how other thermally fragmented products inaccessible by traditional means can be accessed using high temperature flow techniques. This study develops a multi-step approach to achieving productivities of kg/day. Our initial strategy was to study the photophysics of the photochemical reaction and hence to accelerate the reaction by use of a thioxanthone photosensitizer, then to identify a solvent that it is compatible with all the different reactions and lastly to optimize the process to maximize its productivity. The final process has enabled us to avoid a solvent change and, by exploiting the unusual acidity of solvent mixtures containing high

temperature water, to eliminate the need for concentrated HCl as a catalyst, and, hence, to combine two reactions steps into one. Finally, we demonstrate that our approach can transform the yields of other substrates, e.g. **7b** and **7c**, where previous, more traditional batch processing has failed to give usable yields of the final product.

## Results and Discussion

The initial photochemical reaction which ultimately leads to **7a** has been known for some years, but the overall productivity was somewhat low.<sup>13</sup> The overall process starting from **1a** to the target lactone **7a** involves three stages, (see Scheme 1) (i) the initial [2+2] photochemical addition, (ii) hydrolysis of the resulting anhydride and (iii) a combined electrocyclic ring opening and lactonization, which itself occurs via several intermediates, to form **7a**. In the original publication these three steps were carried out in different solvents, which clearly would be problematic for a continuous integrated process.

In order to improve the efficiency of these reactions particularly targeted at scale-up we have investigated a range of photosensitisers (see ESI) and found that isopropylthioxanthone (ITX) to be an efficient triplet sensitizer giving ca. tenfold increase in productivity compared to the unsensitized reaction. We then screened a range of solvents and identified EtOAc as the optimal solvent for photochemistry in terms of productivity and yield (ESI) and sustainability. Using this solvent the photochemistry was scaled-up with the continuous flow Firefly reactor<sup>8c</sup> at 3 kW, (EtOAc, 0.5 M), 1 mole scale in 1.1 hrs, then 5 mole scale in 5.5 hrs with no reactor fouling.

Addition of water to EtOAc allows the hydrolysis to be carried out rapidly as an emulsion and results in aqueous solution of **6a** after separation. The thermal electrocyclic ring opening of **6a** → **7a** was found to proceed slowly at reflux in H<sub>2</sub>O (3 days) but could be catalyzed by 20 mol% HCl, reducing the time to 19 hrs. The resulting product could be isolated in high purity by filtration of the cooled reaction mixture, giving 510 g from a 5 mole photochemical reaction (see ESI). A 24 hour continuous run with the photochemical reactor would give over 2.2 kg of product but with this method would require the use of a 25 L batch reactor for the aqueous thermal reaction. These results, however, opened up the possibility of using flow chemistry to exploit the inherent acidity of superheated H<sub>2</sub>O to eliminate the need for HCl with the added advantage of accelerating the reaction by running it at higher temperatures. Unfortunately, EtOAc is incompatible with H<sub>2</sub>O at high temperatures as it hydrolyses rapidly. By contrast, acetonitrile (CH<sub>3</sub>CN) only reacts slowly with H<sub>2</sub>O even >300 °C.<sup>15-16</sup> In order to implement a fully continuous process it is preferable to avoid solvent change or biphasic mixtures and, although EtOAc gave the highest productivity for the photochemical step, CH<sub>3</sub>CN proved more desirable particularly as it has only marginally worse productivity for the photochemistry but is fully miscible with H<sub>2</sub>O. Therefore, we decided to build the process around using aqueous CH<sub>3</sub>CN for the subsequent steps i.e. carrying out the photochemistry in pure CH<sub>3</sub>CN and then adding an equal volume of H<sub>2</sub>O for the subsequent thermal stages since H<sub>2</sub>O inhibits the photochemistry if added from the outset.

Figure 1 summarizes the key data from a detailed Time Resolved IR (TRIR)<sup>17</sup> study of the reaction of **1a** with **2a** in CD<sub>3</sub>CN – the deuterated solvent was used to avoid IR bands of CH<sub>3</sub>CN masking these regions of the spectrum. Initial experiments with **1a** in the absence of other reagents allowed us to identify the IR bands of the singlet and triplet excited states, <sup>1</sup>[**1a**] and <sup>3</sup>[**1a**], Figure 1A and 1B. This experiment also showed that ca. 60% <sup>1</sup>[**1a**] decays back to the ground state of **1a** rather than to <sup>3</sup>[**1a**], thereby confirming why direct excitation of **1a** is not the most efficient approach to promoting the reaction of <sup>3</sup>[**1a**] with **2a**. Similar experiments with solutions of the photosensitizer thioxanthone, TXO, (not illustrated) allowed the bands of the excited states of the TXO to be identified. Then, using **1a** and TXO together, the rate of energy transfer from <sup>3</sup>[TXO] to **1a** was measured (Figure 1C and 1D). Finally, TRIR data from a mixture containing **1a**, **2a** and TXO confirmed, for the first time, the presence of proposed intermediate diradical **3a** and shows that there is no reformation of **1a**. This indicates that the quantum yield of formation of the diradical **3a** is considerably higher than in the absence of TXO. The spectra (Figure 1E and 1F) also showed

that both of the photoproducts **4a** and **5a** are derived from the same intermediate, **3a**, making it unlikely that one could easily change the ratio of **4a**: **5a** by simple variation of the reaction parameters.

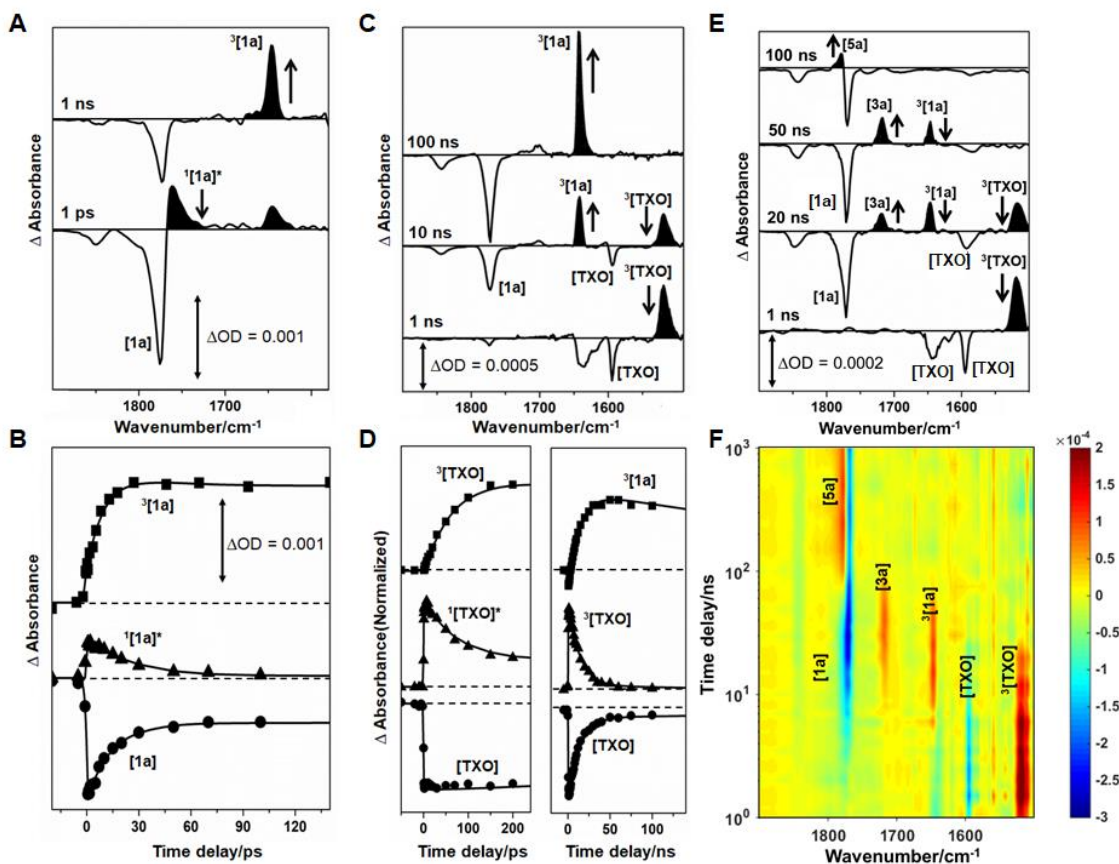


**Figure 1.** Time-resolved IR (TRIR) spectra recorded in CD<sub>3</sub>CN solution to understand the reaction of **1a** with **2a** (A) Spectra obtained 1 ps<sup>18</sup> and 1 ns after 266 nm photoexcitation of **1a** (11 mM) in the absence of other reagents. (B) TRIR kinetic decay traces obtained from the experiment shown in A, showing the bleach and partial recovery of the 1774 cm<sup>-1</sup> band of **1a**, the rise and decay of singlet <sup>1</sup>[**1a**]\*, 1762 cm<sup>-1</sup>, and the formation of triplet <sup>3</sup>[**1a**] (1645 cm<sup>-1</sup>) excited states. (C) TRIR spectra obtained 1, 10 and 100 ns following excitation (355 nm) of mixture of **1a** (12 mM) and TXO (1.2 mM). (D) the corresponding TRIR kinetic decay traces showing the bleach of TXO (1594 cm<sup>-1</sup>); the formation and decay of singlet <sup>1</sup>[TXO]\* (1474 cm<sup>-1</sup>), the concomitant rise of triplet <sup>3</sup>[TXO] (1518 cm<sup>-1</sup>) excited states together with the subsequent decay of <sup>3</sup>[TXO] and formation of <sup>3</sup>[**1a**]. (E) TRIR spectra obtained 1, 20, 50 and 100 ns following excitation (355 nm) of mixture of **1a** (12 mM), TXO( 1.2 mM), and excess **2a** (120 mM) and (F) the corresponding 2D contour map of the TRIR spectra of the mixture showing the assignment of the transient peaks associated with respective intermediates. The time axis is in logarithmic scale. The transient intensity amplitude units are highlighted in colour to indicate the change in IR absorbance ΔOD from blue (-3.0 × 10<sup>-4</sup>) to red (+2.0 × 10<sup>-4</sup>). The global analysis of these TRIR spectra reveal that irradiation initially led to bleaching of TXO and production of <sup>3</sup>[TXO] which decays (τ = 15 ± 3 ns) as the bands of **1a** bleach and <sup>3</sup>[**1a**] is formed. <sup>3</sup>[**1a**] subsequently decay (τ = 12.5 ± 2 ns) to form the bi-radical intermediate **3a** which then decays and the TRIR data also confirms that both photoproducts, **4a** and **5a**, are derived from **3a**.

The development of the integrated process was carried out in three stages. First, using a small autoclave, we studied the batch ring opening and lactonization reaction of **6a** to **7a** in high temperature water (see ESI) to check that (i) the ring opening did occur and (ii) hydrolysis of the lactone did not take place. These experiments were successful with optimal conditions of 200 °C for 10 mins. Transferring this reaction to a continuous pressurized flow reactor revealed a problem, namely that, although the reaction took place, the desired product **7a** precipitated when the water cooled down causing blockages, prior to the release of pressure. Fortunately, the lactone **7a** is soluble in aqueous CH<sub>3</sub>CN, and the reaction still took place with near quantitative yield, when using the CH<sub>3</sub>CN/H<sub>2</sub>O mixture as the solvent, although, the optimal temperature required for maximum throughput (260 °C) was somewhat higher than that in the batch reaction in H<sub>2</sub>O. Then to investigate whether the hydrolysis of **5a** could also be carried out in a high temperature aqueous CH<sub>3</sub>CN, we pumped a solution of **5a** through thermal reactor and found that both reactions could be carried out as a combined process in a single reactor. The reaction worked equally well with a mixture of **4a** and **5a** obtained directly from the photochemical reaction, as opposed to pure **5a**. Thus, it was not necessary to separate the photoproducts **4a** and **5a** prior to hydrolysis. In addition, the reaction in CH<sub>3</sub>CN/H<sub>2</sub>O was carried out with a residence time of < 2.5 mins. These results opened the way for a single integrated process from **1a** → **7a** based on aqueous CH<sub>3</sub>CN.

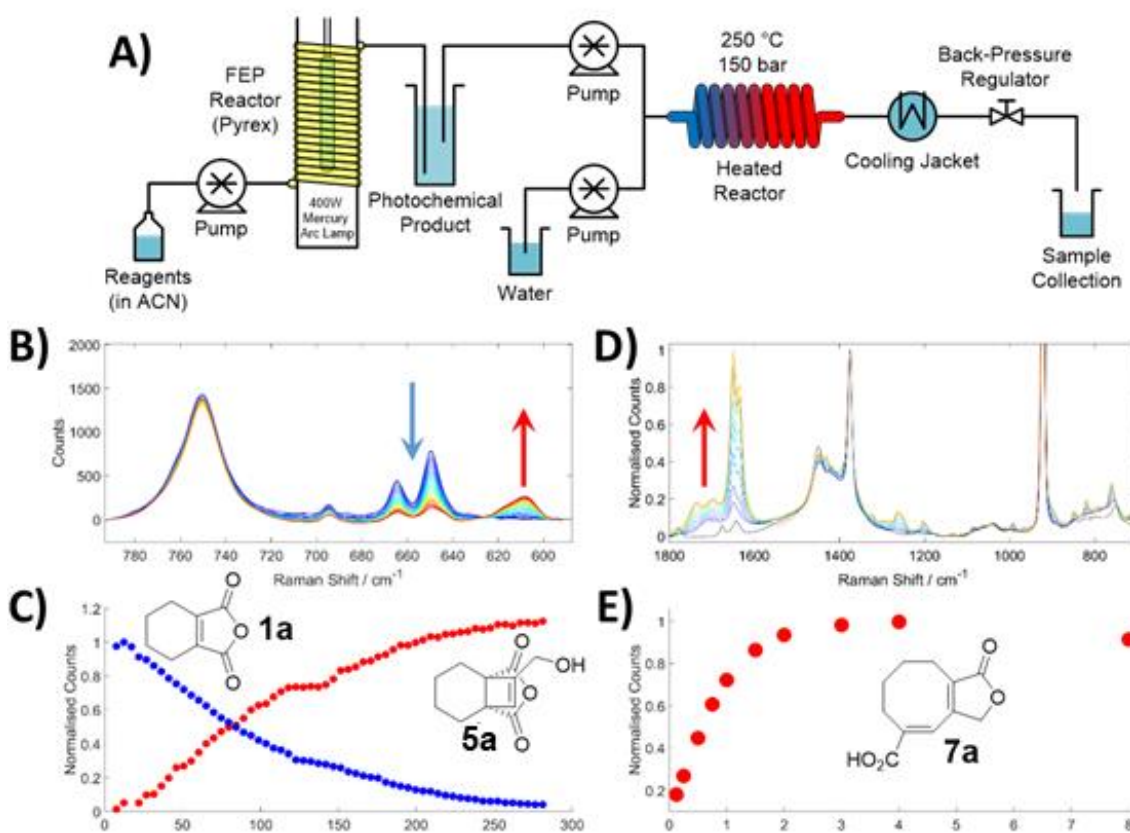


**Figure 2.** Simplified schematic of the integrated chain of photochemical and thermal flow reactors (A), together with Raman spectra from on-line monitoring the formation of the products and intermediates in the smaller scale version of the reactor. (B) Monitoring the UV photolysis with the kinetic traces (C) showing the conversion of **1a** (in blue) and the formation of **5a** (in red); (D) Monitoring of the thermal stage with (E) showing the increase in yield of **7a** (red points) as a function of residence time.



Figure 2A is a schematic diagram of our apparatus, broadly it consists of a fluorinated ethylenepropylene (FEP) tubular photoreactor with a 400 W mercury lamp, filtered by borosilicate glass. Then, after a reservoir to prevent any back pressure reaching the photochemical reactor, the solution is fed into a HPLC pump to generate the pressure needed for the thermal stage. A second pump delivers the H<sub>2</sub>O and the resulting CH<sub>3</sub>CN/H<sub>2</sub>O reaction mixture passes directly into a heated coiled tubular reactor which serves as both preheater and reactor. This is followed by cooldown and pressure release, yielding a solution of the target product **7a**, the hydrolysis product of **4a** and residual TXO. Evaporation of CH<sub>3</sub>CN from this aqueous solution resulted in precipitation of **7a**, in high purity, which could be then separated by filtration from the solution of any remaining diacid **6a** and the hydrolysis products of **4a**.

Using this system, **1a** (0.1 M) with 1.5 eqs of **2a** and TXO (1 mol%) in CH<sub>3</sub>CN were flowed through the photoreactor at 10 ml/min, giving greater than 95% conversion and a 68% yield of **5a**, 41 mmol/h (plus 15% **4a**). This solution was then mixed with water in a 1:1 ratio by volume to give a total flow rate of 20 ml/min and thermally treated at 240 to 260 °C, as summarized in Table 1. At the highest temperature, near quantitative yields of **7a** were obtained for the thermal steps, giving an overall yield of 67% for the daisy-chained process. This corresponds to a productivity of 39 mmol/hr and is a marked improvement over the 44% yield of **7a** obtained via separate batch processing, particularly considering the reduction in overall reaction time from greater than 24 hours to a residence time of just 10 minutes in flow.

**Table 1. Optimisation of large scale 2-step process to form 7a**

Light source	Photochemical				Thermal			Yield <b>6a</b> (%)	Yield <b>7a</b> (%)	Productivity	
	Conc. (M)	Flow rate (ml/min)	Conv. (%)	Yield (%)	Flow rate (ml/min)	Temp. (°C)	Conv. (%)			(mmol/hr.)	(g/day)
1 x 400 W FEP	0.1	10	full	68	20	240	full	8	92	36	181
1 x 400 W FEP	0.1	10	full	68	20	250	full	3	98	39	193
1 x 400 W FEP	0.1	10	full	68	20	260	full	0	>99	39	195
3 x 400 W FEP	0.5	12.5	92	61	25	250	full	2	98	225	1124
Firefly	0.5	30	full	70	-	-	-	-	-	630 <sup>[a]</sup>	3147 <sup>[a]</sup>

<sup>[a]</sup>productivity predicted based on photochemical results only

From these results, it was clear that the maximum throughput of the combined reactor was being limited by the photochemical rather than the thermal reactors. Therefore, we installed two additional identical photoreactors in parallel with the first, thereby at least tripling the productivity of the photochemical reaction. Running these combined reactors together with small changes to the reaction conditions and an increased concentration of substrate to 0.5 M allowed the overall productivity of the daisy-chained sequence to be increased to 225 mmol/hr. For this test run the reactors were successfully held at the desired reaction conditions for 1 hour after equilibration with no evidence of reactor fouling or precipitation of reactants. Extrapolating from this 1 hr period would give an equivalent rate of formation of **7a** of greater than 1.1 kg/day, using lab scale equipment.

Work using a novel tubular quartz reactor, with a 3 kW Hg lamp, gave very promising results for the further scale up of the photochemical step. This so-called 'Firefly' reactor<sup>8c</sup> was used to carry out the photochemical step on 1 mole of **1a** at a 0.5 M concentration in ethyl acetate, using a 30 ml/min flow rate and a 3 kW lamp power. This resulted in full conversion, giving a 70% yield of **5a** at a productivity of 630 mmol/hr. This reaction was subsequently repeated on a 5 mole scale, over the course of 5 hours, with no evidence of fouling within the reactor. These results represent an approximately three-fold increase in productivity and flow rate over the parallel, triple 400 W FEP

reactors, taking the photochemical productivity beyond the current capabilities of our thermal reactor. Process modelling of the thermal reactor using the Process Systems Enterprise (PSE) gPROMS software predicts 82% conversion using similar conditions as reported above in the current reactor, which rises to full conversion and >95% yield if the reactor volume were doubled.<sup>19</sup>

Construction of a larger scale reactor train was not carried out during this project, due to limitations in terms of space and equipment as well as the safety restrictions presented by a University research laboratory. Nevertheless, these results are very promising because they suggest that only a modest increase in scale for the thermal reactor would be required to match the output of the *Firefly* reactor and reach the equivalent of 1 tonne/year, an industrially relevant milestone/benchmark for many pharmaceutical products. Thermal flow chemistry is particularly suited to reactions involving challenging substrates which may decompose at conditions close to those required for their formation. Faster heating, compared to batch reactors of similar productivity, allows the desired conditions to be achieved rapidly, minimizing reaction times, while improved cooling rates help to avoid thermal degradation of unstable products. Therefore, the process intensification that we have achieved with **7a** suggests that we might be able to increase the previously reported low yields for related reactions to a more useful level, see examples in Scheme 1, because the yields for the photochemical stage of those reactions were similar to that in the **7a** system, with the loss of yield occurring mainly in the thermal steps. Thus, we have focused our investigations on thermal flow reactions, while performing the preceding photochemical steps in batch. Some of the starting materials required for these reactions are economically prohibitive for scale-up, so we decided to build a smaller scale thermal reactor, to reduce waste and to run these reactions at a reasonable cost. The performance of this smaller reactor was validated using the synthesis of **7a** and monitored in real time using Raman spectroscopy, Figure 2. This allowed the scalability of the reaction to be investigated, with good agreement between results obtained previously in the larger reactor to those predicted from a gProms model developed using results from the small-scale reactor.

This smaller reactor is described in detail in the ESI but, in brief, it consists of a similar tubular heated reactor as used previously but, with a 0.8 mL heated volume, ca. 50 times smaller. The same aqueous CH<sub>3</sub>CN was used as the solvent for these reactions. The thermal steps in reaction of **1a** with 3-butyn-1-ol (**2b**), have previously required longer reaction times due to less favored formation of the 6-membered lactone **7b** but, in our reactor, a 61% yield of the ring opened product, **7b**, was obtained after only a 2 min residence time at 250 °C. This contrasts favorably to the previously reported 36 hour reflux in xylene.

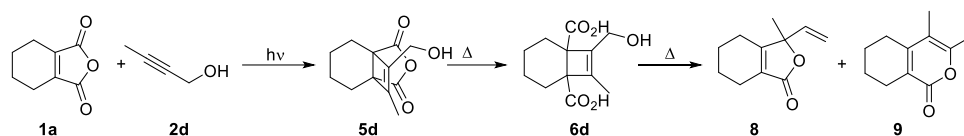
**Table 2.** Optimisation of difficult substrates **5a-d**

Substrate	Temperature (°C)	Flow rate (ml/min)	Yield <b>6a-d</b> (%)	Yield <b>7a-d</b> (%)	Yield <b>8</b> (%)	Yield <b>9</b> (%)
<b>5a</b>	200	0.4	51	35	-	-
<b>5a</b>	225	0.4	10	88	-	-
<b>5a</b>	250	0.4	0	94	-	-
<b>5b</b>	250	0.4	3	61	-	-
<b>5c</b>	260	0.4	36	45	-	-
<b>5c</b>	300	1.2	9	78	-	-
<b>5d</b>	250	0.8	68	0	4	0
<b>5d</b>	300	0.4	9	0	12	34

We then investigated the reaction sequence starting with **1c** and **2a** which ultimately leads to the 7/5 bicyclic ring-opened product **7c**, Scheme 1. When this reaction was originally reported, the methyl ester of this analog was obtained via a series of batch processes over several days with an overall yield of just 4%. Again, good yields had been achieved for the photochemical and esterification steps, with the problem lying in the thermal ring opening steps (6% and later 25%),

due to the increased strain in the 7-membered *cis-trans* diene intermediate and reduced stability of **7c**. With only modest optimization (see ESI), we increased the yield of the thermal stages up to 45% of **7c** plus 36% of **6c**, as shown in table 2. This represents a considerable improvement, especially considering the reduction in thermal reaction time from >24 hrs in batch to ca. 2 minutes in flow. Increasing the temperature of 300 °C gave up to 78% of **7c**, using an increased flow rate to shorten the residence time. However, as there was some evidence for the hydrolysis of CH<sub>3</sub>CN under these conditions, an alternative solvent mixture would be required if this substrate were to be pursued further.

Reaction of **1a** with alcohol, **2d**, gave quite different results, because the steric bulk of the Me group in **2d** appears to seriously hinder the ring expansion sequence. Tolerance of such methyl groups has been shown for analogs containing a larger ring system, although in the case of **5d** batch processing was reported to lead to recovery of the starting material or decomposition. Reacting the photoproduct **5d** in our continuous flow reactor in aqueous CH<sub>3</sub>CN led to the formation of the expected diacid **6d** up to 68% at 250 °C. Higher reaction temperatures appear to promote unusual further reactivity, leading to the formation of two novel compounds, **8** and **9**, which were isolated in reasonable yields (12% and 34% respectively), Scheme 2. The formation of **8** and **9** could occur via a decarboxylation and subsequent cyclisation. Investigations are ongoing to confirm the proposed mechanism and to establish whether this unusual reactivity could be exploited to carry out a range of similar reactions in high temperature water.



**Scheme 2.** Photochemical addition of **1a** and **2d** to **5d** followed by hydrolysis to **6d** and thermal decarboxylation and rearrangement to products **8** and **9**.

## Conclusions

We have successfully integrated photochemical and high temperature water flow reactors to carry out a three- step reaction sequence as a single integrated and continuous process. The addition of a thioxanthone photosensitizer and exploiting the enhanced acidity of high temperature water/acetonitrile mixtures has enabled the reaction time to be reduced from >24 hrs to 10 minutes. This reaction was demonstrated on the equivalent productivity of a > 1 kg/day productivity using lab scale equipment. Although we were operating at the maximum practical scale for a university laboratory, our approach should be simple to scale-up in an appropriate facility, for larger scale production of chemicals. Process analytical technology and modelling were used throughout to support the reaction development, while UV and IR time resolved spectroscopy have been used to provide a deeper understanding of the reaction mechanism. Extending the approach to other substrates has allowed us to increase previously low yields to levels high enough to make those reactions potentially useful for multi-stage synthesis.

## Electronic Supporting Information

Experimental details including details of the reactors, time-resolved infra-red studies, reactor modelling, compound characterisation data and spectra are included in the ESI.

## Acknowledgments

We thank the EPSRC grant (EP/P013341/1) and the EPSRC CDT for Sustainable Chemistry for funding this work. We are grateful to Mr Bryan Tambosco for his help and Dr Charlotte Pearson for their advice. We thank Messrs Richard Wilson, Richard Meehan and Mark Guyler for their technical support.

## References

1. (a) Baumann, M.; Moody, T. S.; Smyth, M.; Wharry, S. A. Perspective on Continuous Flow Chemistry in the Pharmaceutical Industry. *Org. Process Res. Dev.* **2020**, *24*, 1802-1813; (b) Sambigiato, C.; Noël, T. Flow photochemistry: shine some light on those tubes! *Trends Chem.* **2020**, *2*, 92-106; (c) Badman, C.; Cooney, C. L.; Florence, A.; Konstantinov, K.; Krumme, M.; Mascia, S.; Nasr, M.; Trout, B. L. Why We Need Continuous Pharmaceutical Manufacturing and How to Make It Happen. *J. Pharm. Sci.* **2019**, *108*, 3521-3523; (d) Plutschack, M. B.; Pieber, B.; Gilmore, K.; Seeberger, P. H. The Hitchhiker's Guide to Flow Chemistry(II). *Chem. Rev.* **2017**, *117*, 11796-11893; (e) Adamo, A.; Beingessner, R. L.; Behnam, M.; Chen, J.; Jamison, T. F.; Jensen, K. F.; Monbaliu, J.-C. M.; Myerson, A. S.; Revalor, E. M.; Snead, D. R.; Stelzer, T.; Weeranoppanant, N.; Wong, S. Y.; Zhang, P. On-demand continuous-flow production of pharmaceuticals in a compact, reconfigurable system. *Science* **2016**, *352*, 61-67; (f) Gutmann, B.; Cantillo, D.; Kappe, C. O. Continuous-Flow Technology A Tool for the Safe Manufacturing of Active Pharmaceutical Ingredients. *Angew. Chem. Int. Ed.* **2015**, *54*, 6688-6728.
2. a) Donnelly, K.; Baumann, M. Scalability of photochemical reactions in continuous flow mode. *J. Flow Chem.* **2021**, <https://doi.org/10.1007/s41981-021-00168-z> b) Kayahan, E.; Jacobs, M.; Braeken, L.; Thomassen, L. C.; Kuhn, S.; van Gerven, T.; Leblebici, M. E. Dawn of a new era in industrial photochemistry: the scale-up of micro- and mesostructured photoreactors, *Beilstein J. Org. Chem.* **2020**, *16*, 2484–2504.
3. Blanco-Ania, D.; Gawade, S. A.; Zwinkels, L. J. L.; Maartense, L.; Bolster, M. G.; Benningshof, J. C. J.; Rutjes, F. P. J. T. Rapid and Scalable Access into Strained Scaffolds through Continuous Flow Photochemistry, *Org. Process Res. Dev.* **2016**, *20*, 2, 409–413.
4. Luque, A.; Paternoga, J.; Opatz, T. Strain Release Chemistry of Photogenerated Small-Ring Intermediates, *Chem. Eur. J.* **2021**, *27*, 4500.
5. Wong, H. N. C.; Hon, M.-Y.; Tse, C.-W.; Yip, Y.-C.; Tanko, J.; Hudlicky, T. Use of cyclopropanes and their derivatives in organic synthesis. *Chem. Rev.* **1989**, *89*, 165-198.
6. Ebner, C.; Carreira, E. M. Cyclopropanation Strategies in Recent Total Syntheses. *Chem. Rev.* **2017**, *117*, 11651-11679.
7. (a) Politano, F.; Oksdath-Mansilla, G. Light on the Horizon: Current Research and Future Perspectives in Flow Photochemistry. *Org. Process Res. Dev.* **2018**, *22*, 1045-1062; (b) Kärkäs, M. D.; Porco, J. A.; Stephenson, C. R. J. Photochemical Approaches to Complex Chemotypes: Applications in Natural Product Synthesis. *Chem. Rev.* **2016**, *116*, 9683-9747; (c) Ravelli, D.; Protti, S.; Fagnoni, M. Carbon-Carbon Bond Forming Reactions via Photogenerated Intermediates. *Chem. Rev.* **2016**, *116*, 9850-9913; (d) Poplata, S.; Tröster, A.; Zou, Y.-Q.; Bach, T. Recent Advances in the Synthesis of Cyclobutanes by Olefin [2+2] Photocycloaddition Reactions. *Chem. Rev.* **2016**, *116*, 9748-9815; (e) Ghogare, A. A.; Greer, A. Using Singlet Oxygen to Synthesize Natural Products and Drugs. *Chem. Rev.* **2016**, *116*, 9994-10034.; (f) Cambié, D.; Bottecchia, C.; Straathof, N. J. W.; Hessel, V.; Noël, T. Applications of Continuous-Flow Photochemistry in Organic Synthesis,

- Material Science, and Water Treatment. *Chem. Rev.* **2016**, *116*, 10276-10341; (g) Blanco-Ania, D.; Gawade, S. A.; Zwinkels, L. J. L.; Maartense, L.; Bolster, M. G.; Benningshof, J. C. J.; Rutjes, F. P. J. T. Rapid and Scalable Access into Strained Scaffolds through Continuous Flow Photochemistry. *Org. Process Res. Dev.* **2016**, *20*, 409-413.
8. (a) Lee, D. S.; Sharabi, M.; Jefferson-Loveday, R.; Pickering, S. J.; Poliakoff, M.; George, M. W. Scalable Continuous Vortex Reactor for Gram to Kilo Scale for UV and Visible Photochemistry. *Org. Process Res. Dev.* **2020**, *24*, 201-206; (b) Clark, C. A.; Lee, D. S.; Pickering, S. J.; Poliakoff, M.; George, M. W. UV PhotoVap: Demonstrating How a Simple and Versatile Reactor Based on a Conventional Rotary Evaporator Can Be Used for UV Photochemistry. *Org. Process Res. Dev.* **2018**, *22*, 595-599; (c) Elliott, L. D.; Berry, M.; Harji, B.; Klauber, D.; Leonard, J.; Booker-Milburn, K. I. A Small-Footprint, High-Capacity Flow Reactor for UV Photochemical Synthesis on the Kilogram Scale *Org. Process Res. Dev.* **2016**, *20*, 1806-1811; (d) Su, Y.; Kuijpers, K.; Hessel, V.; Noël, T. A convenient numbering-up strategy for the scale-up of gas-liquid photoredox catalysis in flow. *React. Chem. Eng.* **2016**, *1*, 73-81; (e) Beatty, J. W.; Douglas, J. J.; Miller, R.; McAtee, R. C.; Cole, K. P.; Stephenson, C. R. J. Photochemical Perfluoroalkylation with Pyridine N-Oxides: Mechanistic Insights and Performance on a Kilogram Scale. *Chem.* **2016**, *1*, 456-472; (f) Harper, K. C.; Moschetta, E. G.; Bordawekar, S. V.; Wittenberger, S. J. A Laser Driven Flow Chemistry Platform for Scaling Photochemical Reactions with Visible Light. *ACS Cent. Sci.* **2019**, *5*, 109-115.
9. (a) Savage, P. E. A perspective on catalysis in sub- and supercritical water. *J. Supercrit. Fluids* **2009**, *47*, 407-414; (b) Akiya, N.; Savage, P. E. Roles of water for chemical reactions in high-temperature water. *Chem. Rev.* **2002**, *102*, 2725-2750; (c) Galkin, A. A.; Lunin, V. V. Subcritical and supercritical water: a universal medium for chemical reactions. *Russ. Chem. Rev.* **2005**, *74*, 21-35; (d) An, J.; Bagnell, L.; Cablewski, T.; Strauss, C. R. Trainor, R. W. Applications of high-temperature aqueous media for synthetic organic reactions. *J. Org. Chem.* **1997**, *62*, 2505-2511; (e) Kus, N. S. Organic reactions in subcritical and supercritical water. *Tetrahedron* **2012**, *68*, 949-958.
10. a) de Oliveira, K. T.; Servilha, B. M.; Alves, L. de C.; Desiderá, A. L.; Brocksom, T. J. Chapter 14 - The Synthesis of Seven-Membered Rings in Natural Products from Studies. In *Natural Products Chemistry*; Atta-ur-Rahman, Eds.; Elsevier, **2014**; pp 421-463. b) Hu, Y.; Li, L.; Han, J.; Min, L.; Li, C. Recent Advances in the Total Synthesis of Natural Products Containing Eight-Membered Carbocycles (2009–2019). *Chem. Rev.* **2020**, *120*, 5910–5953.
11. Clarke, A. K.; Unsworth, W. P. A happy medium: the synthesis of medicinally important medium-sized rings via ring expansion, *Chem. Sci.* **2020**, *11*, 2876-2881.
12. Booker-Milburn, K. I.; Cowell, J. K.; Harris, L. J. Model studies towards the total synthesis of asteriscanolide. *Tetrahedron Lett.* **1994**, *35*, 3883-3886.
13. (a) Booker-Milburn, K. I.; Delgado Jiménez, F.; Sharpe, A. Sequential ring-opening/cyclisation reactions of bicyclo[4.2.0]oct-7-enes for the synthesis of cyclooctadiene fused lactones: Model studies towards the total synthesis of pachylactone *Tetrahedron* **1999**, *55*, 5889-5902; (b) Booker-Milburn, K. I.; Cowell, J. K.; Delgado Jiménez, F.; Sharpe, A.; White, A. J. Stereoselective intermolecular [2+2] photocycloaddition reactions of tetrahydrophthalic anhydride and derivatives with alkenols and alkynols. *Tetrahedron* **1999**, *55*, 5875-5888 (1999).
14. (a) Booker-Milburn, K. I.; Cowell, J. K.; Sharpe, A.; Jiménez, F. D. Tetrahydrophthalic anhydride and imide: Remarkably efficient partners in photochemical [2+2] cycloaddition reactions with alkenols and alkynols *Chem. Commun.* **1996**, 249-251; (b) Ralph, M. J.; Harrowven, D. C.; Gaulier, S.; Ng, S.; Booker-Milburn, K. I. The Profound Effect of the Ring

Size in the Electrocyclic Opening of Cyclobutene-Fused Bicyclic Systems *Angew. Chem. Int. Ed.* **2015**, *54*, 1527-1531.

15. (a) Venardou, E.; Garcia-Verdugo, E.; Barlow, S. J.; Gorbaty, Y. E.; Poliakov, M. On-line monitoring of the hydrolysis of acetonitrile in near-critical water using Raman spectroscopy. *Vib. Spectrosc.* **35**, 103-109 (2004); (b) Krammer, P.; Vogel, H. Hydrolysis of esters in subcritical and supercritical water. *J. Supercrit. Fluid* **2000**, *16*, 189-206.
16. Care must be taken when carrying out reactions using high temperature water and acetonitrile due to the possible hydrolysis of acetonitrile via acetamide to acetic acid and ammonia. However, except where noted, no evidence of this hydrolysis was found under the reaction conditions studied
17. (a) Kuimova, M. K.; Alsindi, W. Z.; Dyer, J.; Grills, D. C.; Jina, O. S.; Matousek, P.; Parker, A. W.; Portius, P.; Zhong Sun, X.; Towrie, M.; Wilson, C.; Yang, J.; George, M. W. Using picosecond and nanosecond time-resolved infrared spectroscopy for the investigation of excited states and reaction intermediates of inorganic systems. *Dalton Trans.* **2003**, 3996-4006; (b) Towrie, M.; Grills, D. C.; Dyer, J.; Weinstein, J. A.; Matousek, P.; Barton, R.; Bailey, P. D.; Subramaniam, N.; Kwok, W. M.; Ma, C.; Phillips, D.; Parker, A. W.; George, M. W. Development of a broadband picosecond infrared spectrometer and its incorporation into an existing ultrafast time-resolved resonance Raman, UV/Visible, and fluorescence spectroscopic apparatus. *Appl. Spectr.* **2003**, *57*, 367-380.
18. The ps-TRIR spectra obtained 1 ps following direct irradiation of **1a** at 266 nm clearly show the parent bands are bleached and a new transient produced with bands at 1763  $\text{cm}^{-1}$  which is assigned to  $^1n\pi^*$  excited state of **1a**, Figure 1. The presence of a relatively strong  $\nu(\text{C}=\text{O})$  is perhaps slightly surprising for a  $^1n\pi^*$  excited state but is consistent with the excited state being localized mainly on one of the carbonyls and this assignment was supported by DFT calculations (see ESI). The bands of  $^1n\pi^*$  excited state decays at the same rate ( $\tau = 15 (\pm 2)$  ps) as the parent partially reforms and a new band grows in at 1645  $\text{cm}^{-1}$  assigned to formation of the  $^3\pi\pi^*$  excited state of **1a** which subsequently decays back to the parent with a lifetime of 1.05 ( $\pm 0.05$ )  $\mu\text{s}$ , see ESI.
19. Wiseall, C. (2020), *Using computational models to understand CO<sub>2</sub>-rich fluid behaviour, photochemical reactions and high-temperature water reactions*. EngD thesis, University of Nottingham. <http://eprints.nottingham.ac.uk/id/eprint/60501>

# Electronic Supporting Information

## Integrated Multistep Photochemical and Thermal Continuous Flow Reactions; Production of Bicyclic Lactones with Kilogram Productivity.

Rowena A. Howie,<sup>a</sup> Luke D. Elliott,<sup>b</sup> Surajit Kayal,<sup>a</sup> Xue-Zhong Sun,<sup>a</sup> Magnus W. D. Hanson-Heine,<sup>a</sup> Jonathan Hunter,<sup>a</sup> Charlotte A. Clark,<sup>a</sup> Ashley Love,<sup>a</sup> Christopher Wiseall,<sup>a</sup> Darren S. Lee,<sup>a</sup> Martyn Poliakoff,<sup>a</sup> Kevin I. Booker Milburn<sup>b</sup> and Michael W. George<sup>\*a,c</sup>

<sup>a</sup>School of Chemistry, University of Nottingham, University Park, Nottingham, NG7 2RD, UK.

<sup>b</sup>School of Chemistry, University of Bristol, Cantock's Close, Bristol, BS8 1TS, UK.

<sup>c</sup>Department of Chemical and Environmental Engineering, University of Nottingham Ningbo China, 199 Taikang East Road, Ningbo, 315100, China.

\*Email: [mike.george@nottingham.ac.uk](mailto:mike.george@nottingham.ac.uk)

### Table of Contents

1. General Experimental .....	S3
2. Initial Studies on Photochemical and Thermal Steps.....	S4
3.1. Optimization of the [2+2] Photochemistry of 1a and 2a. ....	S4
2.1.1 Sensitizer Screen in Batch .....	S4
2.1.2. Solvent Screen with ITX in Batch.....	S5
2.1.3. Screening Concentration and Lamp Power.....	S5
2.1.4. Transfer to Large Scale Continuous Flow Reactor with a 3 kW Lamp – Predicting the Flow Rate From Batch Results .....	S6
2.2. Homogenous Lactone Hydrolysis Investigation in Batch .....	S7
2.3. Biphasic Lactone Hydrolysis / Aqueous Ring Opening Sequence .....	S8
2.4. Initial Linking of Flow Photochemical and Batch Thermal Reactions .....	S9
2.4.1. 1 Mole Scale Photo/Thermal Reaction Sequence.....	S9
2.4.2. 5 Mole Scale Photo/Thermal Reaction Sequence.....	S9
3. High Temperature Water (HTW) Reactor Set-ups .....	S11
3.1. Reactor Description and Details.....	S11
3.1.1. Large Scale Thermal Flow Reactor .....	S11
3.1.2. Small Scale Thermal Flow Reactor .....	S12
3.1.3. Standard Operating Procedure for Thermal Flow Reactors .....	S13
3.1.4. Batch Thermal Reactions .....	S14
3.2. Photochemical Flow Reactor linked with HTW Reactor .....	S14
3.2.1. Photochemical Set-up .....	S14

3.2.2. Linking of the Photochemical Flow reactor with the HTW Reactor.....	S15
3.2.3. Batch Photochemical Reactions.....	S15
4. Optimisation of Thermal Reaction in High Temperature Water .....	S16
4.1. Batch Ring Expansion/Lactonization of 6a in High Temperature Water/Acetonitrile Mixtures .....	S16
4.2. Continuous Flow Ring Expansion/Lactonization of 6a in High Temperature Water/Acetonitrile Mixtures .....	S17
4.3. Continuous-Flow Combined Hydrolysis and Ring Opening .....	S18
5. Batch Photochemistry of Additional Substrates .....	S19
6. Optimisation of Small Scale Thermal Reactor for the Ring expansion of 5b and 5c.....	S20
7. Characterization Data .....	S22
8. NMR Spectra .....	S27
9. Time Resolved Infrared Spectroscopy (TRIR).....	S34
9.1. Description of Time Resolved Infrared Spectroscopy (TRIR) setup .....	S34
9.2. Time Resolved Infrared Data .....	S35
9.3. Characterization of the transient species .....	S37
9.4. Kinetic rate constants for the sensitized reaction .....	S37
10. Raman Monitoring .....	S40
10.1. Photochemical step.....	S40
10.2. Thermal steps.....	S41
11. gProms Modelling .....	S43
11.1. Model Description.....	S43
12. Density Functional Theory Calculations.....	S44
13. References .....	S48



## 1. General Experimental

Reagents, solvents and gases were purchased from commercial suppliers and used without further purification, unless otherwise described.

Proton nuclear magnetic resonance ( $^1\text{H}$  NMR) spectra and proton-decoupled carbon nuclear magnetic resonance ( $^{13}\text{C}$  NMR) spectra were recorded at 25 °C (unless stated otherwise) using Bruker AV400 (400 MHz) and AV(III)400hd (400 MHz) spectrometers. Chemical shifts for proton are reported in parts per million downfield from tetramethylsilane and are referenced to residual protium in the NMR solvent according to values reported in the literature. Chemical shifts for carbon are reported in parts per million downfield from tetramethylsilane and are referenced to the carbon resonances of the solvent. The solvent peak was referenced to 7.26 ppm for  $^1\text{H}$  and 77.16 ppm for  $^{13}\text{C}$  in  $\text{CDCl}_3$ .

Data are represented as follows: chemical shift, integration, multiplicity (s = singlet, d = doublet, t = triplet, q = quartet, m = multiplet), coupling constants ( $J$ ) is in Hertz (Hz). NMR spectra were processed with MestReNova Software (v 12.0.4-22023).

Yields and conversions for flow experiments were determined by  $^1\text{H}$  NMR using biphenyl as an internal standard.

## 2. Initial Studies on Photochemical and Thermal Steps

### 3.1. Optimization of the [2+2] Photochemistry of 1a and 2a.

#### 2.1.1 Sensitizer Screen in Batch

A screen of commercially available sensitizers identified isopropylthioxanthone (ITX) as the optimal sensitizer for the [2+2] cycloaddition of THPA with propargyl alcohol (Figure S1). As previously reported for kilogram scale synthesis examples,<sup>[1]</sup> ITX is preferred over the parent thioxanthone for synthesis and process applications due to its increased solubility in organic solvents. Compared to the unsensitized reaction, productivity was increased by 10× using ITX, representing a large increase in energy efficiency for the reaction. Under these conditions, benzophenone is only marginally less productive than ITX but the greater extinction coefficient of ITX over BP allows it to be used at lower concentrations with minimal loss of UV transmission and hence productivity.

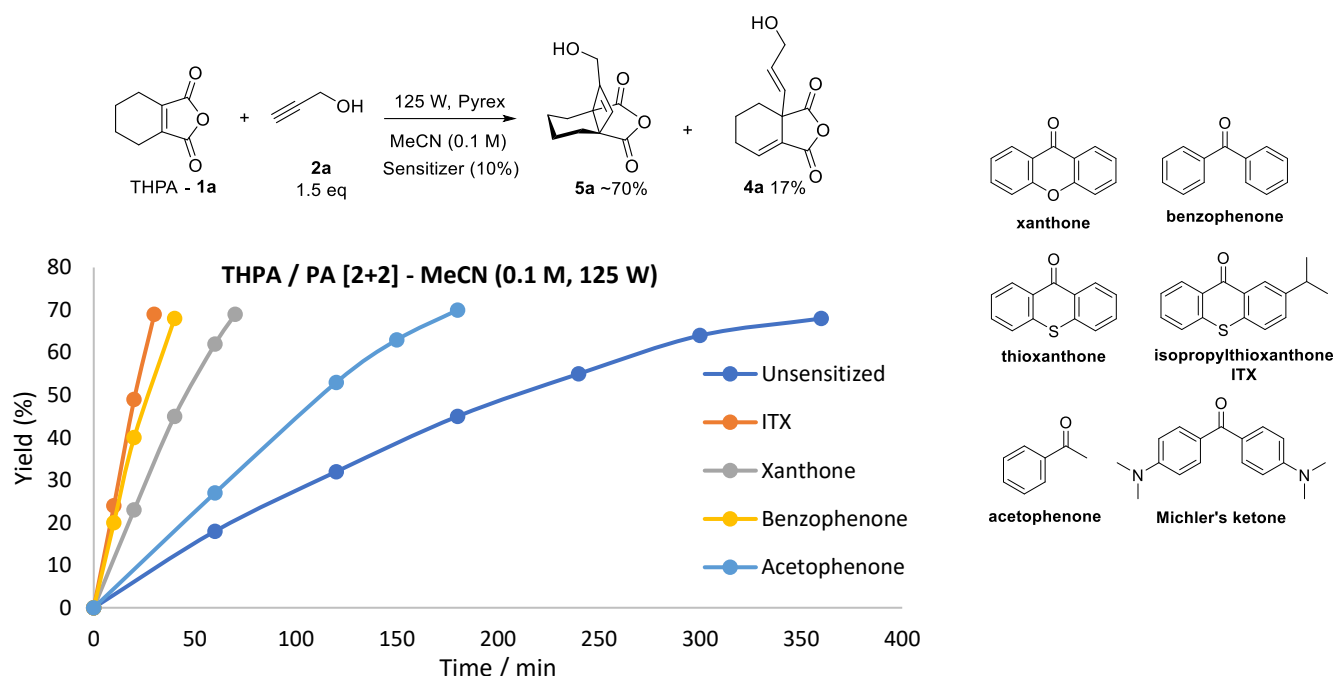


**Figure S1:** Reaction profiles for irradiation of THPA and propargyl alcohol in MeCN (0.1 M) for sensitized (10%) and unsensitized reactions in a 150 ml Pyrex immersion well batch reactor with 125 W Hg lamp

**Table S1:** Initial productivities for [2+2] of THPA with propargyl alcohol for the sensitizer screen in MeCN (0.1 M, 10% sensitizer, 150 ml Pyrex reactor, 125 W Hg lamp)

Sensitizer	$E_T$ (kJ/mol)	Initial productivity (mmol/h)
None	n.a.	2.7
Acetophenone	310 (n)	4
Xanthone	310 (n)	10
Benzophenone	287 (n)	18
Thioxanthone	265 (n)	22
Michler's	255 (p)	No reaction

### 2.1.2. Solvent Screen with ITX in Batch

Having identified isopropylthioxanthone as the optimal sensitizer in acetonitrile, a solvent screen was carried out at the increased concentration of 0.5 M and ITX loading of 1% (Figure S2). EtOAc was identified as the optimal solvent for the reaction giving a superior productivity to the standard MeCN solvent. Its lower cost, toxicity and environmental impact are also attractive features which fit well within the aims of the current work.

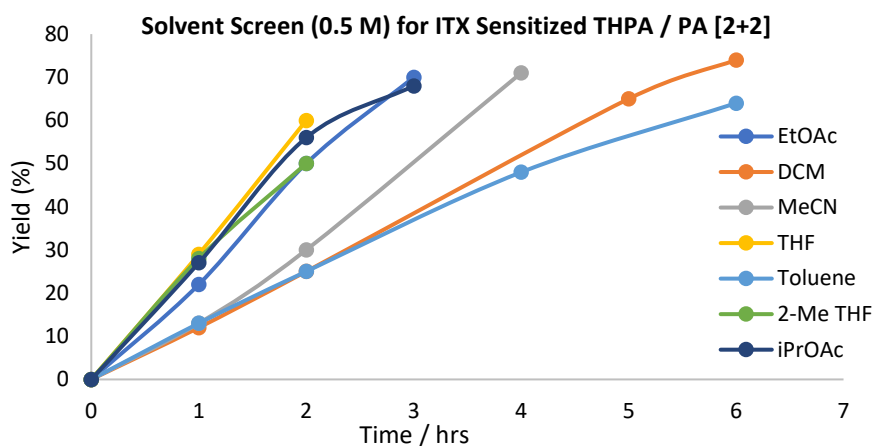


Figure S2: THPA / PA solvent screen (0.5 M, 150ml 1% ITX, 125 W Hg)

### 2.1.3. Screening Concentration and Lamp Power

The optimized solvent (EtOAc) and sensitizer (ITX) conditions were used to screen batch reactions with an increased lamp power of 400 W and concentration of 1.0 M (Figure S3). As expected, the use of a 400 W lamp tripled the productivity of the reaction in comparison to the 125 W results. The reaction tolerates the higher concentration of 1.0 M but a minor decrease in productivity was observed.

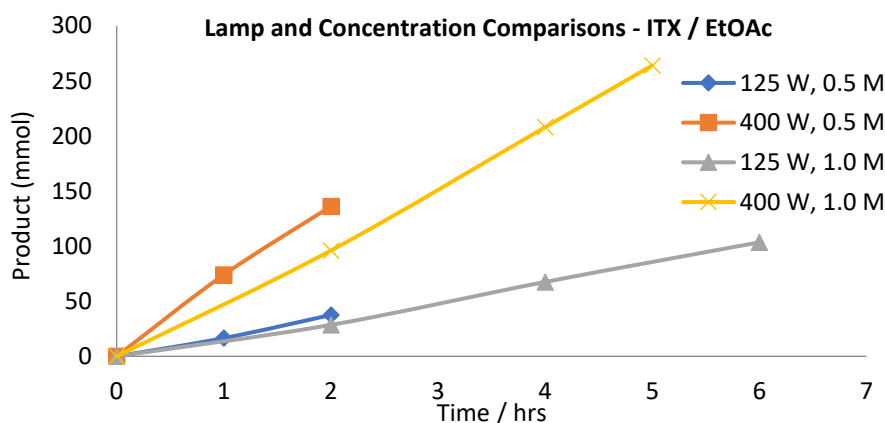
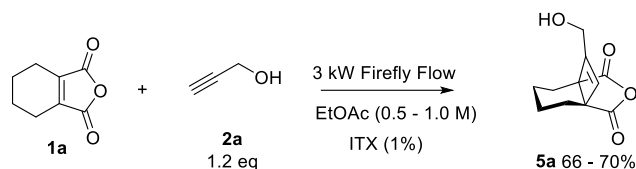


Figure S3: Lamp power comparisons for 125 W (150 ml) and 400 W (400 ml) in EtOAc (0.5 – 1.0 M)

## 2.1.4. Transfer to Large Scale Continuous Flow Reactor with a 3 kW Lamp – Predicting the Flow Rate From Batch Results

The flow reactor (Firefly) used here has been described before and was used without any deviation from the description in the reference.<sup>[1]</sup>



**Scheme S1:** THPA / PA [2+2] with Firefly parallel tube flow reactor

The Firefly at 3 kW was previously shown to give 10× productivity of a 400 W reactor. The solution in the 400 W, 400 ml batch reactor took 2 hrs to reach full conversion at 0.5 M giving an ‘effective flow rate’ of 3.3 ml/min. A likely optimal flow rate is therefore around 33 ml/min. In practice the reaction could be run at 36 ml/min at nearly full conversion.

The productivity for the 1.0 M reaction was slightly reduced and the 400ml solution took 5 hrs to reach full conversion. This gives an ‘effective flow rate’ of 1.3 ml/min and a predicted 3 kW firefly flow rate of 13 ml/min. The experimental results were in agreement with this as demonstrated by a 0.5 mole trial run.

0.5 M, 36 ml/min, 64% = **691 mmol/hr**

0.5 M, 25 ml/min, 65% = **488 mmol/hr**

1.0 M, 16 ml/min, 64% = **616 mmol/hr**

500 mmol (500 ml run) – 76 g THPA

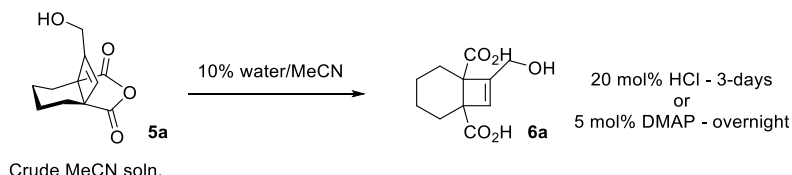
1.0 M, 13 ml/min, 66% = **515 mmol/hr**



For the following large (1 mole +) scale demonstrations, the operational conditions of 0.5 M and 30 ml/min were chosen to give the greatest levels of confidence the reaction would remain at full conversion for the duration of the reaction.

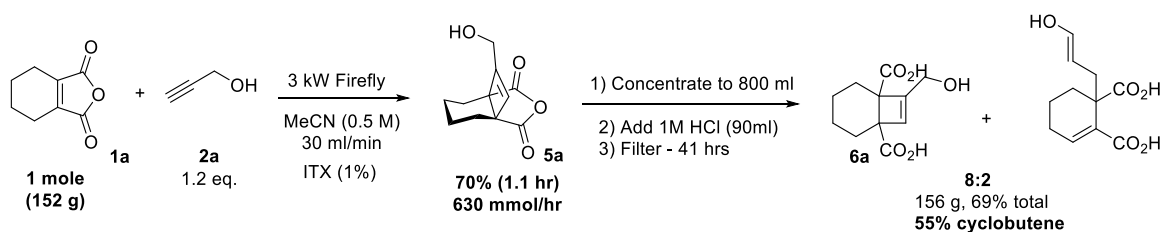
## 2.2. Homogenous Lactone Hydrolysis Investigation in Batch

The addition of 1 M HCl aq. (10% vol) to a crude MeCN (0.5 M) reaction mixture led to the slow hydrolysis over a period of 3 days (Scheme S2). The hydrolysis rate did not appear to be significantly increased by simply heating the reaction. The diacid product precipitated out and could be filtered off in reasonable yield. The addition of DMAP to 10% water in MeCN resulted in a faster hydrolysis but the product did not precipitate out, even after acidifying with HCl.



Scheme S2: Hydrolysis of [2+2] product anhydride

The photochemistry / MeCN hydrolysis sequence was performed on a 1 mole scale with the Firefly at 3 kW (0.5 M, 30 ml/min) to provide diacid for ring opening studies in batch and with the high temperature water flow reactor (Scheme S3).



Scheme S3: Photochemical [2+2] / hydrolysis sequence on 1 mole scale

Prior to hydrolysis, the reaction mixture was concentrated from 2 L to 800 ml before the addition of 1M HCl. The product was isolated, along with the hydrolysed by-product of the photochemical step, by filtration (Figure S4).

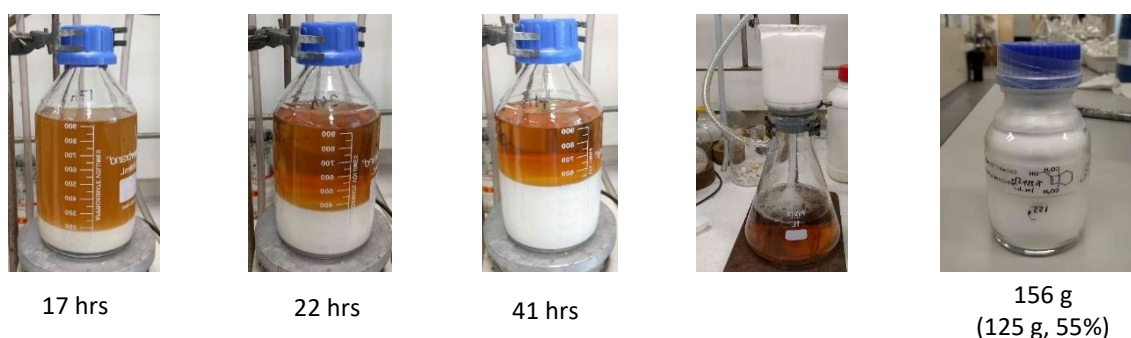
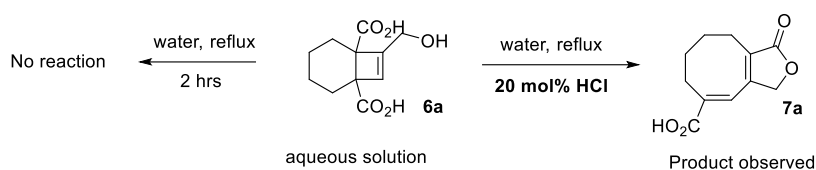


Figure S4: Slow, room temperature hydrolysis of 1 mole scale crude, concentrated photosylate (MeCN)

### 2.3. Biphasic Lactone Hydrolysis / Aqueous Ring Opening Sequence

As an alternative approach to hydrolysis, the crude EtOAc solution was stirred as an emulsion with water. Unlike the MeCN / water hydrolysis, the reaction rate could be increased with heating such that it was at full conversion within 1 hr at 60°C. Since the hydrolysed diacid product was formed as an aqueous solution, this method relies on the electrocyclic ring opening to be carried out in water. Before further optimization, the thermal ring-opening step was investigated.

No significant reaction was observed on heating an aqueous solution at reflux for 2 hours. The addition of catalytic HCl to the aqueous solution successfully accelerated the reaction at reflux and pleasingly, the product precipitated out in high purity after the solution was cooled (Scheme S4).



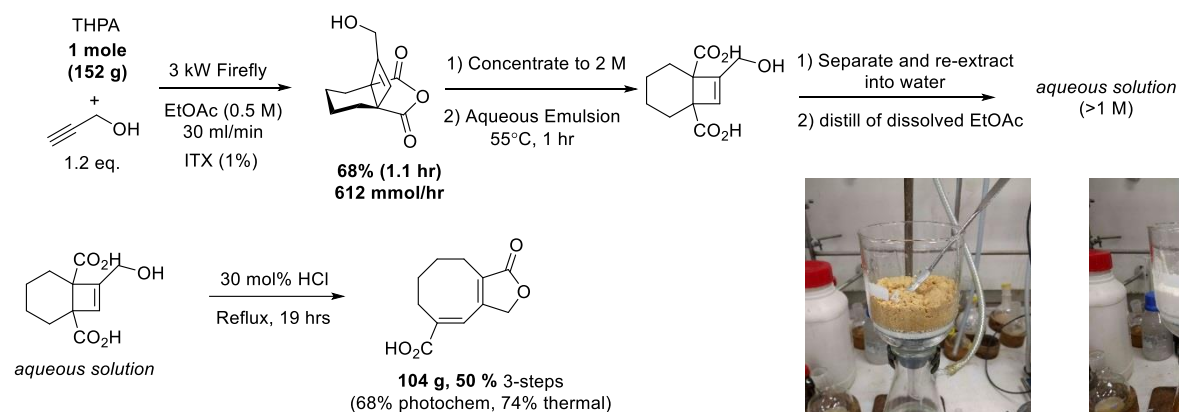
**Scheme S4:** Novel acid catalyzed ring opening of cyclobutene diacid in aqueous solution

In further trial reactions it was found that any significant residual EtOAc dissolved in the aqueous was hydrolyzed to AcOH and EtOH and had the effect of inhibiting the reaction and making purification more difficult. The best results were obtained when excess EtOAc was distilled from the aqueous solution using a rotary evaporator.

## 2.4. Initial Linking of Flow Photochemical and Batch Thermal Reactions

### 2.4.1. 1 Mole Scale Photo/Thermal Reaction Sequence

The optimized reaction sequence was run through on a mole scale to demonstrate the potential for further scale-up (Scheme S5). The photochemistry proceeded at full conversion to give about 70% of the cyclobutene. The addition of hexane (200 ml) to the concentrated photosylate (700 ml) assisted with the separation and allowed the hydrolysed diacid product to be extracted into the aqueous solution more efficiently.

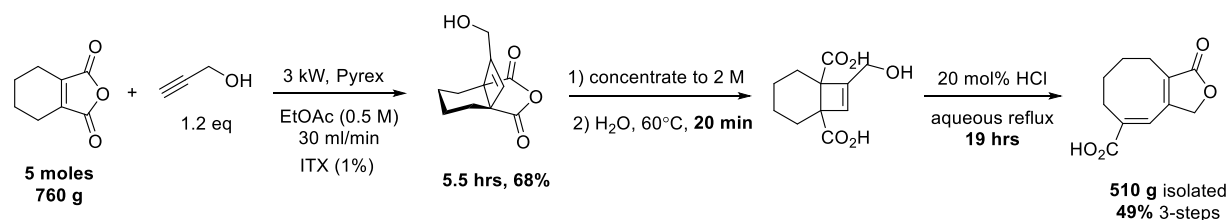


**Scheme S5:** Trial 1 mole scale flow [2+2] photochemistry / hydrolysis / aqueous electrocyclic ring opening

After heating at reflux in acidified aqueous solution, a clumpy suspension of product formed which was filtered to give a soft yellow solid. This was filtered with diethyl ether to give pure product as a free-flowing colourless powder 104 g, 50% - (68% photochem, 74% thermal)

### 2.4.2. 5 Mole Scale Photo/Thermal Reaction Sequence

With increased confidence in the optimized conditions, the reaction sequence was repeated on a 5 mole scale to investigate the robustness of the procedure (Scheme S6).



**Scheme S6:** 5 mole scale flow [2+2] photochemistry / hydrolysis / aqueous electrocyclic ring opening

The photochemical reaction solution was prepared (10 L, 0.5 M, EtOAc) in two 5 L bottles. Each bottle contained THPA (380 g, 2.5 mol) and propargyl alcohol (175 ml, 3 mol) and made up to 5 L volume in EtOAc. The solvent was used as purchased with minimal degassing prior to use by stirring under reduced pressure during THPA addition. Full conversion to product was observed for the duration of the THPA reaction, which took just over 5.5 hours at 30 ml/min (Figure S5, left) with the Firefly parallel

tube flow reactor with Pyrex filter and Hg lamp at 3 kW. This indicates there was no fouling of the reaction tubing due to deposition of degradation by-products.

The photosylate was concentrated to 2.5 L and hydrolyzed by forming an emulsion with water (1.4 L) and hexane (700 ml) at 60°C for 20 mins with an overhead stirrer in a 5 L Radleys Reactor-Ready double jacketed vessel (Figure S5, right). Separation and re-extraction with water (1 L) gave an aqueous solution of the diacid from which dissolved EtOAc was removed by distillation under reduced pressure to give a volume of approximately 3 L.

The aqueous solution was further diluted with water (500 ml) and heated under reflux conditions with the 5 L Radleys Reactor-Ready with 1 mole (83 ml, 12 M) of HCl. Conversion to the ring-opened product was measured by  $^1\text{H-NMR}$  to be 92% after 18 hours. The mixture was cooled after 19 hours before filtering the precipitated product and washing with water, MeOH and Et<sub>2</sub>O to give the product as a powder (510 g, 49% overall, see Figure S6).



**Figure S5:** *left* – 5 mole scale irradiation of THPA with Firefly flow reactor; *right* – 5 mole scale hydrolysis as an emulsion



**Figure S6:** *left* – final filtration of 5 mole scale reaction; *right* – product batches accumulated during studies



## **3. High Temperature Water (HTW) Reactor Set-ups**

### **3.1. Reactor Description and Details**

#### **3.1.1. Large Scale Thermal Flow Reactor**

Large scale continuous flow reactions were carried out using a custom-built flow system constructed primarily from stainless steel Swagelok tubing and fittings, a schematic of which can be seen in Figure **S7**, below. The system in brief is made up of two HPLC pumps, a heated coil reactor with an internal volume of 43.7 ml, a pipe-in-pipe cooling jacket and a manual back pressure regulator (BPR). The heated reactor consists of a 6 m coil of 1/4" OD Swagelok tubing formed around an aluminium heating block, which contains a cartridge heater and is surrounded by an additional band heater. An optional third pump, which can act as a quench to rapidly cool and dilute the reactor outflow is also present. The system temperature is controlled by a Eurotherm heater controller, attached to the reactor and monitored by four K-type thermocouples, two within the heating block and two in flow, downstream of the reactor and the upstream of the BPR. Reagents are introduced to the system via up to three Gilson 305 HPLC pumps, fitted with 5, 10 or 25 SC pump heads depending on the desired flow rate. The system pressure is set by a TESCO manual BPR (26-1700 series) and monitored by three RDP electronics pressure transducers located in flow, just downstream of each pump. A trip system connected to the equipment which isolates power to the pumps and heaters in case of an over-pressure or over-temperature, being recorded in the system and a Swagelok sprung relief valves provides additional overpressure protection.

Care must be taken when designing or working with high pressure continuous flow systems and solvents above their boiling points due to the high temperature, pressure and the potential for high temperature vapours to be released potential causing severe burns. The temperature and pressure ratings of rig components must not be exceeded. The flammability and reactivity of solvents used should also be considered particularly at elevated temperature and pressure, the autoignition temperature must not be exceeded and reactions carried out below these conditions with a safe margin.

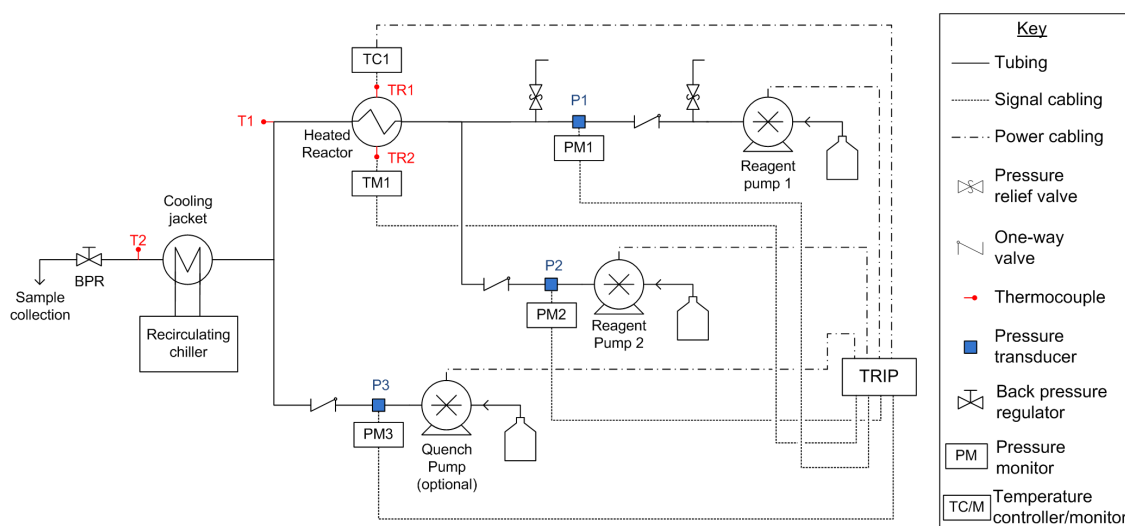


**Figure S7.** Rig diagram for the large-scale continuous flow thermal reactor, showing the positions of and connections between major rig components. Stainless steel tubing is indicated by a solid line, dotted lines show the overtemperature and overpressure inputs to the trip system and dashed lines indicate equipment controlled by the trip system, power to which is disconnected should the trip activate.

### 3.1.2. Small Scale Thermal Flow Reactor

To allow a broader range of substrates to be investigated, a smaller scale thermal reactor and set-up were constructed (Figure S8). This design of this system was similar to that described above, but scaled down to suit a 3 m long coiled reactor constructed from 1/16" OD Swagelok tubing, with an internal volume of 0.77 ml. This gave a total rig volume of less than 2 ml, including reagent feed lines, of which around 1.2 ml is pressurised. Jasco PU-980 HPLC pumps and BP-2080 Back pressure regulator were used in the small scale set-up to suit the lower flow rates required, while needle valves fitted upstream of the pumps allow them to be primed without depressurising the entire system.

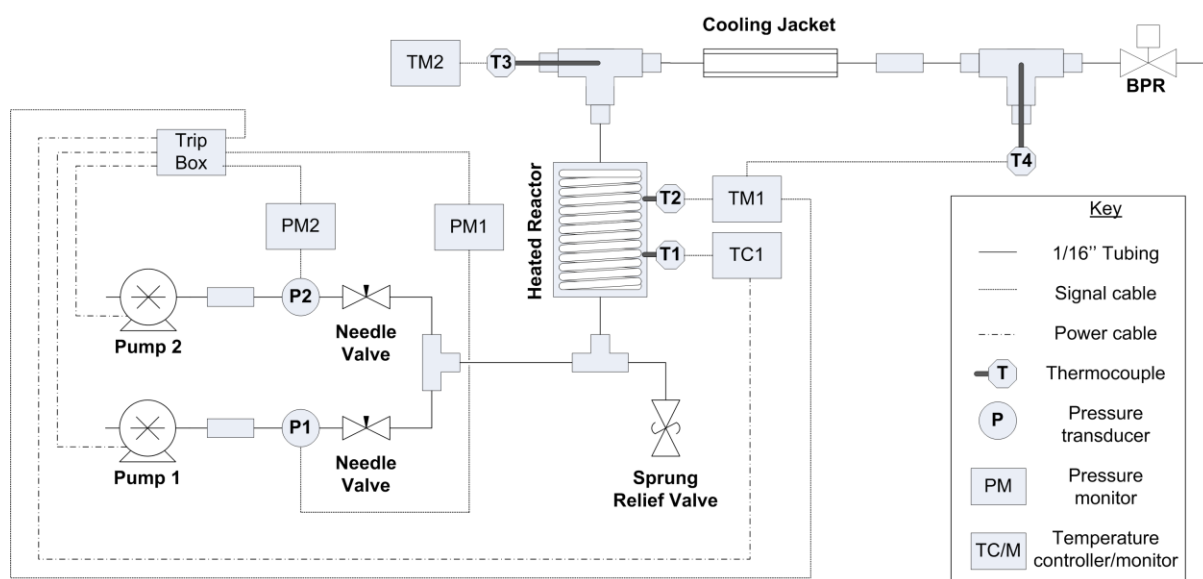


**Figure S8.** Rig diagram for the small scale continuous flow thermal reactor, showing the positions of and connections between major rig components. Stainless steel tubing is indicated by a solid line, dotted lines show the overtemperature and overpressure inputs to the trip system and dashed lines indicate equipment controlled by the trip system, power to which is disconnected should the trip activate.

### 3.1.3. Standard Operating Procedure for Thermal Flow Reactors

A typical continuous flow thermal reaction procedure follows. The standard operating procedures of each size of reactor are the same, with the exceptions of the equilibration periods, priming techniques and method of setting back pressure. For the larger reactor, the minimum equilibration period was taken as the time for three reactor volumes worth of solution to be pumped into the reactor, however this was increased to two total rig volumes for the smaller reactor (>5 reactor volumes), to allow for the increased proportion of non-reactor volume within the system.

#### Start-up

1. Switch on power to system and reset trip. Pressure monitors, temperature monitors, back pressure regulator (BPR) and cooling bath should turn on immediately, pumps and heater should turn on once the trip is reset.
2. Check temperature and pressure trips are set to the correct value.
3. Prime pump(s) using desired reaction solvent. Ensure there is no air in the pump feed lines and the pumps are working efficiently.
4. Once solvent is flowing out of the rig, set the system pressure using the BPR.
5. Check for leaks. If any leaks are found, the system pressure should be reduced to ambient and the fitting re-seated and tightened/replaced as necessary.
6. Turn on cooling bath if used.
7. Turn on heater controller (TC1), set heater temperature, typically 250 °C, and allow reactor temperature to stabilise.

#### Reaction

8. Switch pump feeds to reagents and set pump flow rates as desired.
9. Wait time for equilibrium.
10. Collect sample(s).
11. If multiple samples are to be collected at different conditions, make the necessary changes and repeat equilibrium and sampling process until all samples are collected.

#### Shutdown

12. Substitute solvent for the reagent feeds.
13. Flush reactor at temperature until outflow of system is colourless.
14. Set heaters to zero.
15. Allow system to cool until system is below the boiling point of the solvent in use.
16. Slowly release pressure at BPR, then stop pumps.
17. Turn off system.

To account for minor fluctuations in rig conditions, all samples were collected in triplicate. Once collected, a known volume of each sample was dried under reduced pressure, before biphenyl was added as an external standard and the samples submitted for <sup>1</sup>H NMR in deuterated DMSO.

### 3.1.4. Batch Thermal Reactions

Initial thermal screening reactions were carried out in a series of stainless steel autoclaves with an internal volume of 10 ml, the design of which has been published previously.<sup>[2]</sup>

This reaction set-up allows small scale reactions to be carried out at above the boiling point of the solvents, as the sealed reactors are pressurised autogenously, while attached temperature and pressure monitoring allow the reaction conditions to be monitored throughout. The reaction set-up in brief composes of two wells, one heated and the other water cooled, and the autoclaves can be moved between the wells without interrupting the pressure or temperature monitoring.

The desired reactants and solvent are loaded into a stainless steel autoclave, and the autoclave is sealed, before being placed into either well as required. Short reaction times are possible, as the combination of pre-heating the thermal well and efficient heat transfer to the relatively small reaction vessels allow the reactants to reach the desired temperatures (typically 200-300 °C) in around 7 minutes. The reactants are then held at the desired temperature for 10 minutes (timer started once the reaction temperature is within 5 °C of target), before the autoclave is transferred to the water cooled well, and the temperature rapidly decreased. Full cooling of the reactors takes around 10 minutes, although the internal temperature typically decreases by half within the first 2 minutes.

## 3.2. Photochemical Flow Reactor linked with HTW Reactor

### 3.2.1. Photochemical Set-up

FEP coil reactors,<sup>[3]</sup> similar to those previously described, were used to carry out the photochemical step of these reactions in flow. These reactors consist of one or more layers of thin walled FEP tubing coiled around a central light source. For the initial photochemical flow reactions, FEP tubing (2.7 mm ID 3.1 mm OD, supplied by Adtech) was coiled in a single layer around a borosilicate cylinder into which a quartz immersion wells sized to fit 400 W medium pressure mercury arc lamps, was placed (all glassware and lamps supplied by Photochemical Reactors LTD.). This reactor had an irradiated volume of 75 ml. A Masterflex peristaltic pump with PTFE pump head was then used to flow the photochemical reagents in acetonitrile through the reactor.

To ensure safe containment of the UV lamps, each reactor was wrapped in aluminium foil to minimise stray light, and opaque shields were placed in front of the reactors. Due to the possibility of ozone generation, photochemical reactors were only run inside appropriately extracted boxes. Lamp cooling was provided by a recirculating cooling bath, filled with water and operated at 15 °C. A low-flow cut-off device, supplied by Photochemical Reactors LTD, was used to ensure sufficient cooling flow was maintained throughout. Thin K type thermocouples inserted between the immersion well and the inner layer of FEP tubing allowed reaction temperatures to be estimated.

To ensure that any samples collected were representative of equilibrium conditions, the UV lamps were allowed to reach temperature (with cooling flowing) for 30 minutes before the photochemical reactions were started. Likewise, a minimum of two reactor volumes worth of reagents were pumped before samples were taken. All samples were collected in triplicate and a known volume of each

sample was dried under a flow of nitrogen, before biphenyl was added as an external standard and the samples submitted for  $^1\text{H}$  NMR in deuterated acetonitrile.

To allow scale-up of the daisychain process, three double layer reactors, coiled around quartz immersion wells sized to fit 400 W medium pressure mercury arc lamps, with an inner borosilicate filter placed between the lamp and the immersion well in each case reactors were used. These reactors had an average irradiated volume of 132 ml, and were connected in parallel, with a separate pump feeding each reactor. The combined outflows of which provided the inlet stream of the thermal reactor.

### **3.2.2. Linking of the Photochemical Flow reactor with the HTW Reactor**

To allow the photochemical and thermal steps of this reaction to be combined into a single continuous flow operation, a daisy-chained system was developed, see main text Figure 2. Up to three FEP coil reactors, operating in parallel, were fitted upstream of the thermal system described above, with the outflow of each photoreactor combined to provide the reagent feed for the thermal reactor.

### **3.2.3. Batch Photochemical Reactions**

Batch photochemical reactions were carried out in a commercially available 100 ml borosilicate immersion well reactor, surrounding a 125 W medium pressure mercury arc lamp.

## 4. Optimisation of Thermal Reaction in High Temperature Water

### 4.1. Batch Ring Expansion/Lactonization of 6a in High Temperature Water/Acetonitrile Mixtures

Batch synthesis of **7a** ((*E*)-1-oxo-1,3,6,7,8,9-hexahydrocycloocta[*c*]furan-5-carboxylic acid) from **6a** (7-(hydroxymethyl)bicyclo[4.2.0]oct-7-ene-1,6-dicarboxylic acid) in high temperature water and high temperature water containing solvent mixtures.

#### Standard Procedure

Diacid **6a** (57 mg, 0.25 mmol) and solvent (water or water/acetonitrile mixture, 5 ml) was added to stainless steel autoclave. The autoclave was then sealed, heated and held at the reaction temperature for 10 minutes, before being rapidly water cooled. Once fully cooled the contents of the reactor were transferred to a measuring cylinder to check for any loss of solvent, which may indicate a reactor leak, before sampling. For reactions in water where precipitation of the product occurred, samples were either filtered to obtain the pure product or made up to a known volume with acetone before a subsample was dried under reduced pressure and biphenyl added as an external standard to allow semi-quantitative <sup>1</sup>H NMR analysis (Table **S2**).

**Table S2:** The effect of reaction temperature on batch electrocyclic ring opening reactions in HTW

Solvent	Reaction temperature (°C)	Yield of ring opened product (%)	Conversion of diacid (%)
Water	100	0	0
Water	120	0	0
Water	140	5	5
Water	160	22	22
Water	180	60	65
Water	200	99	Full
Water	220	81	Full
Water plus trace ethyl acetate	200	87	Full
50:50 Water:Acetonitrile	200	94	Full

Using pure water as the solvent, full conversion and near quantitative yields were achieved for the 10 minute reaction at 200 °C, the reaction did not reach completion within the 10 minute reaction time below this temperature and some decomposition of the product was observed at 220 °C. Even trace quantities of ethyl acetate within the solvent mixture, lead to an appreciable drop in yield, and increase in reaction pressure. Near equivalent yields to pure water were observed at 200 °C when using a 50:50 v/v mixture of acetonitrile and water, and the reaction products remained in solution even after cooling.

## 4.2. Continuous Flow Ring Expansion/Lactonization of 6a in High Temperature Water/Acetonitrile Mixtures

Continuous flow synthesis of **7a** ((E)-1-oxo-1,3,6,7,8,9-hexahydrocycloocta[c]furan-5-carboxylic acid) from **6a** (7-(hydroxymethyl)bicyclo[4.2.0]oct-7-ene-1,6-dicarboxylic acid) in high temperature water and high temperature water containing solvent mixtures. These reactions were carried out in the larger of the thermal reactors, and followed the standard operating procedure described above (Table S3).

**Table S3:** Screening continuous flow conditions for electrocyclic ring opening of **6a** to **7a** in HTW

Temperature (°C)	Flow rate (ml/min)	Solvent ratio (H <sub>2</sub> O:ACN)	Yield <sup>1</sup> H NMR (isolated) (%)	Conversion (%)
200	3.8	100:0	68	93
200	5.1	100:0	66	84
200	7.6	100:0	55	68
200	15.2	100:0	33	38
210	7.5	50:50	81	88
220	7.4	50:50	95	95
200	8	25:75	44 (42)	52
220	8	25:75	85 (79)	89
220	16	25:75	75	73
220	18	25:75	61	58
240	16	25:75	83	87
260	16	25:75	92	92

For the reactions carried out in water, the reactor temperature was set to 200 °C and pressure to 100 bar, a 0.05 M starting solution of diacid in water was introduced to the reactor, at the flow rates shown and an additional water feed at the same flow rate was introduced via the quench pump downstream of the reactor, to dilute the outflow and minimise the accumulation of solid within the reactor due to precipitation of **7a** although a large volume of solid was subsequently removed from the reactor post reaction, indicating product accumulation had occurred and potentially explaining the lower than predicted yields.

For reactions in acetonitrile water mixtures, the system pressure was 100 bar, reagent concentrations of 0.06 M of diacid made up in the appropriate solvent mixture were used at the flow rate shown, and no quench pump was required, as reagents and products remained in solution. Isolated yields were obtained for two sets of conditions, via removal of the acetonitrile under reduced pressure and filtration, showing good agreement with yield obtained by NMR, and excellent purity.

### 4.3. Continuous-Flow Combined Hydrolysis and Ring Opening

Combined hydrolysis and ring opening of **5a** (8-(hydroxymethyl)-4,5,6,7-tetrahydro-1H,3H-3a,7a-ethenoisobenzofuran-1,3-dione) to **7a** ((*E*)-1-oxo-1,3,6,7,8,9-hexahydrocycloocta[*c*]furan-5-carboxylic acid).

Combined hydrolysis and ring opening reaction in batch indicated full conversion of the photoproduct **5a** (0.05M in 5 ml solvent) and at least 95% yield of **7a** were obtained in a 10 minute reaction at 200 °C for solvent mixtures containing a minimum of 25% water. Below this percentage diacid **6a** was recovered in addition to **7a**.

Similar yields were obtained when using crude photoproduct (approx. 0.06 M of **5a** in acetonitrile) diluted with the appropriate volume of water. In this case additional peaks believed to correspond to the hydrolysis products of non-bridged photoproduct **4a** and any remaining propargyl alcohol were also observed via NMR.

For reactions carried out in continuous flow, crude photochemical solutions were used (containing approx. 0.06M of **5a** in acetonitrile) and the optimal solvent ratio was found to be 50:50 acetonitrile to water, which was found to increase the rate of hydrolysis. A higher pressure of 150 bar was used to minimise expansion of the higher volatility solvent mixture. Two pumps were used to generate the required solvent mixture in situ, with matched flow rate of water introduced by pump 1 and photoproduct in CH<sub>3</sub>CN introduced via pump 2.

**Table S4:** Screening continuous flow conditions for combined hydrolysis / electrocyclic ring opening of **5a** to **7a** in HTW

Starting material	Temperature (°C)	Flow rate (ml/min)	Water (%)	Acetonitrile (%)	Yield of ring opened product (%)	Yield of diacid (%)	Conversion (%)
<b>5a</b>	200	Batch	100	0	95	0	Full
<b>5a</b>	200	Batch	50	50	95	0	Full
<b>5a</b>	200	Batch	25	75	95	0	99
<b>5a</b>	200	Batch	10	90	35	40	78
<b>5a</b>	200	Batch	5	95	23	40	64
<b>5a</b>	200	Batch	0	100	7	0	28
Crude	200	Batch	50	50	94	0	Full
Crude	260	34	50	50	95	1	Full



## 5. Batch Photochemistry of Additional Substrates

Batch photochemical reactions were carried out in a 100 ml borosilicate immersion well photoreactor, fitted with a water cooled 125 W Hg arc lamp, all obtained from Photochemical Reactors LTD. Prior to irradiation, solutions were degassed by passing a flow of nitrogen through the solution for 15 minutes.

### 8-(2-hydroxyethyl)-4,5,6,7-tetrahydro-1*H*,3*H*-3a,7a-ethenoisobenzofuran-1,3-dione (**5b**)

A solution of 3,4,5,6 tetrahydrophthalic acid anhydride (1.52 g, 10 mmol) and 3-butyn-1-ol (0.76 ml, 10 mmol) in acetonitrile (100 ml) was irradiated for 3 hours. Half of the solution (50 ml) was retained without further purification for reactions using the crude photochemical product. The solvent was removed from the remaining 50 ml of photochemical reaction mixture under reduced pressure and flash chromatography of the residue (0-50% EtOAc/Heptane) afforded the title compound as a pale yellow oil (0.82 g, 74%); (*R<sub>f</sub>* 0.28, 50% EtOAc:/Heptane). Further elution gave 2-(3'-hydroxy-1'-butenyl)-2,3,4,5-tetrahydrothalic anhydride (**4b**) as a pale yellow oil (0.14 g, 12%); (*R<sub>f</sub>* 0.18, 50% EtOAc:/Heptane).

### 7-(hydroxymethyl)-5,6-dihydro-1*H*,3*H*,4*H*-3a,6a-ethenocyclopenta[*c*]furan-1,3-dione (**5c**)

A solution of 1-cyclopentene-1,2dicarboxylic anhydride (0.95 g, 6.9 mmol) and propargyl alcohol (0.42 ml, 6.9 mmol) in acetonitrile (100 ml) was irradiated for 3 hours. This yielded a solution containing the title compound in 79% yield via <sup>1</sup>H NMR against a biphenyl external standard which was used for thermal reactions without further purification.

### 8-(hydroxymethyl)-9-methyl-4,5,6,7-tetrahydro-1*H*,3*H*-3a,7a-ethenoisobenzofuran-1,3-dione (**5d**)

A solution of 3,4,5,6 tetrahydrophthalic acid anhydride (1.52 g, 10 mmol) and 2-butyn-1-ol (0.75 ml, 10 mmol) in acetonitrile (100 ml) was irradiated for 4 hours. This yielded a solution containing the title compound in 73% yield via <sup>1</sup>H NMR against a biphenyl external standard which was used for thermal reactions without further purification.

## 6. Optimisation of Small Scale Thermal Reactor for the Ring expansion of **5b** and **5c**.

Continuous flow synthesis of (E)-1-oxo-3,4,7,8,9,10-hexahydro-1H-cycloocta[c]pyran-6-carboxylic acid (**7b**) from purified and crude photoproduct (**5b**)

These reactions were carried out in the smaller of the thermal reactors, and followed the standard operating procedure described above. Reactions carried out at 150 bar using either purified **5b** (70 mM in acetonitrile) or crude photochemical solutions (containing approx. 70 mM of **5b** in acetonitrile). Similar results were obtained in either case. Two pumps were used to generate the required solvent mixture in situ, with matched flow rate of water introduced by pump 1 and photoproduct in acetonitrile introduced via pump 2. Flow rates quoted are the total flow rate, calculate as a sum of all water and acetonitrile flow rates. Yields were obtained via <sup>1</sup>H NMR against a biphenyl external standard and calculated based on an average of two samples, normalised against a measured starting material sample, and were corrected for dilution, pump efficiency and sample evaporation during collection. > 95% conversion of the starting anhydride was observed in each case.

**Table S5:** Screening continuous flow conditions for formation of **7b** from **5b**

Substrate	Temperature (°C)	Flow rate (ml/min)	ACN:H <sub>2</sub> O ratio	Diacid yield (%)	Ring opened yield (%)
Purified	200	0.4	1:1	51	25
Purified	225	0.4	1:1	17	57
Purified	250	0.2	1:1	0	62
Purified	250	0.4	1:1	0	61
Crude	200	0.2	1:1	28	28
Crude	200	0.4	1:1	66	26
Crude	200	0.8	1:1	84	15
Crude	225	0.2	1:1	5	59
Crude	225	0.4	1:1	22	54
Crude	225	0.8	1:1	55	43
Crude	250	0.4	1:1	3	61
Crude	250	0.6	1:1	7	60
Crude	250	0.8	1:1	11	50
Crude	260	0.4	1:1	0	49
Crude	260	0.8	1:1	8	57
Crude	260	1.2	1:1	18	48
Crude	250	0.4	3:5	0	57
Crude	250	0.4	5:3	14	50

Continuous flow synthesis of 1-oxo-3,6,7,8-tetrahydro-1H-cyclohepta[c]furan-5-carboxylic acid (**7c**) from crude photoproduct (**5c**)

These reactions were carried out in the smaller of the thermal reactors, and followed the standard operating procedure described above. Reactions carried out at 150 bar using crude photochemical solutions, which were diluted with acetonitrile to improve solubility giving 33mM concentrations of **5c**. Two pumps were used to generate the required 1:1 solvent mixture in situ, with matched flow rate of water introduced by pump 1 and photoproduct in acetonitrile introduced via pump 2. Flow rates quoted are the total flow rate, calculate as a sum of all water and acetonitrile flow rates Yields were

obtained via  $^1\text{H}$  NMR against a biphenyl external standard and calculated based on an average of two samples, normalised against a measured starting material sample, and were corrected for dilution, pump efficiency and sample evaporation during collection. Greater than 95% conversion of the starting anhydride was observed in each case. \* indicates evidence of acetonitrile hydrolysis during reaction or conditions likely to result in sure hydrolysis.

**Table S6:** Screening continuous flow conditions for formation of **7c** from **5c**

Temperature (°C)	Flow rate (ml/min)	Diacid yield (%)	Ring opened yield (%)
200	0.4	95	0
225	0.4	Quant.	0
250	0.4	48	28
260	0.4	36	45
260	0.2	14	53
250	0.2	26	39
250	0.1	9	41
235	0.1	38	41
235	0.04	3	9
280*	0.4	4	50
280*	0.8	20	48
300*	0.8	2	72
300*	1.2	9	78
320*	1.2	0	62
320*	1.6	1	66

Continuous flow thermal reaction of 8-(hydroxymethyl)-9-methyl-4,5,6,7-tetrahydro-1H,3H-3a,7a-ethenoisobenzofuran-1,3-dione (**5d**)

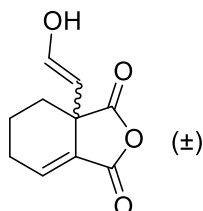
These reactions were carried out in the smaller of the thermal reactors, and followed the standard operating procedure described above. Reactions carried out at 150 bar using crude photochemical solutions (containing approx. 64 mM of **5d** in acetonitrile). Two pumps were used to generate the required 1:1 solvent mixture in situ, with matched flow rate of water introduced by pump 1 and photoproduct in acetonitrile introduced via pump 2. Flow rates quoted are the total flow rate, calculate as a sum of all water and acetonitrile flow rates Yields were obtained via  $^1\text{H}$  NMR against a biphenyl external standard and calculated based on an average of two samples, normalised against a measured starting material sample, and were corrected for dilution, pump efficiency and sample evaporation during collection. \* indicates evidence of acetonitrile hydrolysis during reaction or conditions likely to result in such hydrolysis.

**Table S7:** Screening continuous flow conditions for thermolysis of **5d**

Reaction temperature (°C)	Total flow rate (ml/min)	Diacid yield <b>6d</b> (%)	Yield <b>8</b> (%)	Yield <b>9</b> (%)
250	0.8	68	4	0
275*	0.4	20	10	25
275*	0.8	45	5	15
300*	0.4	9	12	34
300*	0.8	35	11	31
300*	1.2	45	9	21

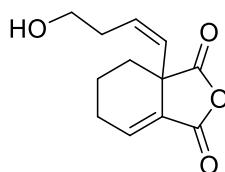
## 7. Characterization Data

Compounds **4a-b**, **5a-d**, **6a** and **7a** were prepared in agreement with data reported in the literature.



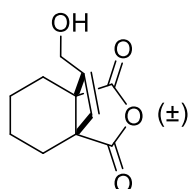
**(4a)** (*E*)-3a-(3-hydroxyprop-1-en-1-yl)-3a,4,5,6-tetrahydroisobenzofuran-1,3-dione<sup>[4]</sup>

<sup>1</sup>H NMR (400 MHz, CDCl<sub>3</sub>, 25 °C, TMS):  $\delta$ =7.13 (t, *J*=3.7 Hz, 1H, CH), 5.75 (d, *J*=15.6 Hz, 1H, CH), 5.70 (dt, *J*=15.6, 3.5 Hz, 1H, CH), 4.18 (d, *J*=3.5 Hz, 2H, CH<sub>2</sub>), 3.75 (br, 1H, OH), 2.50-2.22 (m, 2H, CH<sub>2</sub>), 2.19-2.13 (m, 1H, CH<sub>2A</sub>), 1.89-1.54 (m, 3H, CH<sub>2</sub> + CH<sub>2B</sub>); <sup>13</sup>C NMR (100 MHz, CDCl<sub>3</sub>, 25 °C, TMS):  $\delta$ =172.0 (CO), 163.4 (CO), 142.1 (CH), 135.6 (CH), 128.5 (C), 128.3 (CH), 62.4 (CH<sub>2</sub>), 50.2 (C), 27.4 (CH<sub>2</sub>), 25.3 (CH<sub>2</sub>), 16.5 (CH<sub>2</sub>).



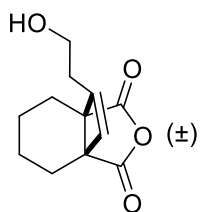
**(4b)** 2-(3'-hydroxy-1'-butenyl)-2,3,4,5-tetrahydrothalic anhydride<sup>[4]</sup>

<sup>1</sup>H NMR (400 MHz, CDCl<sub>3</sub>, 25 °C, TMS):  $\delta$ =7.07 (t, *J*=3.6 Hz, 1H, CH), 5.53-5.49 (m, 2H, 2x CH), 4.85 (b, 1H, OH), 3.58 (td, *J*=6.5, 1.2 Hz, 2H, CH<sub>2</sub>), 2.44-2.18 (m, 4H, 2x CH<sub>2</sub>), 2.10-2.04 (m, 1H, CH<sub>2A</sub>), 1.82-1.56 (m, 2H, CH<sub>2</sub>), 1.55-1.46 (m, 1H, CH<sub>2B</sub>); <sup>13</sup>C NMR (100 MHz, CDCl<sub>3</sub>, 25 °C, TMS):  $\delta$ =172.2 (CO), 163.5 (CO), 142.3 (CH), 133.4 (CH), 129.8 (CH), 128.1 (C), 61.4 (C), 50.3 (C), 35.3 (CH<sub>2</sub>), 27.2 (CH<sub>2</sub>), 25.2 (CH<sub>2</sub>), 16.2 (CH<sub>2</sub>).



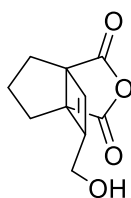
**(5a)** 8-(hydroxymethyl)-4,5,6,7-tetrahydro-1*H*,3*H*-3a,7a-ethenoisobenzofuran-1,3-dione<sup>[5]</sup>

<sup>1</sup>H NMR (400 MHz, CDCl<sub>3</sub>, 25 °C, TMS):  $\delta$ =6.28 (t, *J*=1.8 Hz, 1H, CH), 4.20 (d, *J*=1.8 Hz, 2H, CH<sub>2</sub>), 3.32 (b, 1H, OH), 2.10-1.94 (m, 4H, 2x CH<sub>2</sub>), 1.68-1.56 (m, 2H, CH<sub>2</sub>), 1.54-1.41 (m, 2H, CH<sub>2</sub>); <sup>13</sup>C NMR (100 MHz, CD<sub>3</sub>CN, 25 °C, TMS):  $\delta$ =173.8 (CO), 172.8 (CO), 155.9 (C), 134.4 (CH), 58.2 (CH<sub>2</sub>), 54.5 (C), 51.8 (C), 25.3 (CH<sub>2</sub>), 24.5 (CH<sub>2</sub>), 19.7 (CH<sub>2</sub>), 19.6 (CH<sub>2</sub>).



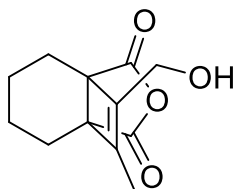
**(5b)** 8-(2-hydroxyethyl)-4,5,6,7-tetrahydro-1*H*,3*H*-3*a*,7*a*-ethenoisobenzofuran-1,3-dione<sup>[5]</sup>

<sup>1</sup>H NMR (400 MHz, CDCl<sub>3</sub>, 25 °C, TMS): δ=6.17 (t, *J*=1.7 Hz, 1H, CH), 3.74 (td, *J*=6.3, 1.7 Hz, 2H, CH<sub>2</sub>), 2.46 (b, 1H, OH), 2.45-2.29 (m, 2H, CH<sub>2</sub>), 2.08-1.89 (m, 4H, 2xCH<sub>2</sub>), 1.67-1.54 (m, 2H, CH<sub>2</sub>), 1.53-1.39 (m, 2H, CH<sub>2</sub>); <sup>13</sup>C NMR (100 MHz, CDCl<sub>3</sub>, 25 °C, TMS): δ=172.65 (CO), 172.63 (CO), 153.8 (CH), 135.0 (C), 59.0 (CH<sub>2</sub>), 54.7 (C), 51.1 (C), 31.4 (CH<sub>2</sub>), 25.2 (CH<sub>2</sub>), 24.1 (CH<sub>2</sub>), 19.5 (CH<sub>2</sub>), 19.3 (CH<sub>2</sub>); HRMS (ESI) *m/z* [M+H]<sup>+</sup> calcd for C<sub>12</sub>H<sub>15</sub>O<sub>4</sub>: 223.0965, found: 223.0955.



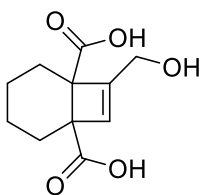
**(5c)** 7-(hydroxymethyl)-5,6-dihydro-1*H*,3*H*,4*H*-3*a*,6*a*-ethenocyclopenta[*c*]furan-1,3-dione<sup>[4]</sup>

<sup>1</sup>H NMR (400 MHz, (CD<sub>3</sub>)<sub>2</sub>SO, 25 °C, TMS): δ=6.26 (t, *J*=1.9 Hz, 1H, CH), 5.13 (b, 1H, OH), 4.05 (dd, *J*=16.2, 1.9 Hz, 1H, CH<sub>2A</sub>), 3.96 (dd, *J*=16.2, 1.6 Hz, 1H, CH<sub>2B</sub>), 2.10-1.82 (m, 5H, 2x CH<sub>2</sub> + CH<sub>2A</sub>), 1.74-1.68 (m, 1H, CH<sub>2B</sub>).



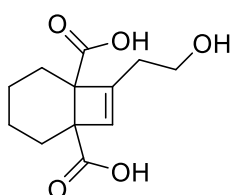
**(5d)** 8-(hydroxymethyl)-9-methyl-4,5,6,7-tetrahydro-1*H*,3*H*-3*a*,7*a*-etheno-isobenzofuran-1,3-dione<sup>[5]</sup>

<sup>1</sup>H NMR (400 MHz, CDCl<sub>3</sub>, 25 °C, TMS): δ=4.24 (q, *J*=1.3 Hz, 2H, CH<sub>2</sub>), 2.44 (b, 1H, OH), 2.09-2.01 (m, 2H, CH<sub>2</sub>), 1.98-1.91 (m, 2H, CH<sub>2</sub>), 1.82 (t, *J*=1.3 Hz, 3H, CH<sub>3</sub>), 1.67-1.45 (m, 4H, 2x CH<sub>2</sub>); <sup>13</sup>C NMR (100 MHz, CDCl<sub>3</sub>, 25 °C, TMS): δ=172.9 (CO), 172.1 (CO), 145.4 (C), 144.2 (C), 57.0 (CH<sub>2</sub>), 53.1 (C), 52.1 (C), 24.5 (CH<sub>2</sub>), 23.7 (CH<sub>2</sub>), 19.74 (CH<sub>2</sub>), 19.71 (CH<sub>2</sub>), 11.3 (CH<sub>3</sub>); HRMS (ESI) *m/z* [M+Na]<sup>+</sup> calcd for C<sub>12</sub>H<sub>14</sub>NaO<sub>4</sub>: 245.0784, found: 245.0783.



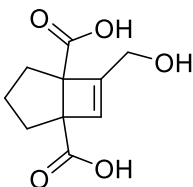
**(6a)** 7-(hydroxymethyl)bicyclo[4.2.0]oct-7-ene-1,6-dicarboxylic acid<sup>[6]</sup>

<sup>1</sup>H NMR (400 MHz, (CD<sub>3</sub>)<sub>2</sub>CO, 25°C, TMS): δ=10.56 (b, 2H, OH), 6.11 (app. t, *J*=1.8 Hz, 1H, CH), 4.24 (dd, *J*=15.3, 1.8 Hz, 1H, CH<sub>2A</sub>), 4.16 (dd, *J*=15.3, 1.6 Hz, 1H, CH<sub>2B</sub>), 3.00 (b, 1H, OH), 2.20-2.09 (m, 2H, CH<sub>2</sub>), 1.92-1.85 (m, 1H, CH<sub>2A</sub>), 1.80-1.72 (m, 1H, CH<sub>2B</sub>), 1.65-1.54 (m, 4H, 2x CH<sub>2</sub>); <sup>13</sup>C NMR (75 MHz, (CD<sub>3</sub>)<sub>2</sub>SO, 25 °C, TMS): δ=175.0 (CO), 174.5 (CO), 151.6 (C), 129.8 (CH), 57.7 (CH<sub>2</sub>), 56.2 (C), 54.0 (C), 26.2 (CH<sub>2</sub>), 25.8 (CH<sub>2</sub>), 15.74 (CH<sub>2</sub>), 15.67 (CH<sub>2</sub>).



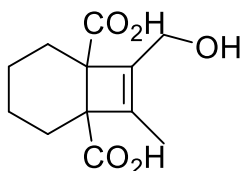
**(6b)** 7-(2-hydroxyethyl)bicyclo[4.2.0]oct-7-ene-1,6-dicarboxylic acid – Observed but not isolated

<sup>1</sup>H NMR (400 MHz, (CD<sub>3</sub>)<sub>2</sub>SO, 25°C, TMS): δ=12.1 (b, 2H, 2x OH), 5.93 (t, *J*=1.7 Hz, 1H, CH), 4.54 (b, 1H, OH), 3.56 (t, *J*=7.2 Hz, 2H, CH<sub>2</sub>), 2.27-2.11 (m, 2H, CH<sub>2</sub>), 2.03-1.89 (m, 2H, CH<sub>2</sub>), 1.74-1.59 (m, 2H, CH<sub>2</sub>), 1.57-1.36 (m, 4H, 2x CH<sub>2</sub>).



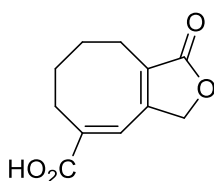
**(6c)** 6-(hydroxymethyl)bicyclo[3.2.0]hept-6-ene-1,5-dicarboxylic acid – Observed but not isolated

<sup>1</sup>H NMR (400 MHz, (CD<sub>3</sub>)<sub>2</sub>SO, 25°C, TMS): δ=12.19 (b, 2H, 2x OH), 5.81 (t, *J*=1.9 Hz, 1H, CH), 4.82 (b, 1H, OH), 3.96 (dd, *J*=15.7, 24.5 Hz, 1H, CH<sub>2</sub>), 1.82-1.64 (m, 4H, 2x (CH<sub>2</sub>), 1.61-1.53 (m, 2H, CH<sub>2</sub>).



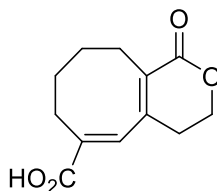
**(6d)** 7-(hydroxymethyl)-8-methylbicyclo[4.2.0]oct-7-ene-1,6-dicarboxylic acid

$^1\text{H}$  NMR (400 MHz,  $(\text{CD}_3)_2\text{SO}$ , 25°C, TMS):  $\delta$ =4.09-3.91 (m, 2H,  $\text{CH}_2$ ), 1.99-1.83 (m, 2H,  $\text{CH}_2$ ), 1.74-1.59 (m, 5H,  $\text{CH}_3 + \text{CH}_2$ ), 1.55-1.42 (m, 3H,  $\text{CH}_2 + \text{CH}_{2\text{A}}$ ), 1.40-1.29 (m, 1H,  $\text{CH}_{2\text{B}}$ );  $^{13}\text{C}$  NMR (100 MHz,  $(\text{CD}_3)_2\text{SO}$ , 25 °C, TMS):  $\delta$ =175.4 (CO), 175.1 (CO), 142.2 (C), 139.8 (C), 56.4 ( $\text{CH}_2$ ), 55.7 (C), 55.2 (C), 25.3 ( $\text{CH}_2$ ), 24.5 ( $\text{CH}_2$ ), 15.84 ( $\text{CH}_2$ ), 15.83 ( $\text{CH}_2$ ), 11.5 ( $\text{CH}_3$ ); HRMS (ESI)  $m/z$   $[\text{M}+\text{Na}]^+$  calcd for  $\text{C}_{12}\text{H}_{16}\text{NaO}_5$ : 263.0890, found: 263.0893; IR (ATR):  $\nu/\text{cm}^{-1}$  1708 (s, C=O), 1689 (s, C=O), 1637 (m, C=C).



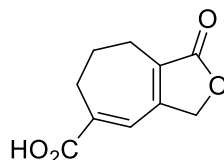
**(7a)** (*E*)-1-oxo-1,3,6,7,8,9-hexahydrocycloocta[*c*]furan-5-carboxylic acid<sup>[4]</sup>

$^1\text{H}$  NMR (400 MHz,  $(\text{CD}_3)_2\text{CO}$ , 25°C, TMS):  $\delta$ =11.09 (b, 1H, OH), 7.27 (s, 1H, CH), 4.79 (td,  $J$ =2.6, 0.9 Hz, 2H,  $\text{CH}_2$ ), 2.67-2.62 (m, 2H,  $\text{CH}_2$ ), 2.45-2.40 (m, 2H,  $\text{CH}_2$ ), 1.87-1.79 (m, 2H,  $\text{CH}_2$ ), 1.73-1.65 (m, 2H,  $\text{CH}_2$ );  $^{13}\text{C}$  NMR (100 MHz,  $(\text{CD}_3)_2\text{SO}$ , 25 °C, TMS):  $\delta$ =174.1 (CO), 152.1 (CO), 152.1 (C), 137.6 (C), 129.0 (CH), 128.6 (C), 71.0 ( $\text{CH}_2$ ), 25.7 ( $\text{CH}_2$ ), 25.0 ( $\text{CH}_2$ ), 24.8 ( $\text{CH}_2$ ), 20.4 ( $\text{CH}_2$ ).



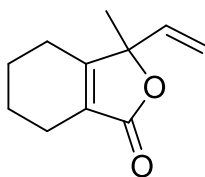
**(7b)** (*E*)-1-oxo-3,4,7,8,9,10-hexahydro-1*H*-cycloocta[*c*]pyran-6-carboxylic acid

$^1\text{H}$  NMR (400 MHz,  $\text{CD}_3\text{CN}$ , 25°C, TMS):  $\delta$ =7.14 (s, 1H, CH), 4.34 (t,  $J$ =6.2 Hz, 2H,  $\text{CH}_2$ ), 2.47 (t,  $J$ =6.2 Hz, 2H,  $\text{CH}_2$ ), 2.42-2.00 (br m, 4H, 2x  $\text{CH}_2$ ), 1.59-1.35 (br m, 4H, 2x  $\text{CH}_2$ );  $^{13}\text{C}$  NMR (100 MHz,  $\text{CD}_3\text{CN}$ , 25 °C, TMS):  $\delta$ =168.4 (CO), 166.3 (CO), 147.5 (C), 136.6 (C), 136.4 (CH), 128.8 (C), 66.9 ( $\text{CH}_2$ ), 28.4 ( $\text{CH}_2$ ), 28.1 ( $\text{CH}_2$ ), 27.7 ( $\text{CH}_2$ ), 24.3 ( $\text{CH}_2$ ), 23.4 ( $\text{CH}_2$ ); HRMS (ESI)  $m/z$   $[\text{M}+\text{H}]^+$  calcd for  $\text{C}_{12}\text{H}_{15}\text{O}_4$ : 223.0965, found: 223.0959.



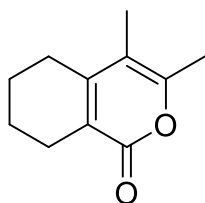
**(7c)** 1-oxo-3,6,7,8-tetrahydro-1*H*-cyclohepta[*c*]furan-5-carboxylic acid

$^1\text{H}$  NMR (400 MHz,  $\text{CD}_3\text{CN}$ ,  $25^\circ\text{C}$ , TMS):  $\delta=7.06$  (s, 1H, CH), 4.77 (t,  $J=2.9$  Hz, 2H,  $\text{CH}_2$ ), 2.78-2.73 (m, 2H,  $\text{CH}_2$ ), 2.56-2.50 (m, 2H,  $\text{CH}_2$ ), 1.91-1.85 (m, 2H,  $\text{CH}_2$ );  $^{13}\text{C}$  NMR (100 MHz,  $(\text{CD}_3)_2\text{SO}$ ,  $25^\circ\text{C}$ , TMS):  $\delta=173.9$  (CO), 168.0 (CO), 142.5 (C), 130.7 (C), 125.7 (CH), 71.1 ( $\text{CH}_2$ ), 29.2 ( $\text{CH}_2$ ), 26.8 ( $\text{CH}_2$ ), 21.5 ( $\text{CH}_2$ ); HRMS (ESI)  $m/z$   $[\text{M}+\text{H}]^+$  calcd for  $\text{C}_{10}\text{H}_{11}\text{O}_4$ : 195.0652, found: 195.0660.



**(8)** 3-methyl-3-vinyl-4,5,6,7-tetrahydroisobenzofuran-1(3*H*)-one

$^1\text{H}$  NMR (400 MHz,  $\text{CDCl}_3$ ,  $25^\circ\text{C}$ , TMS):  $\delta=5.75$  (dd,  $J=17.3$  Hz, 10.7 Hz, 1H; CH), 5.34 (d,  $J=17.3$ , 1H,  $\text{CH}_{2\text{A}}$ ), 5.21 (d,  $J=10.7$ , 1H,  $\text{CH}_{2\text{B}}$ ), 2.24-2.14 (m, 4H, 2x  $\text{CH}_2$ ), 1.77-1.65 (m, 4H, 2x  $\text{CH}_2$ ), 1.50 (s, 3H,  $\text{CH}_3$ );  $^{13}\text{C}$  NMR (100 MHz,  $\text{CDCl}_3$ ,  $25^\circ\text{C}$ , TMS):  $\delta=173.0$  (CO), 166.6 (C), 137.1 (CH), 125.4 (C), 116.2 ( $\text{CH}_2$ ), 87.3 (C), 22.2 ( $\text{CH}_3$ ), 22.1 ( $\text{CH}_2$ ), 21.8 ( $\text{CH}_2$ ), 21.7 ( $\text{CH}_2$ ), 20.0 ( $\text{CH}_2$ ); HRMS (ESI)  $m/z$   $[\text{M}+\text{H}]^+$  calcd for  $\text{C}_{11}\text{H}_{15}\text{O}_2$ : 179.1067, found: 179.1024; IR (ATR):  $\nu/\text{cm}^{-1}$  1748 (s, C=O), 1678 (m, C=C), 1641 (m, C=C).

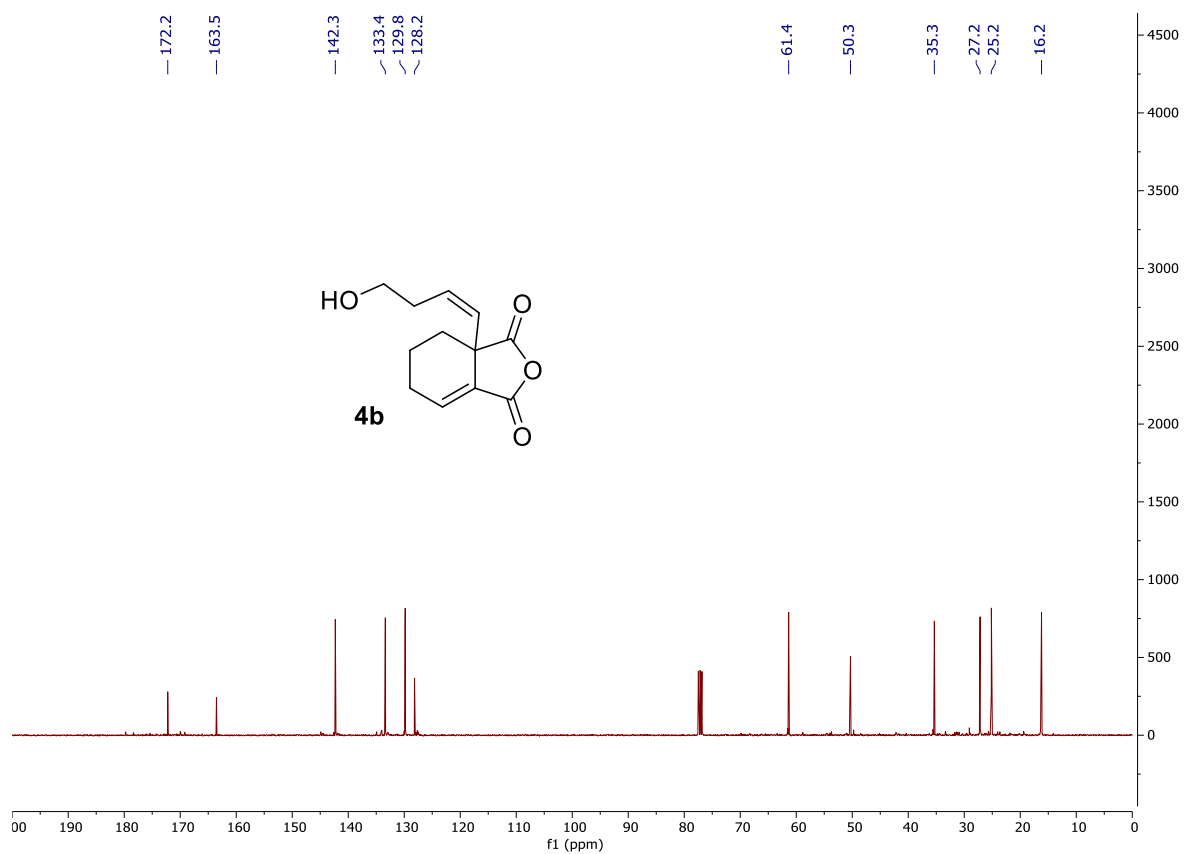
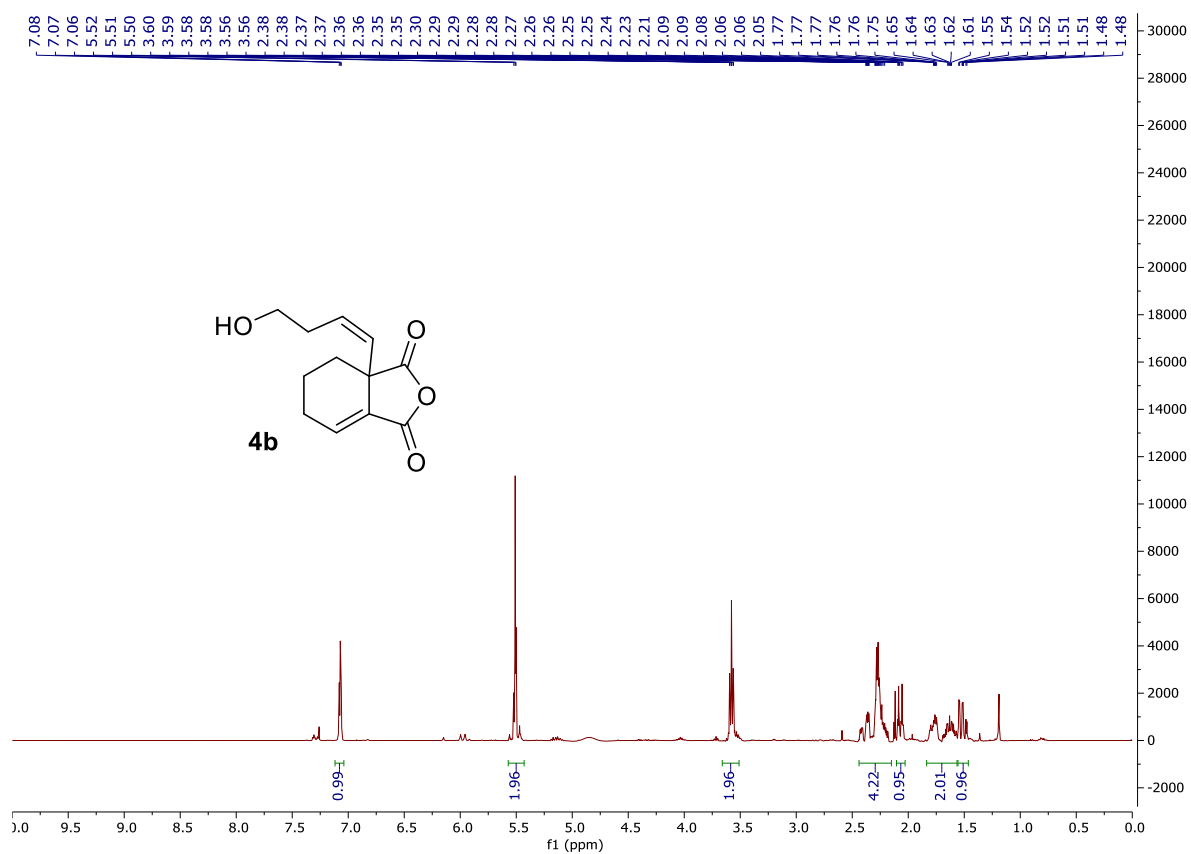


**(9)** 3,4-dimethyl-5,6,7,8-tetrahydro-1*H*-isochromen-1-one

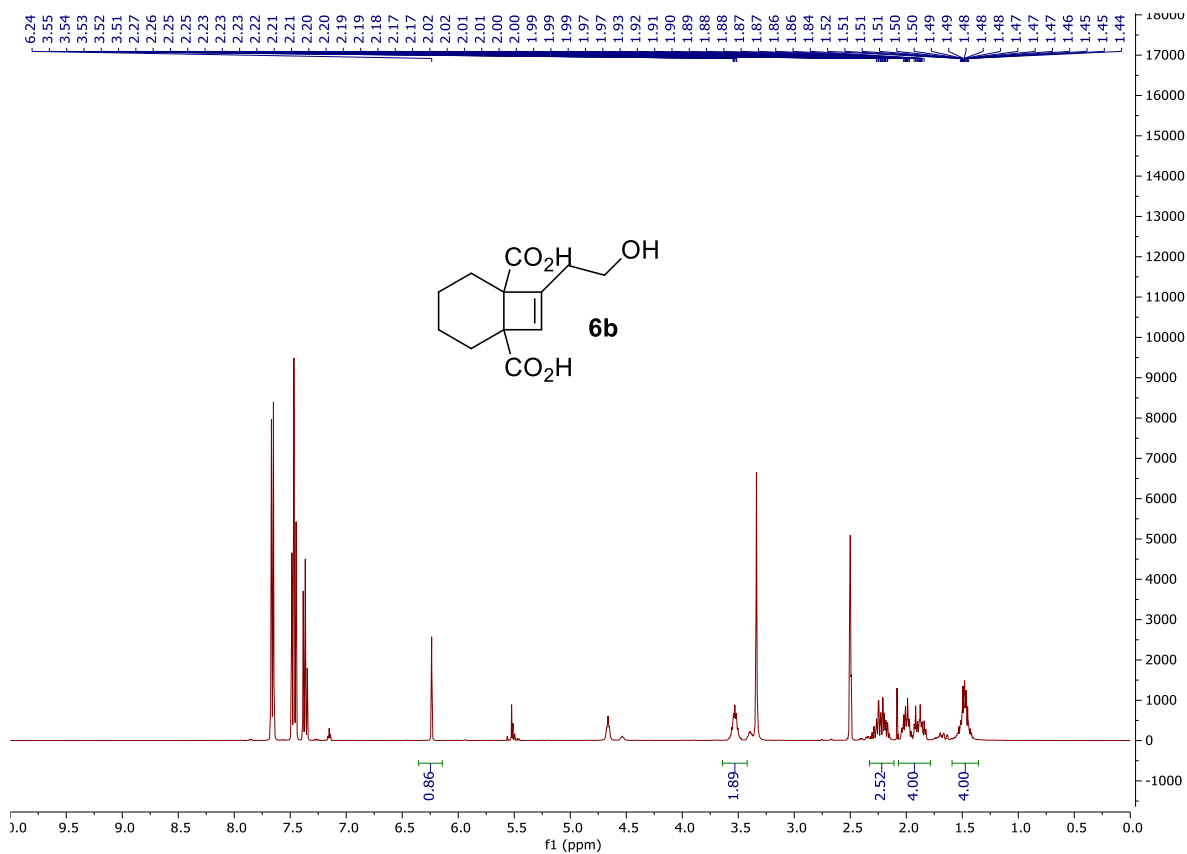
$^1\text{H}$  NMR (400 MHz,  $\text{CDCl}_3$ ,  $25^\circ\text{C}$ , TMS):  $\delta=2.47$ -2.35 (m, 4H, 2x  $\text{CH}_2$ ), 2.19 (s, 3H,  $\text{CH}_3$ ), 1.87 (s, 3H,  $\text{CH}_3$ ), 1.76-1.63 (m, 4H, 2x  $\text{CH}_2$ );  $^{13}\text{C}$  NMR (100 MHz,  $\text{CDCl}_3$ ,  $25^\circ\text{C}$ , TMS):  $\delta=163.8$  (CO), 153.1 (C), 152.3 (C), 120.2 (C), 111.3 (C), 27.2 ( $\text{CH}_2$ ), 23.6 ( $\text{CH}_2$ ), 21.9 ( $\text{CH}_2$ ), 21.5 ( $\text{CH}_2$ ), 17.4 ( $\text{CH}_3$ ), 12.1 ( $\text{CH}_3$ ); HRMS (ESI)  $m/z$   $[\text{M}+\text{Na}]^+$  calcd for  $\text{C}_{11}\text{H}_{14}\text{NaO}_2$ : 201.0886, found: 201.0894; IR (ATR):  $\nu/\text{cm}^{-1}$  1695 (s, C=O), 1643 (s, C=C), 1565 (s, C=C).



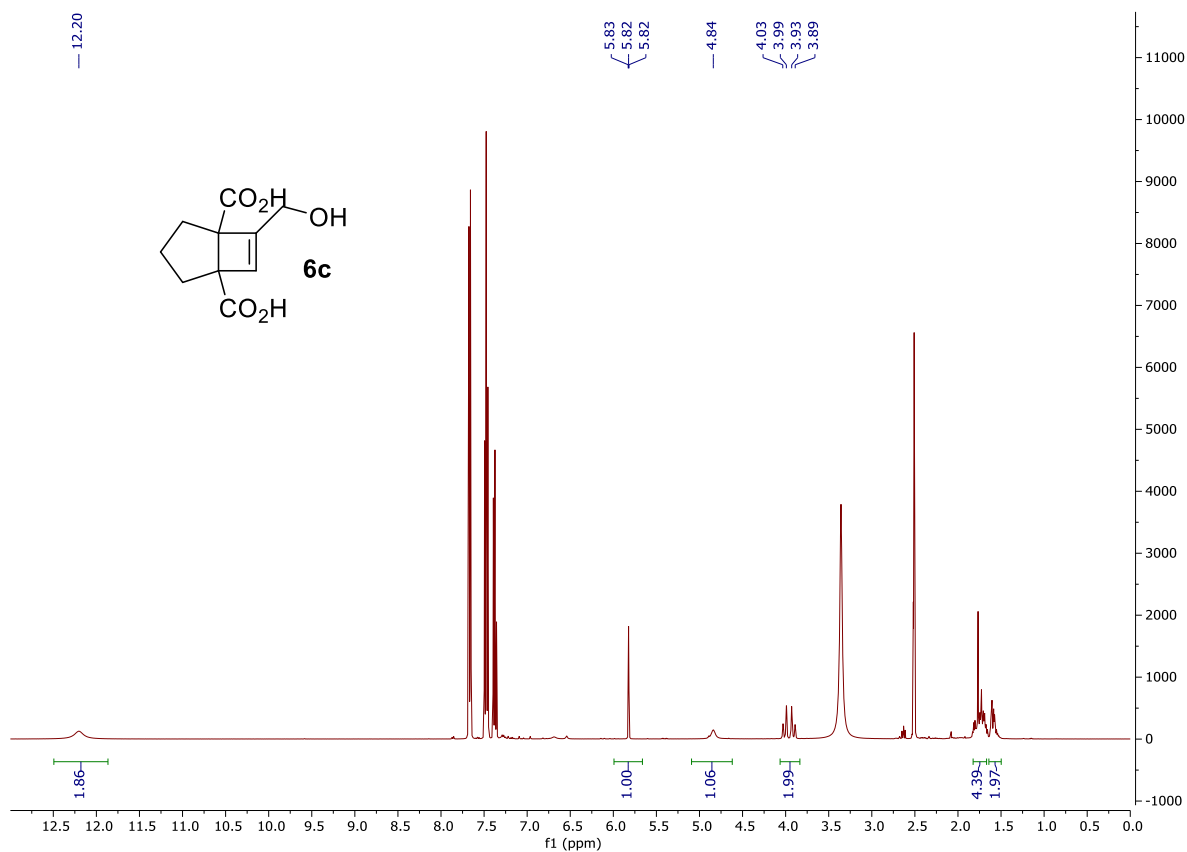
## 8. NMR Spectra

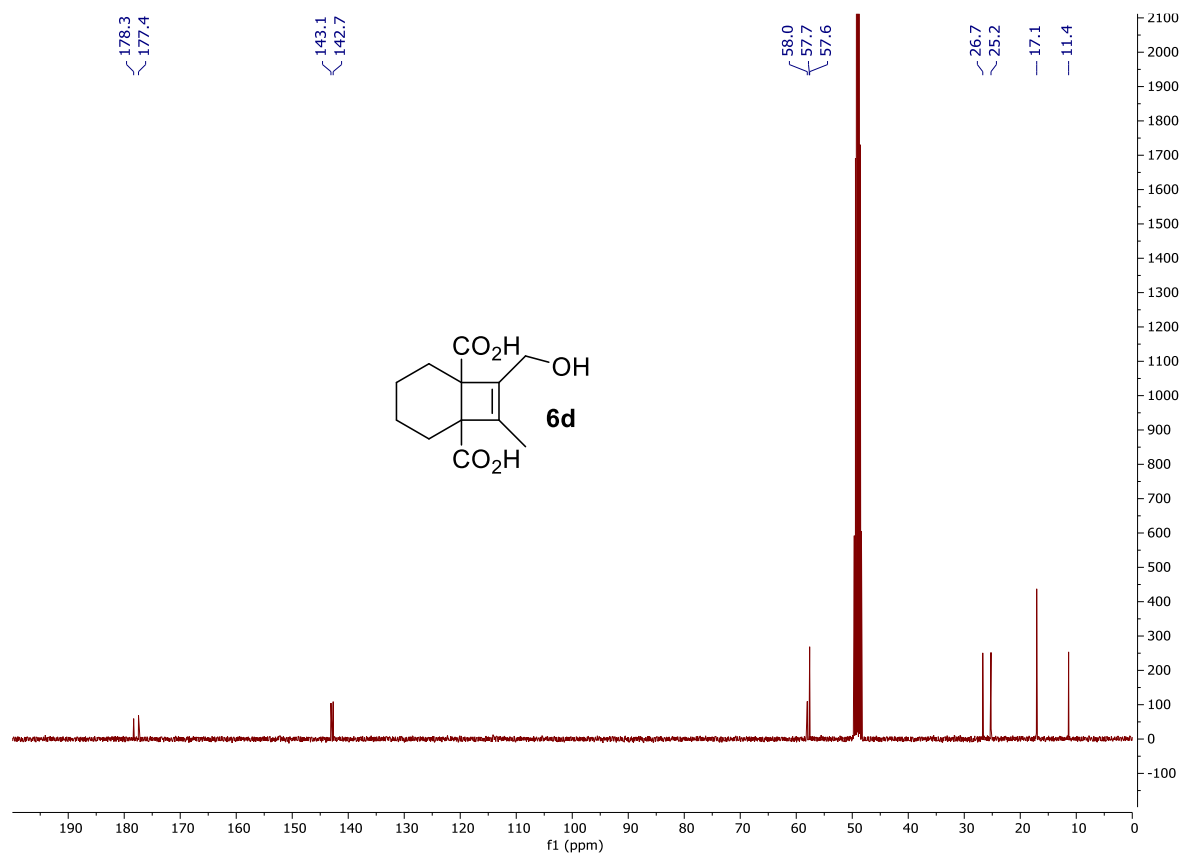
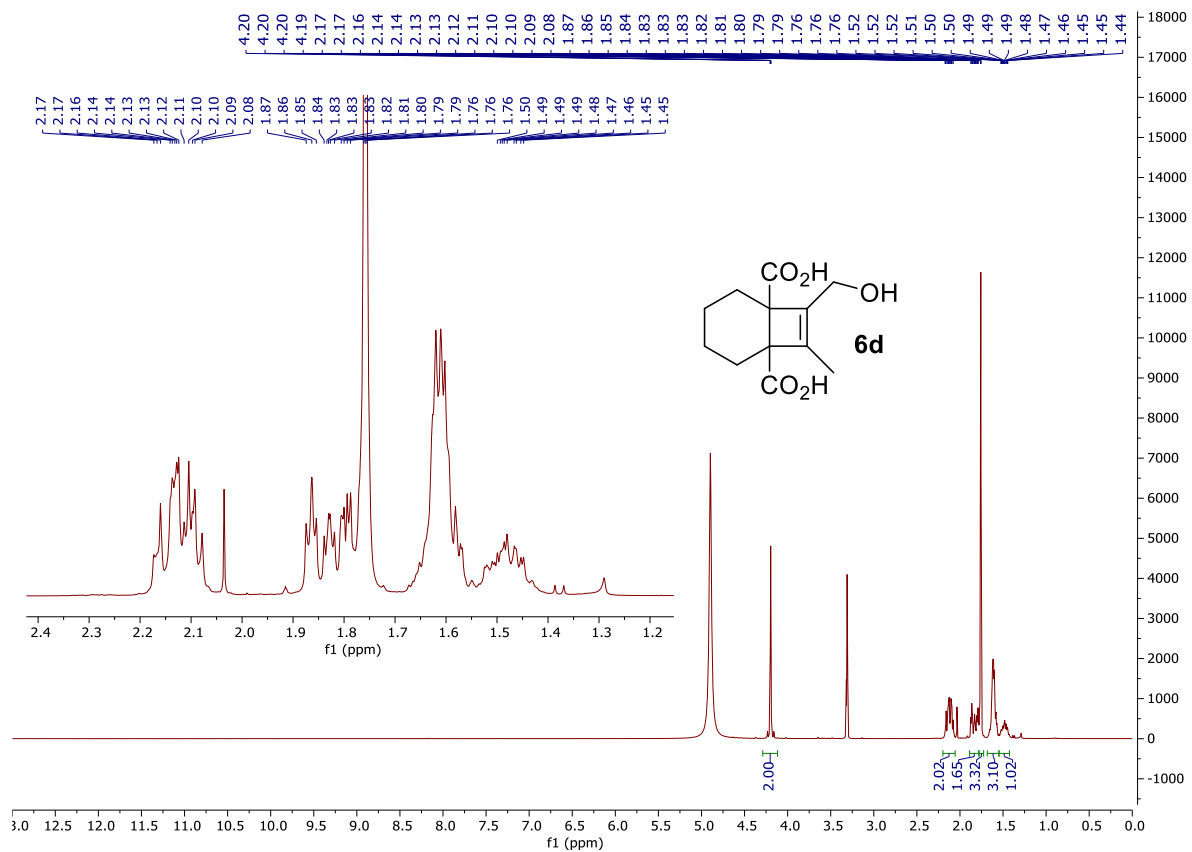


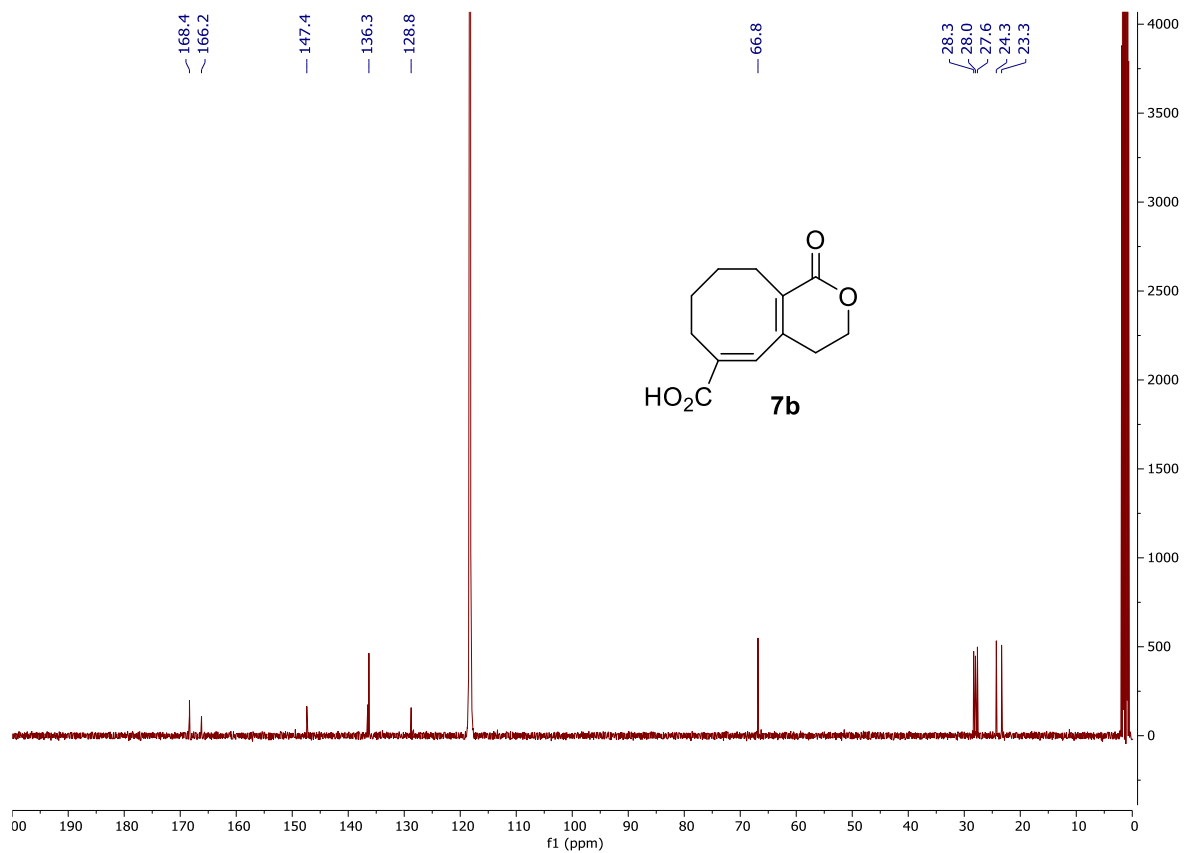
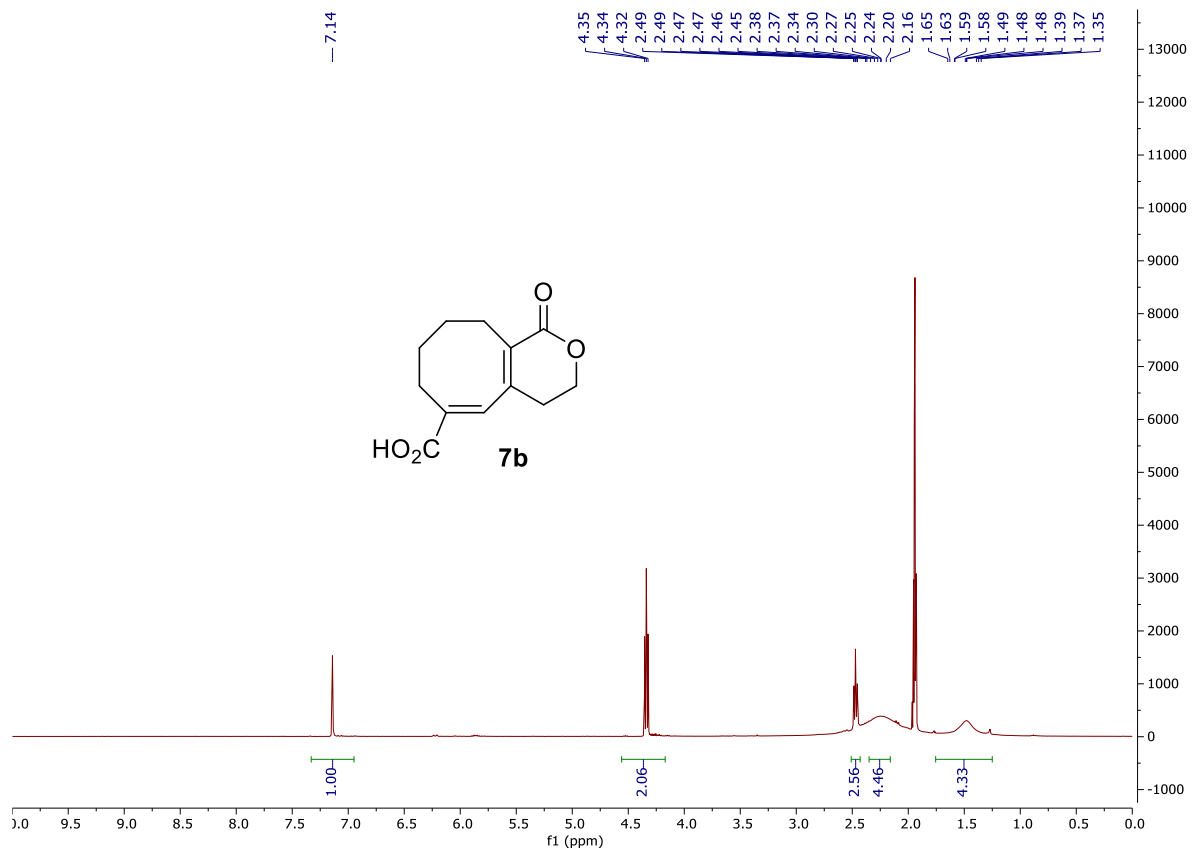
**6b – Observed in the presence of biphenyl (7.3 – 7.8 ppm) but not isolated**

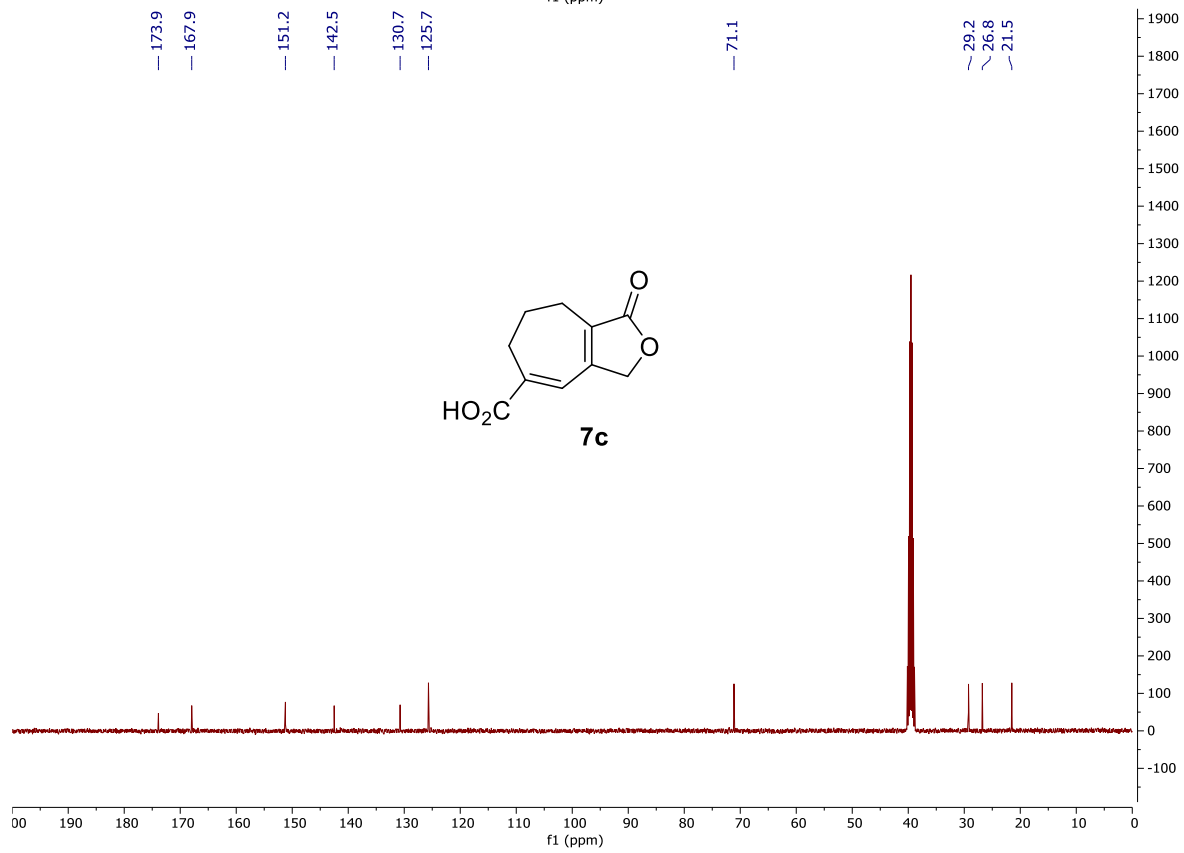
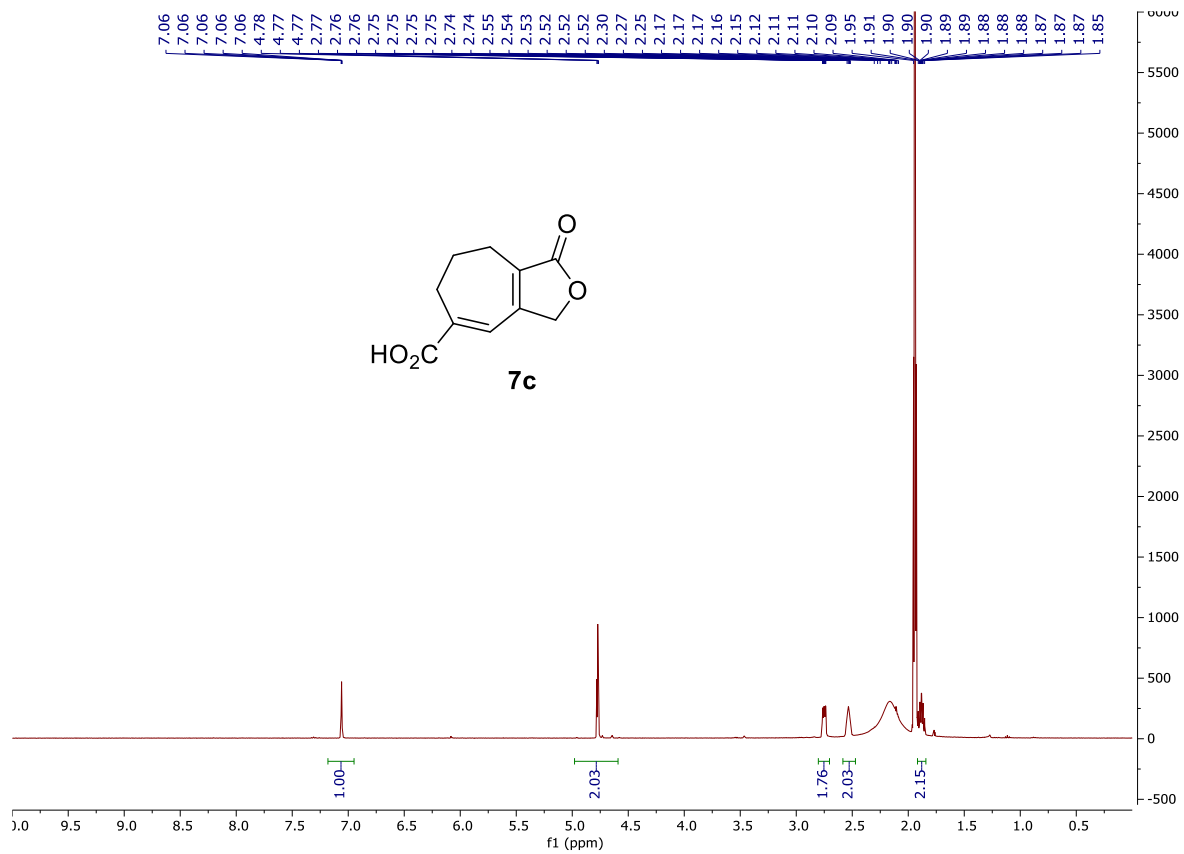


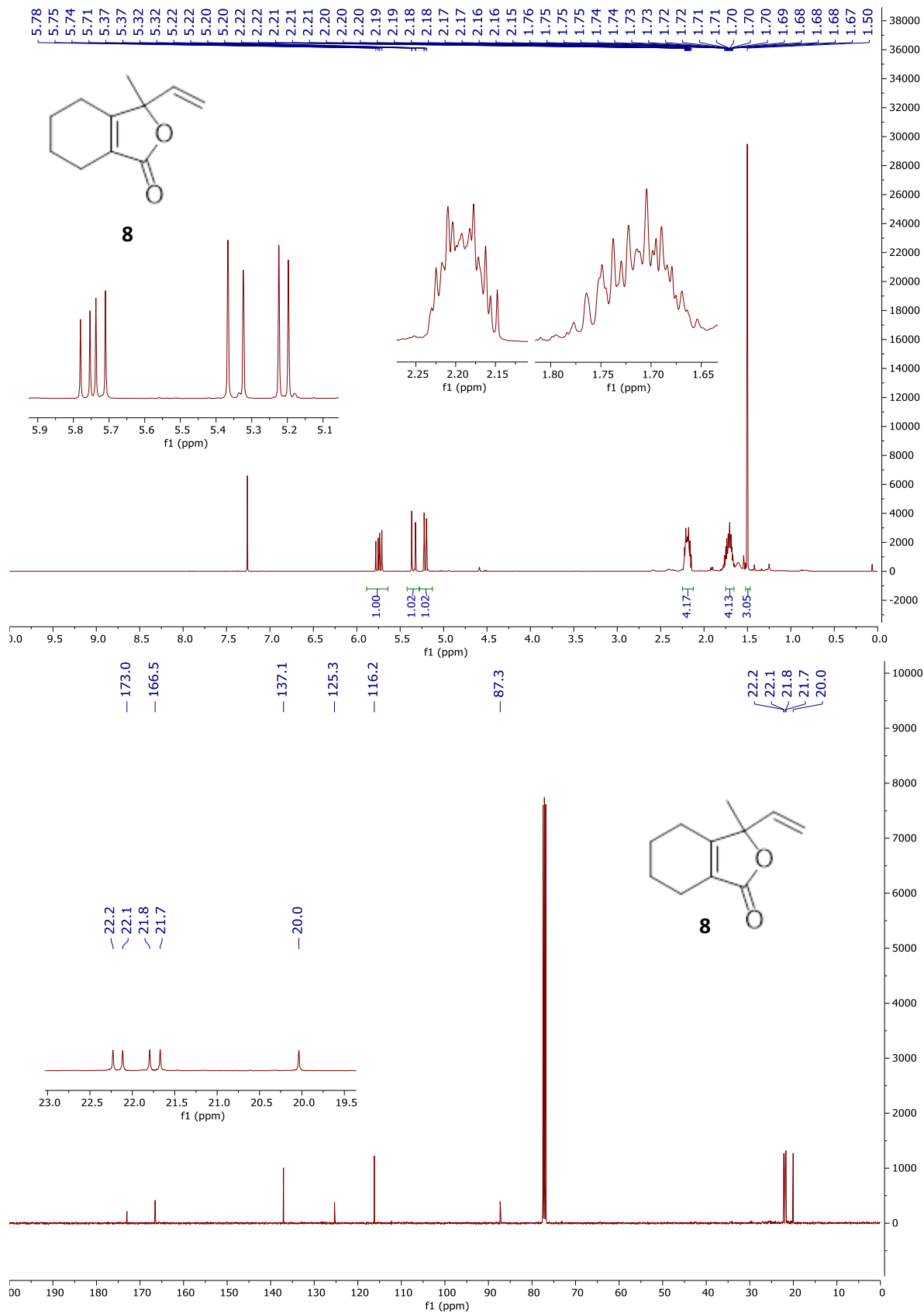
**6c - Observed in the presence of biphenyl (7.3 – 7.8 ppm) but not isolated**

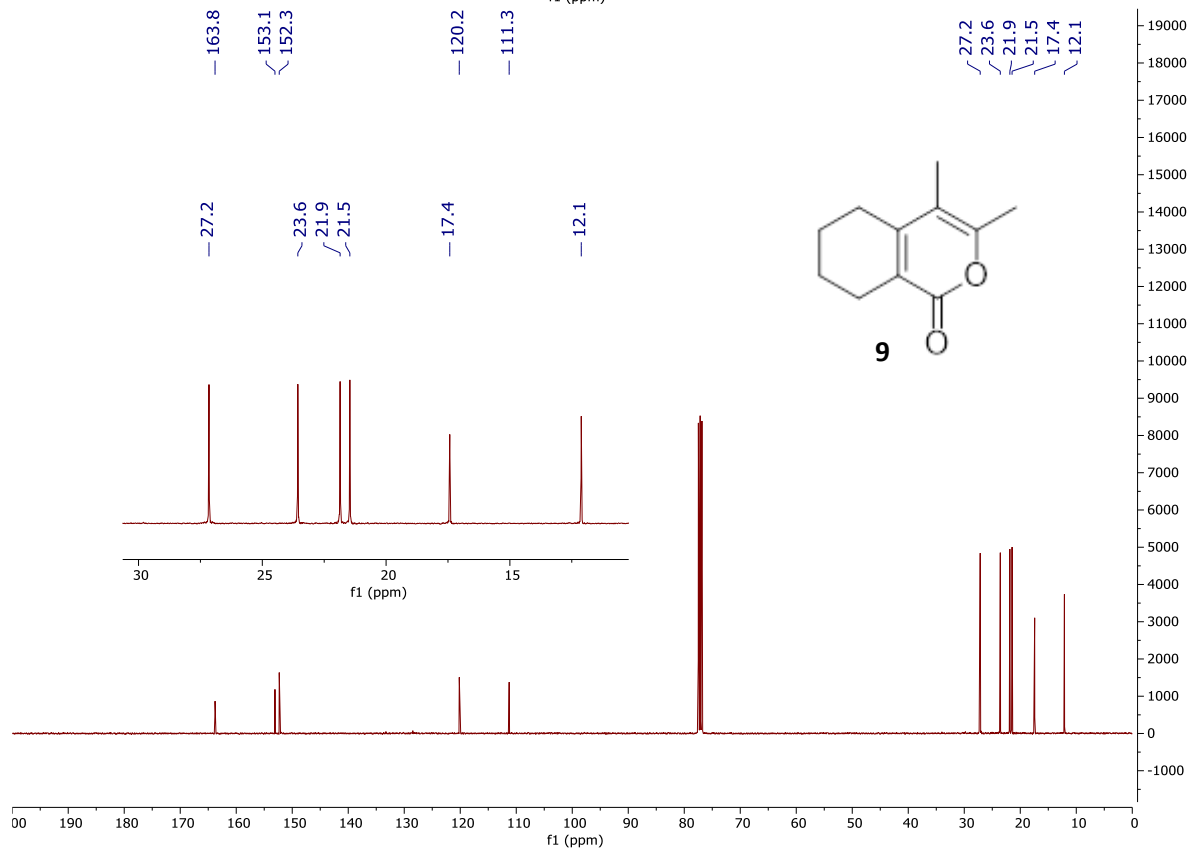
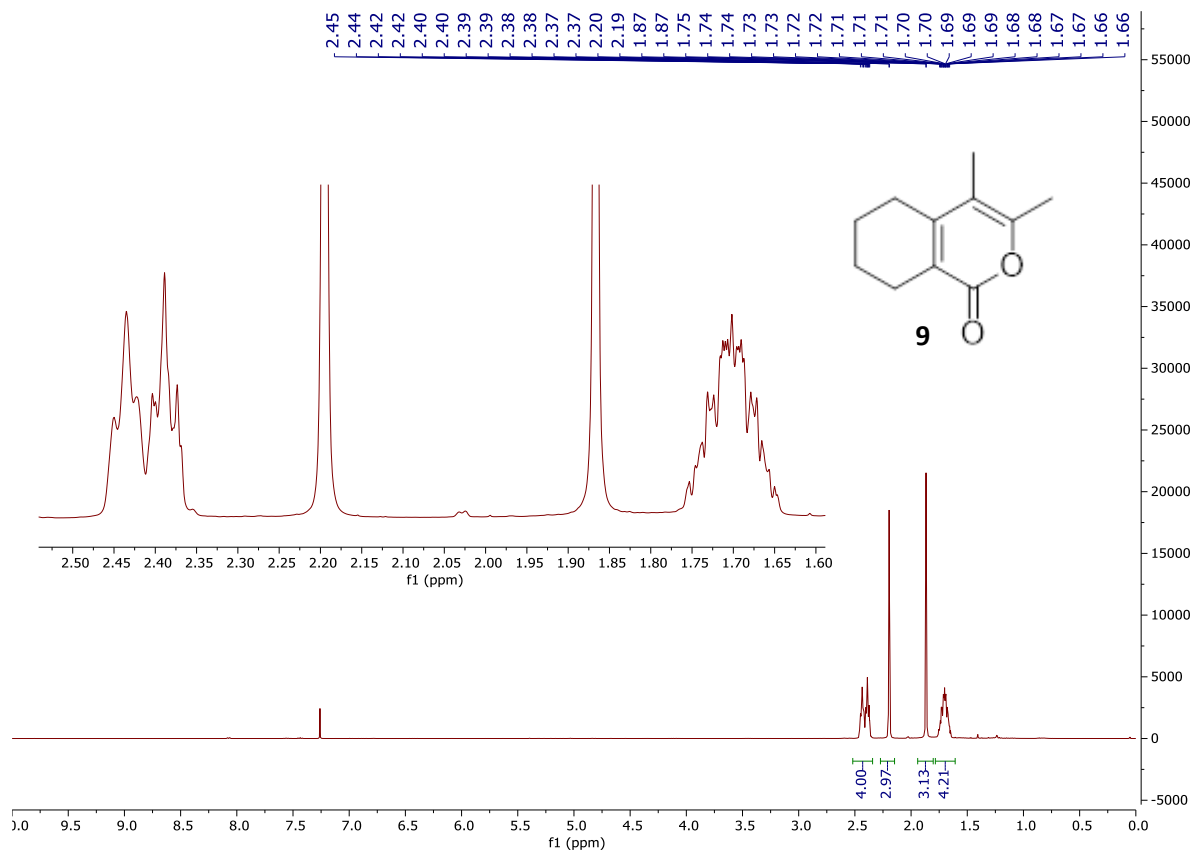












## **9. Time Resolved Infrared Spectroscopy (TRIR)**

### **9.1. Description of Time Resolved Infrared Spectroscopy (TRIR) setup**

The TRIR spectroscopy apparatus at the Nottingham has been described previously.<sup>[7]</sup> Briefly, fundamental pulses (800 nm, 100 fs, 80 MHz) are generated with a commercial Ti:Sapphire oscillator (Spectra-Physics MaiTai) and fundamental pulses are amplified in a Ti:Sapphire amplifier (Spectra-Physics SpitfirePro) to produce 800 nm, 100 fs, 1kHz, 2 mJ pulses. Half of the output is used to pump a TOPAS-C (Light Conversion) to produce tunable IR pulses using a difference frequency generator and the other part of the output is used to pump a harmonic generator (Time Plate Tripler, Miniopic Technology) to produce either 400 nm and 266 nm 100 fs pulses. The 400/266 nm pulses are used as pump beam and are focused onto the sample and delayed up to 2 ns with respect to the IR pulses by a translational stage (LMA Actuator, Aerotech). Part of the IR pulse is reflected onto a single-element mercury cadmium telluride (MCT) detector (Kolmar Technology) to serve as a reference, and the rest of the output is used as the probe and is focused and overlaps with the pump beam at the sample position. The polarization of the pump pulse was set at the magic angle (54.7°) relative to the probe pulse to avoid rotational diffusion. The broad-band transmitted probe pulse is detected with an 128 element MCT array detector (Infrared Associates). The array detector is mounted in the focal plane of a 250 mm IR spectrograph (DK240, Spectra Product) with a 150 grooves/mm grating. For TRIR measurements on timescales > 0.5 ns, a Q-switched Nd : YVO laser (ACE- 25QSPXHP/MOPA, Advanced Optical Technology, UK) was employed as a pump source which is synchronized to the Spitfire Pro amplifier.



## 9.2. Time Resolved Infrared Data

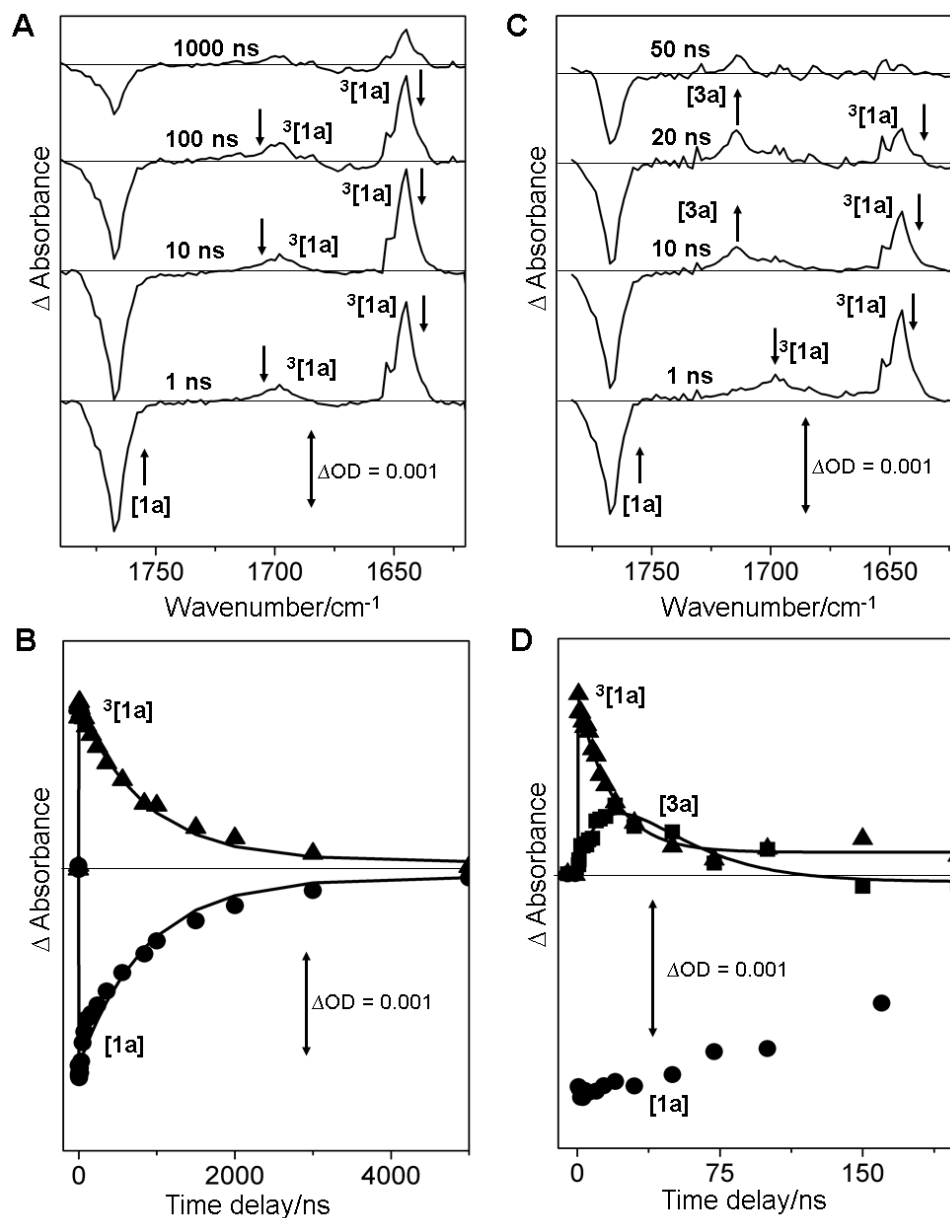


**Figure S9.** (A) ns TRIR spectra of **1a** (11 mM) in CD<sub>3</sub>CN at selected pump-probe time delays. The bands at 1645 cm<sup>-1</sup>, 1700 cm<sup>-1</sup> is assigned to the <sup>3</sup>ππ\* state of **1a**. (B) TRIR decay traces obtained from the ns experiment as shown in A. The decay of <sup>3</sup>[**1a**] (1645 cm<sup>-1</sup> peak intensity kinetics) state and bleach recovery (1774 cm<sup>-1</sup> peak intensity kinetics) are with lifetime of 1.05 (± 0.05) μs (C) ns TRIR spectra of mixture of **1a** (11 mM) and **2a** (120 mM) at selected pump-probe time delays. (D) TRIR decay traces obtained from the ns experiment as shown in C, showing the quenching of the <sup>3</sup>[**1a**], formation and decay of bi-radical intermediate **3a** and partial bleach recovery of **1a**. The decay of <sup>3</sup>[**1a**] state is associated with the formation of **3a** with time constant of 20(±2) ns.

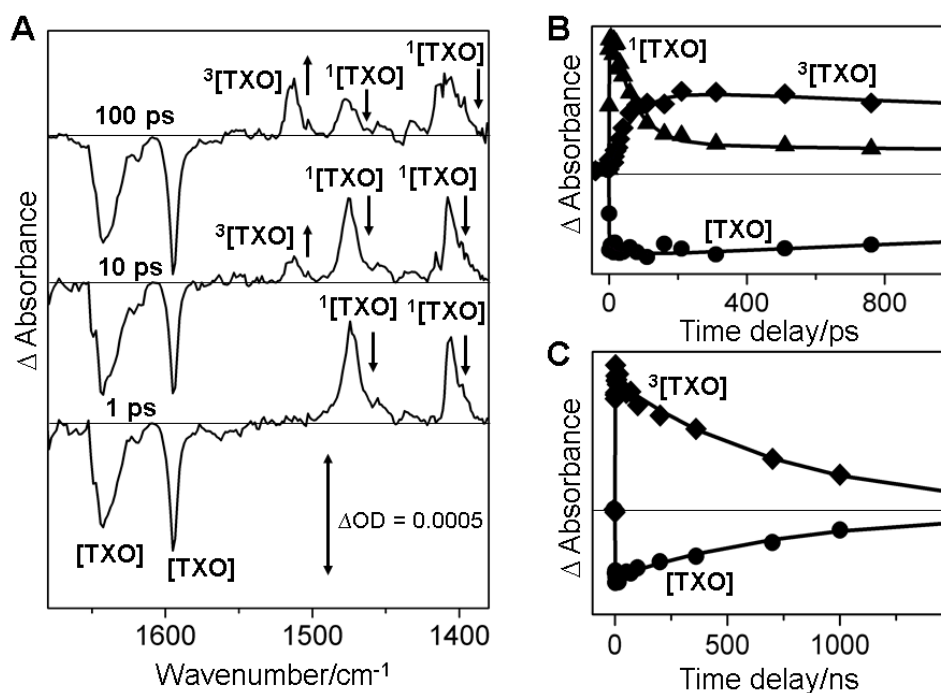


**Figure S10.** (A) ps TRIR spectra of TXO at selected pump-probe time delays in CD<sub>3</sub>CN after 355 nm photoexcitation. (B) ps TRIR kinetic traces showing decay of <sup>1</sup>[TXO] state, formation of <sup>3</sup>[TXO] state and partial bleach recovery of ground state. The singlet state decays with the lifetime of 60(±4) ps. The decay of excited singlet state is associated with the formation of <sup>3</sup>[TXO] state. (C) ns TRIR kinetic traces showing decay of <sup>3</sup>[TXO] state and bleach recovery kinetics. The lifetime of the triplet state is 760(±30) ns.

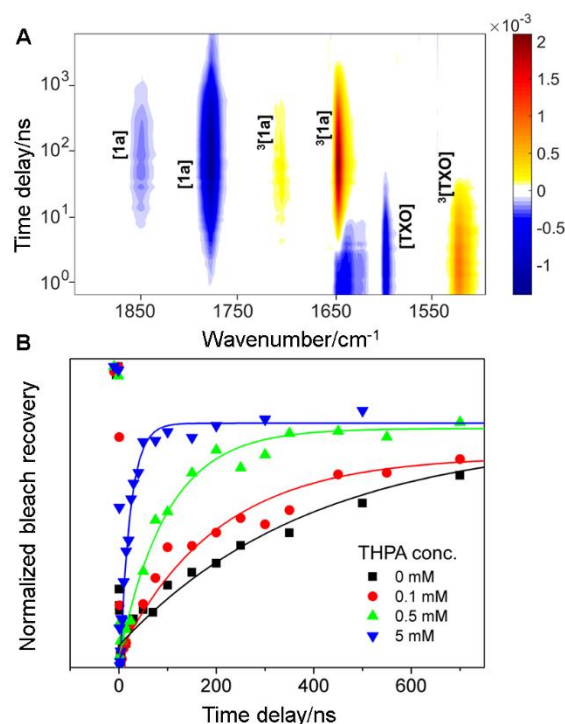


**Figure S11.** (A) 2D contour map of the TRIR spectra of the mixture of TXO(1.2 mM)+**1a**(12 mM) in CD<sub>3</sub>CN solution after 355 nm photoexcitation. (B) Bleach recovery kinetics of [TXO] with the indicated concentration of **1a** (THPA). The obtained bimolecular rate constant is  $k_q = 6.7 \times 10^9 \text{ M}^{-1}\text{s}^{-1}$ .

### 9.3. Characterization of the transient species:

The photoexcitation of TXO (at 355 nm) in presence of **1a** (THPA) and propargyl alcohol generates  $^3[\text{TXO}]$ ,  $^3[\mathbf{1a}]$ , **3a** and the final products **5a (major)** and **4a (minor)**. The TRIR studies include complete excited state characterization of **TXO**, **1a** by direct photoexcitation followed by quenching studies of the **TXO+1a** and **TXO+1a+propargyl alcohol** reaction mixtures. Our initial studies confirm that PAOH alone has little effect on the excited triplet state lifetime of TXO.

The ns TRIR spectra at selected time delays after 355 nm photoexcitation (TXO is excited exclusively) of TXO (1.2 mM)+**1a** (12 mM) in CD<sub>3</sub>CN are presented in **Figure S10**. In the ns timescale, both the  $^3[\text{TXO}]$  and  $^3[\mathbf{1a}]$  contribute to the TRIR signal. The assignment of the vibrational modes to the individual species is done by performing TRIR studies on TXO and **1a** separately (Figure **S10** and Figure **S9** respectively). Because the ns TRIR spectra of **1a** ( $\lambda_{\text{exc}} = 266 \text{ nm}$ ) alone show bleaches at 1774 cm<sup>-1</sup> and triplet excited state bands at 1700, 1645 cm<sup>-1</sup> (Figure **S9**), we assigned these bands safely to the ground state **1a** and  $^3[\mathbf{1a}]$  respectively. Bleaches at 1637 and 1594 cm<sup>-1</sup> are due to the **TXO** and the 1518cm<sup>-1</sup> band is assigned to the  $^3[\text{TXO}]$  based on the TRIR experiments on TXO alone (Figure **S10**)The formation of  $^3[\mathbf{1a}]$  following the 355 nm excitation confirms the triplet-triplet energy transfer process.

### 9.4. Kinetic rate constants for the sensitized reaction:

The ns TRIR studies on the **TXO+1a** mixture after 355 nm photoexcitation allows us to isolate the reaction kinetics for the generation of  $^3[\mathbf{1a}]$  and its return to the ground state. We performed a global kinetic analysis to obtain quantitative information on the kinetics. From the above discussion, it follows that at least three kinetic components – $^3[\text{TXO}]$ ,  $^3[\mathbf{1a}]$ , and infinite component are required to completely describe the ns TRIR data. Indeed, three kinetic components describe the data in a satisfactory manner. The resulting time constants are  $\tau_1 = 12.9 (\pm 2) \text{ ns}$  and  $\tau_2 = 536 (\pm 25) \text{ ns}$  and a long-lived component. The  $\tau_1$  is the lifetime of  $^3[\text{TXO}]$  state, and  $\tau_2$  is the lifetime of  $^3[\mathbf{1a}]$  state. The triplet energy transfer from the excited **TXO** to the ground state of **1a** leads to a strongly reduced  $^3[\text{TXO}]$  state lifetime (in absence of THPAA the  $^3[\text{TXO}]$  lifetime is 760 ( $\pm 30$ ) ns). The triplet energy transfer rate  $k_T$  is obtained by the following equation:

$$k_T = \frac{1}{\tau} - \frac{1}{\tau_0} = 7.7 \times 10^7 \text{ s}^{-1} \dots\dots\dots (\text{S1})$$

where  $\tau$  is the triplet lifetime in the presence of quencher and  $\tau_0$  is triplet lifetime in the absence of quencher. For bimolecular quenching experiments, in the low concentration limit of the quencher (dynamic quenching), the kinetics is often pseudo-first order. The plot of the quenching rate constants

(Figure S11(B)) versus **1a** concentrations confirms a linear relationship indicating that in this concentration regime the quenching is controlled by diffusion.

Next, we explored the kinetics of the [2+2] photocycloaddition reaction by studying the kinetics of the **TXO+1a+2a** solution. We have to consider many different chemical species for the kinetic analysis. Therefore, kinetics of the IR bands associated with the individual species are considered for the detailed kinetic analysis. Selected kinetic traces associated with the various species are presented in Figure S12. After excitation of TXO, the  $^3[\text{TXO}]$  state ( $1518\text{ cm}^{-1}$  mode) decays with the time constant of  $\tau_{\text{decay}} = 15(\pm 3)$  ns with the bleach recovery ( $1594\text{ cm}^{-1}$ ) with the time constant of  $\tau_{\text{recovery}} = 14(\pm 2)$  ns. The decay of the  $^3[\text{TXO}]$  state is associated with the formation of the  $^3[\mathbf{1a}]$  ( $1645\text{ cm}^{-1}$ ,  $\tau_{\text{rise}} = 12.5(\pm 2)$  ns). The bimolecular reaction between  $^3\text{THPAA}$  with PAOH leads to the formation of bi-radical species ( $1715\text{ cm}^{-1}$ ) with the time constant of  $28(\pm 4)$  ns. The decay of the radical species with the time constant of  $37.4(\pm 5)$  ns leads to the formation of final product ( $1778\text{ cm}^{-1}$  mode)

Upon 266 nm excitation of **1a**, the singlet excited state ( $^1[\mathbf{1a}]$ ) rapidly decays to the ground state predominantly through ultrafast internal conversion. Beside ultrafast internal conversion, it yields  $^3[\mathbf{1a}]$  with triplet quantum yield of  $\eta_{\text{ISC}} \approx 0.33$  (obtained from bleach recovery). From the direct TRIR measurements of **1a+2a** mixture, we conclude that the long-lived triplet state of **1a** involves in the [2+2] cycloaddition reaction, not the singlet excited state. The triplet-triplet energy transfer (TTET)

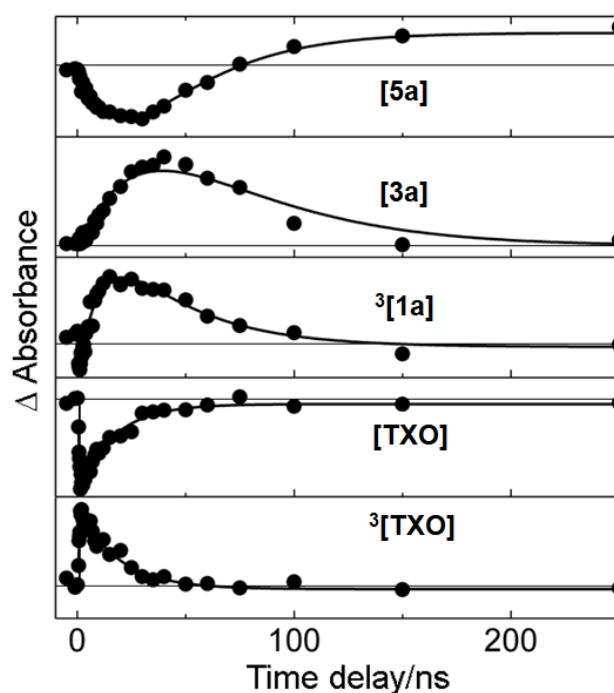


**Figure S12.** Peak position kinetics of IR modes associated with various species after photoexciting ( $\lambda_{\text{exc}} = 355\text{ nm}$ ) a solution of **TXO** (1.2 mM)+**1a** (12 mM)+**2a** (120 mM) in  $\text{CD}_3\text{CN}$ .

quantum yield from  $^3[1a]$  to the ground state  $2a$  (at a particular concentration) can be obtained by the following equation:

$$\Phi_{TTET} = \frac{1/\tau}{1/\tau + 1/\tau_0} \dots\dots\dots (S2)$$

Where  $\tau$  is the lifetime of  $^3[1a]$  state in the presence of quencher  $2a$  and  $\tau_0$  is the lifetime  $^3[1a]$  state in the absence of quencher. The complete quantum yield of the  $3a$  formation is therefore

$$\Phi_{diradical-non\ sensitized} = \eta_{ISC,1a} \times \Phi_{TTET(3[1a] \rightarrow 2a)} \dots\dots\dots (S3)$$

Our calculation yields  $\Phi_{diradical-non\ sensitized} \approx 0.32$  for the quantum yield of the formation of  $3a$  by direct photoexcitation. Using equation (2) we obtain the TTET from the  $^3[TXO]$  to the ground state of  $1a$  and the energy transfer efficiency from  $^3[1a]$  to  $2a$ . The total quantum yield formation of  $3a$  bi-radical for the sensitized reaction is given by

$$\Phi_{bi-radical-sensitized} = \eta_{ISC,TXO} \times \Phi_{TTET(3[TXO] \rightarrow [1a])} \times \Phi_{TTET(3[1a] \rightarrow [2a])} \dots\dots (S4)$$

The triplet quantum yield of TXO ( $\eta_{ISC,TXO}$ ) in ACN is 0.66. By applying equation (2) we can obtain  $\Phi_{TTET(3[TXO] \rightarrow [1a])}$  and  $\Phi_{TTET(3[1a] \rightarrow [2a])}$ . Overall we found  $\Phi_{bi-radical-sensitized} \approx 0.61$  in  $CD_3CN$ . Similar kinetic analysis in  $CH_2Cl_2$  solvent yields  $\Phi_{bi-radical-sensitized} \approx 0.53$ .

## 10. Raman Monitoring

### 10.1. Photochemical step

Raman spectroscopic measurements of the photochemical step were performed using a Kaiser Optical Systems Inc. RXN2 spectrometer, equipped with a sapphire tipped MarqMetrix BallProbe®. The photolysis was performed in an immersion well reactor using a 125 W medium pressure mercury lamp from Photochemical Reactors LTD. The Raman probe was inserted within an external sampling loop which was fed with the circulating reaction mixture *via* peristaltic pumps, in order to avoid exposure of the spectrometer detector to the mercury lamp light. The Spectra were collected using an excitation wavelength of 785 nm with a 400 mW laser power and a detector exposure time of 30 s with 10 averaged scans. The spectra collected during the course of the reaction are displayed in Figure S13.

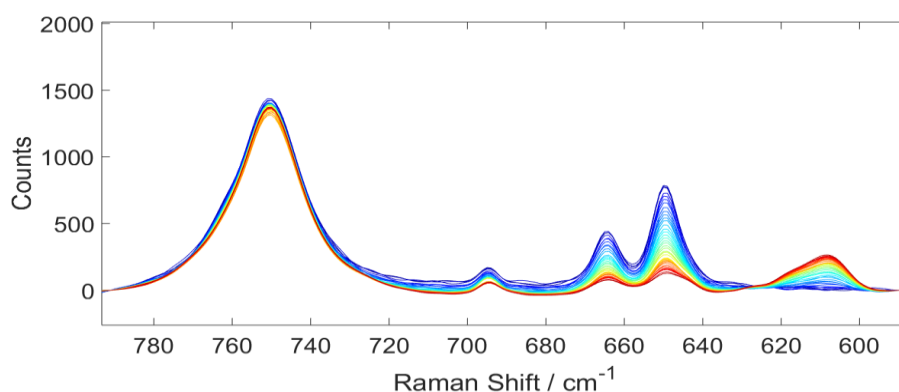


**Figure S13** – Raman spectra of the photolysis with time (blue to red) in the ring and bridged skeleton region showing the depletion of the THPA at ca. 650 and at 665  $\text{cm}^{-1}$  and the growth of the bridged product peak at 607  $\text{cm}^{-1}$ .

From these spectra the kinetics of the reaction could be monitored by tracking the normalised intensity of the THPA starting material vibration at 665  $\text{cm}^{-1}$  and the bridged product at 607  $\text{cm}^{-1}$  as a function of time (**Figure S14**).

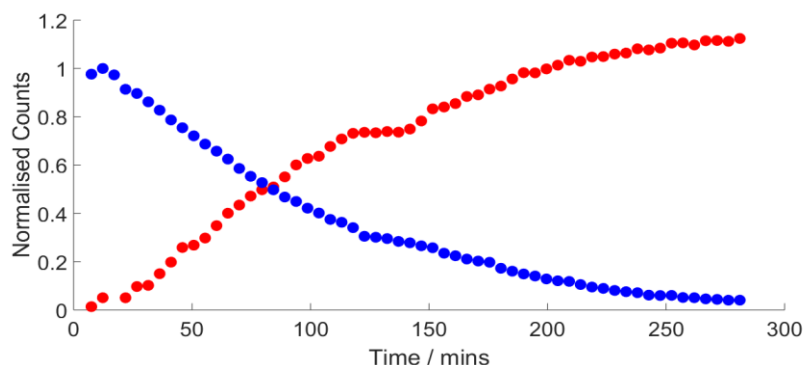


**Figure S14** – Kinetics of the photochemical step obtained from the normalised intensity of the THPA starting material vibration at 665  $\text{cm}^{-1}$  (blue) and the bridged product at 607  $\text{cm}^{-1}$  (red).

During the course of the reaction the carbonyl region of the Raman spectrum also exhibited this behaviour with the disappearance of the THPA vibrations at *ca.* 1677, 1773 and 1845  $\text{cm}^{-1}$  and the appearance of the bridged product peak at 1642  $\text{cm}^{-1}$ . This is demonstrated in Figure S15.

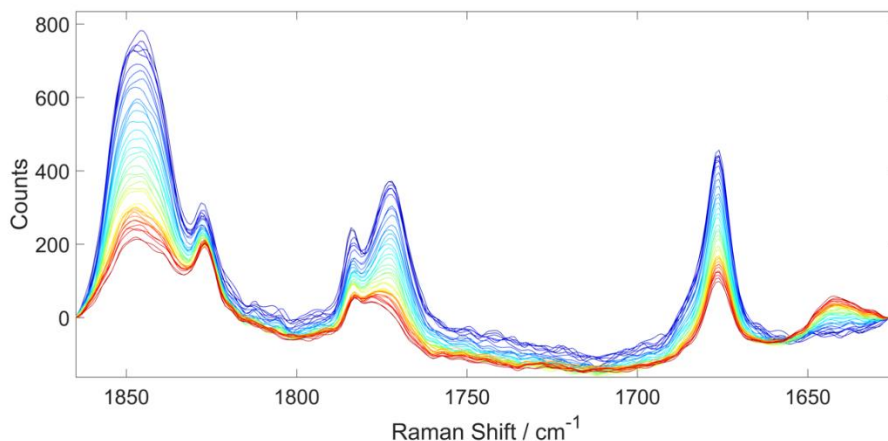


**Figure S15** – Raman spectra of the photolysis with time (blue to red) in the carbonyl region showing the depletion of the THPA at *ca.* 1677, 1773 and 1845  $\text{cm}^{-1}$  and the growth of the bridged product peak at 1642  $\text{cm}^{-1}$ .

## 10.2. Thermal steps

Raman spectroscopic measurements of the thermal reaction was again achieved using a Kaiser Optical Systems Inc. RXN2 spectrometer, equipped with a sapphire tipped MarqMetrix BallProbe<sup>®</sup>. These spectra were collected with the same detector exposure and laser power (30 s, 10 scans and 400 mW power) as the photochemical step, however the sampling was obtained *via* the submerging of the probe in a sample collection vessel of the outlet of the thermal flow reactor. The thermal reaction was run at 225°C and 150 bar, at residence times ranging from 0.125 to 8 mins. Normalised Raman spectra of the product and starting material are shown in Figure S16.

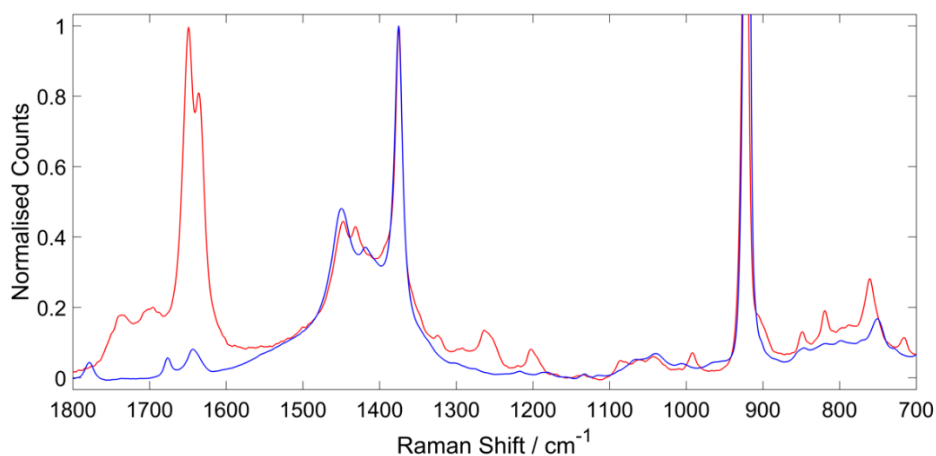


**Figure S16** – Normalised Raman spectra of the both the starting material (blue) and product 7a (red) of the thermal step of the reaction.

The Spectra in Figure S17 show the effect of the residence time on the yield of the product, as indicated by the height of the characteristic **7a** product modes. This is particularly evident for the 1650  $\text{cm}^{-1}$  vibration. Using the height of this mode and plotting it as a function of residence time, it can be seen that the yield of the product increases as the residence time within the thermal reactor increases from 0.125 to 7 mins. However as this residence time increases past this to 8 mins, the yield starts to decrease due to the formation of side products (Figure S18).

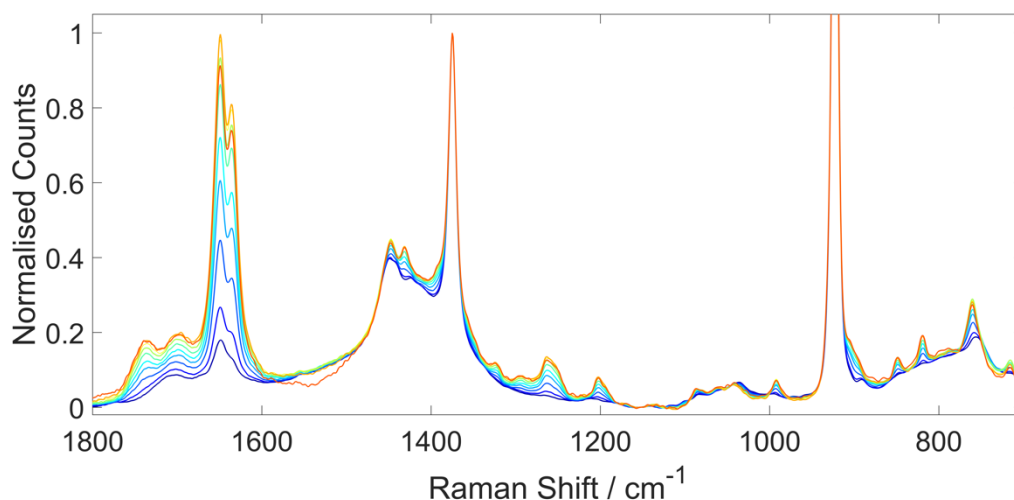


**Figure S17** – Normalised Raman spectra of the progression of the thermal reaction with increasing residence time (blue to red) displaying the growth of the characteristic **7a** product modes until 8 min (dark red) where the product yield decreases. This is reflected in a lower intensity of the product's 1650  $\text{cm}^{-1}$  vibration.

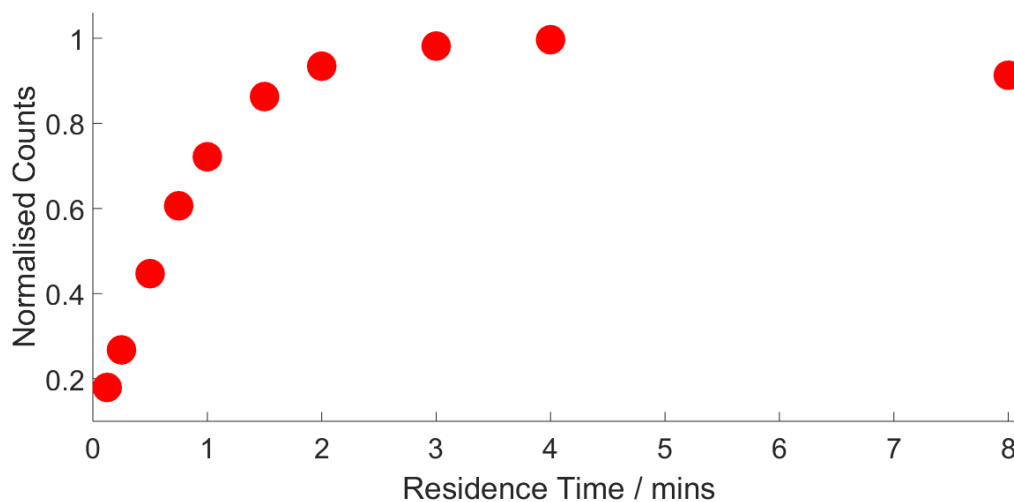


**Figure S18** – The intensity of the **7a** product vibration at 1650  $\text{cm}^{-1}$  from the normalised Raman spectra of the thermal reaction. This shows the increase in the product yield with increasing residence time until after ca. 5 mins where the yield starts to decrease as side products form.



## 11. gProms Modelling

Process modelling of the thermal reaction of **5a** to **7a** was carried out using gPROMS modelling software to allow the effect of changing the reaction scale on the performance of the reaction to be investigated, such as would be the case should the Firefly photoreactor be combined with the thermal rig, which would require elevated flow rates.

### 11.1. Model Description

A schematic of the reactor model is shown in Figure S19, showing a coiled reactor that is placed inside a heating block, depicted in red. The model of the high temperature thermal coil reactor has been developed within Process Systems Enterprise's gPROMS® *ProcessBuilder 1.3.1*. The inner diameter of the reactor tube is 0.305 cm, with a coil diameter of 7 cm and length of 600 cm. The temperature of the heating block, as measured by a K-type thermocouple inside the heating block, is assumed to be the fixed temperature of the reactor wall. The initial concentration concentrations are calculated at standard temperature and pressure, before being introduced into the reactor where it can change depending on conditions.

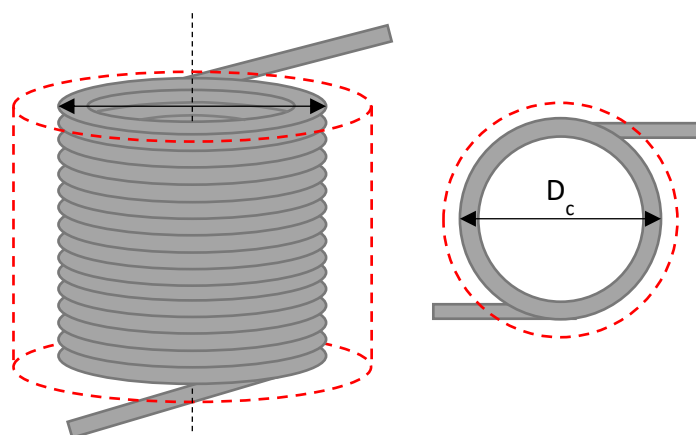
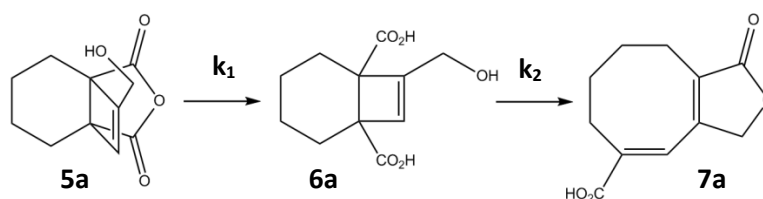


**Figure S19** - A schematic of the model, showing the coiled tubular reactor inside a heating block shown in red.

The physical properties, such as density, viscosity or thermal conductivity, of the reaction mixture were calculated using the Peng-Robinson Advanced 1978 (PR-78A) equation of state (EoS).<sup>[8]</sup> Due to the low concentration of reagents, the physical properties calculated for this system were assumed to be equal to that of the solvent. The mathematical relationships of the model have been developed from engineering principles so that, with parameter estimation, a semi-empirical model can be developed to predict behaviour outside of the experimental space. The following two reaction scheme (Scheme S7) was initially used, where reaction 1 is hydrolysis of the anhydride motif in **5a** and reaction 2 is the electrocyclic ring opening of **6a**, which occurs via multiple fast-lived intermediates.



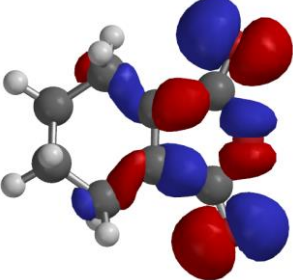
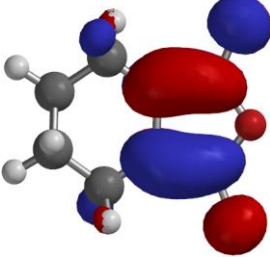
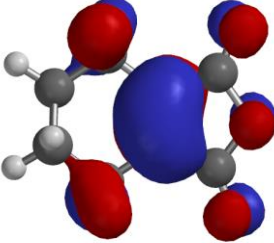
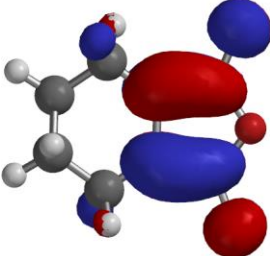
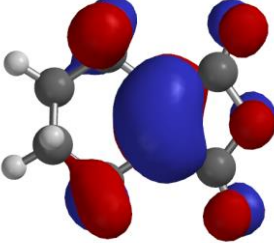
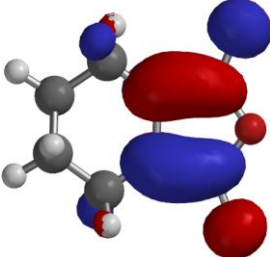
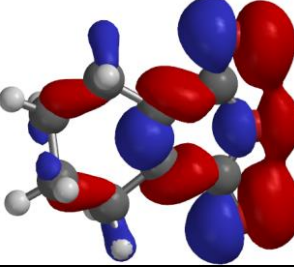
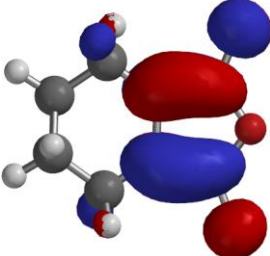
**Scheme S7** - The two steps of the thermal reaction, where the bridged product (**5a**) of the photochemical step is hydrolysed to **6a**, which then undergoes a rearrangement to form the 8 membered ring compound (**7a**).

## 12. Density Functional Theory Calculations

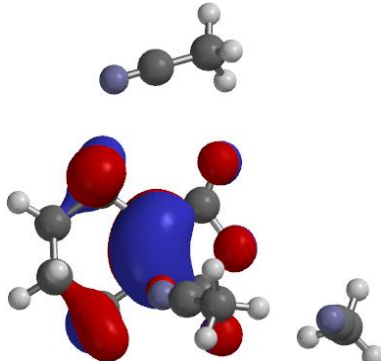
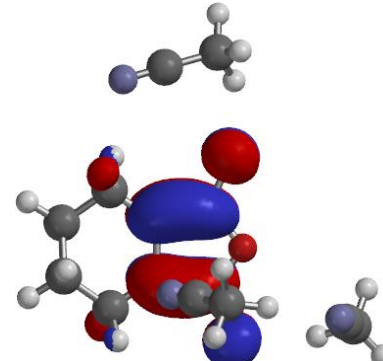
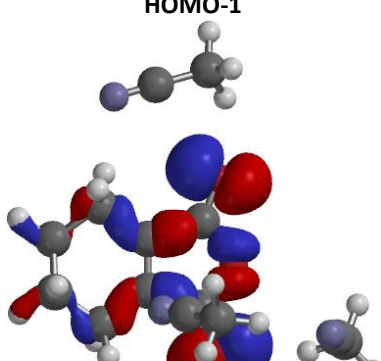
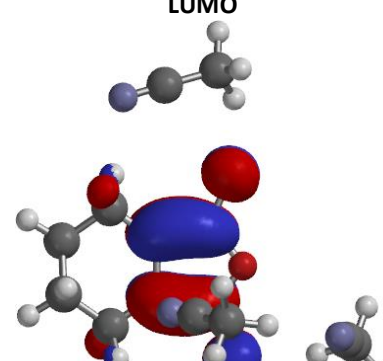
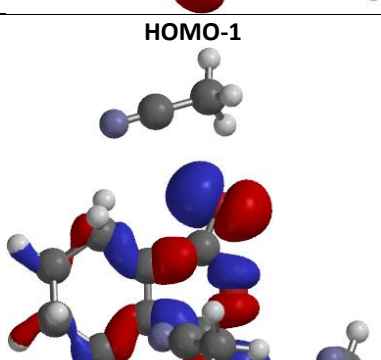
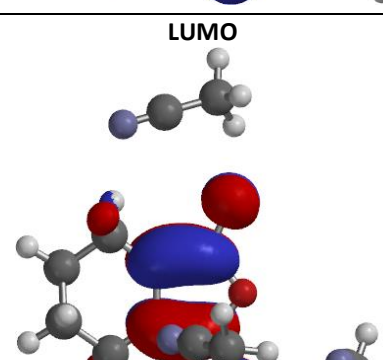
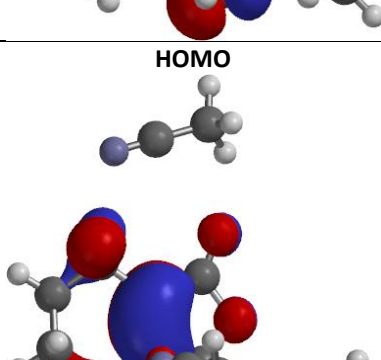
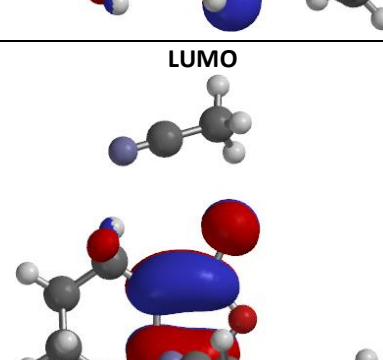
Density functional theory (DFT) calculations were carried out for **1a**,  $^1[1a]$ , and  $^3[1a]$  using the Q-Chem quantum chemistry software package.<sup>[9]</sup> Kohn-Sham DFT calculations of the lowest energy electronic states with singlet and triplet multiplicity (**1a** and  $^3[1a]$ ) were carried out using the B3LYP exchange-correlation functional and the 6-311G(d,p) electronic basis set.<sup>[10,11]</sup> Geometry optimizations, harmonic vibrational frequency calculations and molecular orbital calculations were performed both *in vacuo* and including an explicit solvent model consisting of three MeCN molecules initially positioned around the carbonyl groups. The  $^1[1a]$  excited state was calculated using an excited state DFT self-consistent field procedure during both the geometry optimization and harmonic frequency calculations, in which an electron was moved from the highest occupied molecular orbital (HOMO) to the lowest unoccupied molecular orbital (LUMO) and the maximum-overlap-method was used to prevent variational collapse to the ground state.<sup>[12]</sup> Time-Dependent DFT (TDDFT) calculations of electronic excitations from the ground state were carried out using the CAM-B3LYP exchange-correlation functional,<sup>[13]</sup> both in vacuo and in explicit solvent with a state-specific polarizable continuum model (PCM) solvent with a dielectric constant of 37.5 and an optical dielectric constant of 1.81.

TDDFT calculations indicate that the lowest singlet and triplet electronic excitations of **1a** that correspond to the formation of  $^1[1a]$  and  $^3[1a]$ , have  $n\pi^*$  and  $\pi\pi^*$  orbital excitation character, respectively, when solvated by MeCN (see Table S8 and S9). Orbital analysis in **Figure S20** then shows that the n-orbital involving the carbonyl oxygen atoms becomes increasingly localized onto only one of the two carbonyl groups as the  $^1[1a]$  geometry relaxes. This in turn leads to a change in the bonding of the excited state where the double bonding character in only one of the carbonyl bonds is depleted. This observation is consistent with the presence of the experimental peak at  $1762\text{ cm}^{-1}$  in the carbonyl stretching region of the TRIR of **1a**, and a corresponding single carbonyl stretching mode is predicted from the harmonic vibrational analysis of the  $n\pi^*$   $^1[1a]$  species with a vibrational frequency of  $1759\text{ cm}^{-1}$ .

**Table S8:** Dominant orbital contributions and excitation energies (in eV) for the lowest two singlet and triplet electronic excitations of **1a** calculated *in vacuo* using TDDFT.

State	Donor MO	Acceptor MO	Excitation Energies
T <sub>1</sub>	HOMO 	LUMO 	3.35
T <sub>2</sub>	HOMO-1 	LUMO 	3.80
S <sub>1</sub>	HOMO-1 	LUMO 	4.25
S <sub>2</sub>	HOMO-2 	LUMO 	4.88

**Table S9:** Dominant orbital contributions and excitation energies (in eV) for the lowest two singlet and triplet electronic excitations of **1a** calculated in explicit solvent using SS-TDDFT.

State	Donor MO	Acceptor MO	Excitation Energies
T <sub>1</sub>	HOMO 	LUMO 	3.09
T <sub>2</sub>	HOMO-1 	LUMO 	3.98
S <sub>1</sub>	HOMO-1 	LUMO 	4.46
S <sub>2</sub>	HOMO 	LUMO 	4.81

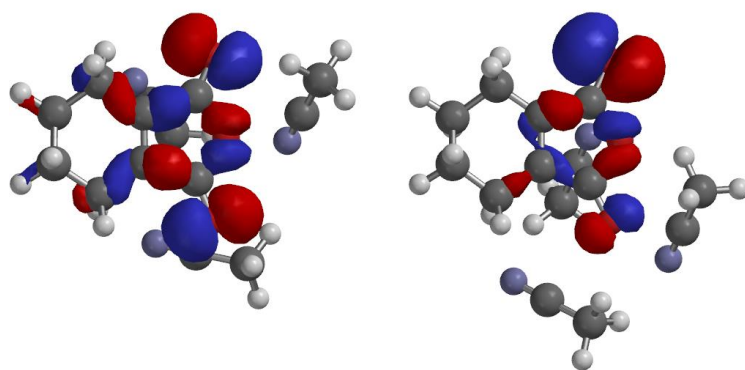


**Figure S20** - The highest energy occupied oxygen n-orbital in the ground state electronic configuration shown for the solvated **1a** geometry (left) and **<sup>1</sup>[1a]** geometry (right).

## 13. References

1. Elliott, L. D.; Berry, M.; Harji, B.; Klauber, D.; Leonard, J.; Booker-Milburn, K. I. *Org. Process Res. Dev.* **2016**, *20*, 1806-1811.
2. Dudd, L. M.; Venardou, E.; Garcia-Verdugo, E.; Licence, P.; Blake, A. J.; Wilson, C.; Poliakoff, M. *Green Chem.*, **2003**, *5*, 187-192.
3. Hook, B. D. A.; Dohle, W.; Hirst, P. R.; Pickworth, M.; Berry, M. B.; Booker-Milburn, K. I. *J. Org. Chem.*, **2005**, *70*, 7558-7564.
4. Booker-Milburn, K. I.; Cowell J. K.; Delgado-Jiménez, F.; Sharpe, A.; White A. J. *Tetrahedron*, **1999**, *55*, 5875-5888.
5. Ralph, M. J.; Harrowven, D. C.; Gaulier, S.; Ng, S.; Booker-Milburn, K. I. *Angew. Chemie - Int. Ed.* **2015**, *54*, 1527-1531.
6. a) Booker-Milburn, K. I.; Delgado-Jimenez, F.; Sharpe, A. *Tetrahedron*, **1999**, *55*, 5889-5902. b) Booker-Milburn, K. I.; Cowell, J. K.; Harris, L. J. *Tetrahedron*, **1997**, *53*, 12319-12338.
7. Brennan, P.; George, M. W.; Jina, O. S.; Long, C.; McKenna, j.; Pryce, M. T.; Sun, X.; Vuong, K. Q. *Organometallics*, **2008**, *27*, 3671-3680.
8. Robinson D. B.; Peng, D. Y. The characterization of the heptanes and heavier fractions for the GPA Peng–Robinson programs, Gas processors association. (**1978**).
9. Shao, Y.; Gan, Z.; Epifanovsky, E.; Gilbert, A.T.B.; Wormit, M.; Kussmann, J.; Lange, A.W.; Behn, A.; Deng, J.; Feng, X.; Ghosh, D.; Goldey, M.; Horn, P.R.; Jacobson, L.D.; Kaliman, I.; Khaliullin, R.Z.; Kuś, T.; Landau, A.; Liu, J.; Proynov, E.I.; Rhee, Y.M.; Richard, R.M.; Rohrdanz, M.A.; Steele, R.P.; Sundstrom, E.J.; Woodcock, H.L.; Zimmerman, P.M.; Zuev, D.; Albrecht, B.; Alguire, E.; Austin, B.; Beran, G.J.O.; Bernard, Y.A.; Berquist, E.; Brandhorst, K.; Bravaya, K.B.; Brown, S.T.; Casanova, D.; Chang, C.-M.; Chen, Y.; Chien, S.H.; Closser, K.D.; Crittenden, D.L.; Diedenhofen, M.; DiStasio, R.A.; Do, H.; Dutoi, A.D.; Edgar, R.G.; Fatehi, S.; Fusti-Molnar, L.; Ghysels, A.; Golubeva-Zadorozhnaya, A.; Gomes, J.; Hanson-Heine, M.W.D.; Harbach, P.H.P.; Hauser, A.W.; Hohenstein, E.G.; Holden, Z.C.; Jagau, T.; Ji, C.H.; Kaduk, B.; Khistyayev, K.; Kim, J.; Kim, J.; King, R.A.; Klunzinger, P.; Kosenkov, D.; Kowalczyk, T.; Krauter, C.M.; Lao, K.U.; Laurent, A.D.; Lawler, K.V.; Levchenko, S.V.; Lin, C.Y.; Liu, F.; Livshits, E.; Lochan, R.C.; Luenser, A.; Manohar, P.; Manzer, S.F.; Mao, S.-P.; Mardirossian, N.; Marenich, A.V.; Maurer, S.A.; Mayhall, N.J.; Neuscammann, E.; Oana, C.M.; Olivares-Amaya, R.; O'Neill, D.P.; Parkhill, J.A.; Perrine, T.M.; Peverati, R.; Prociuk, A.; Rehn, D.R.; Rosta, E.; Russ, N.J.; Sharada, S.M.; Sharma, S.; Small, D.W.; Sodt, A.; Stein, T.; Stück, D.; Su, Y.-C.; Thom, A.J.W.; Tsuchimochi, T.; Vanovschi, V.; Vogt, L.; Vydrov, O.; Wang, T.; Watson, M.A.; Wenzel, J.; White, A.; Williams, C.F.; Yang, J.; Yeganeh, S.; Yost, S.R.; You, Z.-Q.; Zhang, I.Y.; Zhang, X.; Zhao, Y.; Brooks, B.R.; Chan, G.K.L.; Chipman, D.M.; Cramer, C.J.; Goddard, W.A.; Gordon, M.S.; Hehre, W.J.; Klamt, A.; Schaefer, H.F.; Schmidt, M.W.; Sherrill, C.D.; Truhlar, D.G.; Warshel, A.; Xu, X.; Aspuru-Guzik, A.; Baer, R.; Bell, A.T.; Besley, N.A.; Chai, J.-D.; Dreuw, A.; Dunietz, B.D.; Furlani, T.R.; Gwaltney, S.R.; Hsu, C.-P.; Jung, Y.; Kong, J.; Lambrecht, D.S.; Liang, W.; Ochsenfeld, C.; Rassolov, V.A.; Slipchenko, L.V.; Subotnik, J.E.; Van Voorhis, T.; Herbert, J.M.; Krylov, A.I.; Gill, P.M.W.; Head-Gordon, M. *Mol. Phys.*, **2014**, *113*, 184-215.
10. Becke, A. D. *J. Chem.*, **1993**, *98*, 5648-5652.

11. Stephens, P. J.; Devlin, F. J.; Chabalowski, C. F.; Frisch, M. J. *J. Phys. Chem.*, **1994**, *98*, 11623-11627.
12. Gilbert, A. T. B.; Besley, N. A.; Gill, P. M. W. *Phys. Chem. A*, **2008**, *112*, 13164-13171.
13. Yanai, T.; Tew, D. P.; Handy, N. C. *Chem. Phys. Lett.*, **2004**, *393*, 51-57.